# INFORMATION TO USERS

This manuscript has been reproduced from the microfilm master. UMI films the text directly from the original or copy submitted. Thus, some thesis and dissertation copies are in typewriter face, while others may be from any type of computer printer.

**The quality of this reproduction is dependent upon the quality of the copy submitted.** Broken or indistinct print, colored or poor quality illustrations and photographs, print bleedthrough, substandard margins, and improper alignment can adversely affect reproduction.

In the unlikely event that the author did not send UMI a complete manuscript and there are missing pages, these will be noted. Also, if unauthorized copyright material had to be removed, a note will indicate the deletion.

Oversize materials (e.g., maps, drawings, charts) are reproduced by sectioning the original, beginning at the upper left-hand corner and continuing from left to right in equal sections with small overlaps.

Photographs included in the original manuscript have been reproduced xerographically in this copy. Higher quality 6" x 9" black and white photographic prints are available for any photographs or illustrations appearing in this copy for an additional charge. Contact UMI directly to order.

Bell & Howell Information and Learning
300 North Zeeb Road, Ann Arbor, MI 48106-1346 USA
800-521-0600

# RICE UNIVERSITY

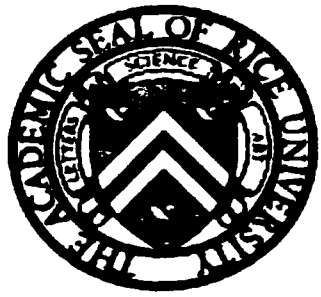


# Platelet Transport and Surface Reactions in Mural Thrombosis

by

**Shih-Hsin Kao**

**Doctor of Philosophy**

Houston, Texas

May, 2000

UMI Number: 9969279

UMI Microform 9969279


Bell & Howell Information and Learning Company
300 North Zeeb Road
P.O. Box 1346
Ann Arbor, MI 48106-1346

RICE UNIVERSITY

# Platelet Transport and Surface Reactions in Mural Thrombosis

by

**Shih-Hsin Kao**

A THESIS SUBMITTED
IN PARTIAL FULFILLMENT OF THE
REQUIREMENTS FOR THE DEGREE

**Doctor of Philosophy**

APPROVED, THESIS COMMITTEE:

Larry V. McIntire, E.D. Butcher Professor
Department of Chemical Engineering and Bioengineering
Chair, Department of Bioengineering
Chair, Institute for Biosciences and Bioengineering

J. David Hellums, A. J. Hartsook Professor Emeritus
Department of Chemical Engineering and Bioengineering

Jennifer L. West, T.N. Law Assistant Professor
Department of Bioengineering

Joel L. Moake, Associate Director
J. W. Cox Laboratory for Biomedical Engineering
Professor of Medicine, Baylor College of Medicine

Houston, Texas
May, 2000

## Abstract

## Platelet Transport and Surface Reactions in Mural Thrombosis

by

**Shih-Hsin Kao**

Due to the complexity of mural thrombosis, involving blood flow patterns, blood cellular and protein components, and multiple surface reactions, some fundamental mechanisms of the blood clot formation process are still difficult to resolve. This thesis focuses on three key areas that contribute to an understanding of flow effects and platelet-surface interactions in mural thrombosis. First, a mathematical model based on a constitutive equation that accounts for lateral motions of red blood cells (RBCs) by collision and viscosity effects is presented. It predicts the steady-state RBC distributions and blood velocity profiles under different shear rates and hematocrits in a parallel-plate flow chamber. The platelet drift velocity toward the wall due to the plasma counter flow is calculated directly from these RBC distributions, and higher wall concentrations of platelets are predicted at higher shear rates and larger hematocrits, as have been observed experimentally. Second, utilizing a novel flow cytometric analysis, measurements of the platelet activation status after platelets adhere onto the microspheres coated with vWf, insoluble collagen fibrils, or soluble collagen monomers are presented. The platelets adhering on immobilized fibrillar collagen express a higher percentage of activated GpIIb-IIIa receptors and more P-selectin than do those on vWf- and soluble collagen-coated surfaces. This finding explains why platelets adhere separately on vWf-coated surfaces but form large aggregates on fibrillar collagen-coated surfaces in flow chamber

experiments. In addition, it indicates that immobilized collagen structures affect the thrombogenicity of surfaces. Further studies using this protocol reveal that $Ca^{2+}$ released from intracellular pools is involved in signal transduction pathways that lead to the conformation change of GpIIb-IIIa and the surface expression of P-selectin after platelets interact with collagen. Finally, using a combination of viscometric and flow cytometric methods, originally designed to study receptor-ligand binding forces, an unexpected interaction phenomenon was discovered between the platelet receptor GpIb-IX-V complex and immobilized vWf. Platelet adhesion via GpIb-IX-V onto the microspheres with high vWf coating density is enhanced as the shear rate increases. This enhancement is not due to the shear-induced platelet activation, cytoskeletal rearrangement by calpains, or secondary flows in the cone-and-plate viscometer at high shear rates.

***The heavens declare the glory of God; the skies proclaim the work of His hands.***

***Day after day they pour forth speech; night after night they display knowledge.***

***There is no speech or language where their voice is not heard.***

***Their voice goes out into all the earth, their words to the ends of the world.***

**(Psalms 19: 1-4a; NIV)**

# Acknowledgments

I would like to express my sincere appreciation to:

- Dr. Larry V. McIntire, my thesis advisor, for providing me the freedom to explore different directions in this research and his continuous support.
- Dr. J. David Hellums, Dr. Joel L. Moake, and Dr. Jennifer L. West for serving on my thesis committee.
- Dr. Thomas Chow, Marcella E. Estrella, and Nancy A. Turner for their technical assistance and helpful discussions.
- Dr. Jan Hewitt for helping me in thesis writing.
- Arnez Washington, Sherry Nassar, and Maria Modelska for their excellent administrative assistance.
- My friends in the Cox Laboratory for their enlightening discussions and making this a fruitful and enjoyable period of my life.
- My parents, sister and brother for their love, patience, and understanding.
- My brothers and sisters in Houston Chinese Church for their intercession prayers.

This work was supported financially by NIH Grants No. HL-18672, NS-23327, and the Robert A. Welch Foundation Grant No. C-938.

# Table of Contents

# List of Figures

# Chapter 1

## Mural Thrombosis: Flow Patterns, Blood Components and Surface Reactions Are Interconnected

Mural thrombosis is the blood clot formation on altered endovascular surfaces or cardiovascular devices anywhere in the circulation as a pathological consequence of activating hemostatic mechanisms under variable flow conditions. Under normal circumstances, the determinants of hemostasis are carefully regulated to ensure that the blood fluidity is maintained. The same hemostatic elements are poised to respond effectively and rapidly to acute vascular injury by forming a protective hemostatic clot, thereby preventing excessive blood loss. However, pathologic processes that alter the normal balance among hemostatic determinants can lead either to inadequate hemostasis, producing hemorrhage, or excessive hemostasis, resulting in thrombosis.

Pathologic mural thrombosis is a clinical manifestation in cardiovascular and cerebrovascular diseases, the first and third fatal causes in USA respectively. For example, in patients with acute myocardial infarction, an acute thrombus, often associated with atherosclerotic plaque rupture, occludes the artery that supplies the damaged area. In the case of ischemic stroke, thrombi or emboli from an atherosclerotic plaque or other causes result in an intra- or extracranial interruption in the arterial blood supply, causing brain infarction and consequent neurologic symptoms. Current therapies

provide only moderate protection from these pathological states. To aid in developing more potent therapeutics, essential mechanisms of mural thrombosis must be understood.

## 1.1 Determinants of Mural Thrombosis

The concept of the pathogenesis of mural thrombosis involves three primary interactions between blood flow, blood components (soluble and cellular constituents), and the blood vessel wall, as proposed by Rudolph Virchow in 19th century [1]. As a thrombogenic surface is exposed to circulating blood, platelets and coagulation factors are delivered to the surface by blood flow. Platelets may adhere, aggregate, and release their granular components. In addition, thrombin, which is also a potent platelet activator, is generated via the intrinsic or extrinsic coagulation cascades and catalyzes fibrin network formation. The resulting thrombi will narrow or even obstruct the blood passage. Unstable blood clots may be dislodged or broken by shear forces and form emboli. In the natural process of restoring normal blood flow, plasmin is generated to dissolve the fibrin network and leukocytes are recruited to scavenge the degraded thrombi. Therefore, mural thrombosis is a highly dynamic process, and blood flow patterns, blood components, and surface reactions are interconnected in causing blood clot formation. Without considering all three determinants of mural thrombosis, the clinical and experimental findings may be not easy to interpret accurately. The effects of these thrombogenic factors are reviewed in the next sections.

**Flow Patterns**

Flow patterns affect the distribution of blood cells and the mass transport of blood components between the blood stream and the vessel wall. Under normal circumstances, blood tends to flow in a laminar pattern in which the center of the flow channel possesses the greatest velocity with the shear rate (velocity gradient) approaching zero, and the wall possesses zero velocity with a maximum shear rate. Because of the range of vessel sizes and volumetric blood flow rates, the wall shear rates corresponding to the different regions of the vascular system vary greatly. Owing primarily to differences in cell size and membrane flexibility, red blood cells accumulate at the center of the flow channel and are depleted close to the wall, whereas platelets are concentrated in the near-wall region [2-7]. This enrichment of platelets near the wall ensures an adequate primary hemostatic response following the exposure of thrombogenic surfaces to flowing blood.

Flow may not only cause non-uniform distributions of blood cells but may also affect cell functions. In the near-wall region where platelets are concentrated, there is the highest shear rate of the flow channel, which may reach abnormal levels in a stenosed artery [8,9]. Many experimental observations have shown that shear stress induces platelet activation [10-12]. When pathologic levels of the shear stress (>50 dynes/cm$^2$) are applied to platelet rich plasma (PRP), platelets change morphology, secrete many substances and aggregate. Platelet aggregation in response to pathologically elevated shear stresses is not an artifact of cell lysis, but rather depends on the presence of plasma von Willebrand factor (vWf) and functional platelet receptors GpIb-IX-V and GpIIb-IIIa (also known as

the integrin $\alpha_{IIb}\beta_3$) [13-18]. Using an optically modified cone-and-plate viscometer, capable of simultaneously monitoring cytoplasmic ionized calcium $[Ca^{2+}]_i$ and platelet aggregation, it has been shown that the $[Ca^{2+}]_i$ elevation is accompanied by synchronous aggregation, and both responses are dependent on shear stress and vWf [19,20]. The GpIb-IX-V and the extracellular $Ca^{2+}$ are absolutely required for vWf–mediated $[Ca^{2+}]_i$ changes and platelet aggregations under high shear conditions. The high shear forces can also induce the activation of platelet GpIIb-IIIa receptors, often reported as an increase in binding of the monoclonal antibody PAC-1 [21], which recognizes specifically the high affinity conformation of this receptor.

The composition and geometry of a blood vessel play an important role in determining the flow pattern and the mass transport. In the vascular system, thrombi and atherosclerotic plaques preferentially occur at locations such as bifurcations, T-junctions, highly curved vessels, regions near valves, and vessels with abruptly changing diameters [22,23]. Complex vessel geometries can cause secondary flow patterns, including streamline separation, stagnant regions, vortex formation, and even local turbulence. Those conditions increase the residence time between blood cells/plasma proteins and the vessel wall, leading to a potential increase in the local concentration or deposition of the components necessary for thrombus and plaque formation. As the heart pumps blood continually, the main effects of pulsatile blood motion are prevalent in the aorta and major arteries; however, they are encountered down to the level of the arterioles and even in capillaries where residual pulsations have been recorded. The pressure driven

oscillatory motion of blood may cause transient flow reversal and radial vessel dilatation, depending on the thickness and elasticity of the vessel wall.

Both abnormally increased flow with high shear and the reduced flow with stasis predispose to mural thrombosis, and the structures of blood clots formed are varied at different shear conditions. In the arterial system, especially at a vessel bifurcation or an aortic stenosis, blood experiences high flow velocities and thus high shear forces, even a potential for turbulent flow. Once endothelial injury or dysfunction induces thrombus development, the generation of even a modestly sized thrombus mechanically encroaching on the vascular lumen perturbs the laminar flow pattern, complex and time-dependent flow patterns then emerge, and local shear forces may increase significantly. As a result, shear-dependent platelet activation and deposition are promoted, and interactions between platelets and the vessel wall increase because of increased collisions resulting from local vortex or spiral flow patterns. Typically, the thrombi developed under these arterial conditions are relatively platelet-rich (so-called "white" thrombi). In the venous system, thrombi develop primarily in the states of relatively low flow and stasis. Most venous thrombi begin as platelet nidi in the valve cusps of deep calf veins, and then tissue thromboplastin is released, initiating coagulation cascades and forming fibrin networks that trap red blood cells. Reduced flow limits the dilution of procoagulant and proaggregatory substances, thereby further facilitating this process. The typical vein thrombi are rich in fibrin and red blood cells (so-called "red" thrombi).

**Blood Components**

Blood is a rather complex fluid, containing a large variety of plasma proteins and a number of blood cells. The rheological properties of blood are strongly dependent on those blood components. Increases in blood viscosity can be due to increased hematocrit (red blood cell counts), loss of red blood cell deformability, or increased concentrations of certain plasma proteins, such as fibrinogen and immunoglobulins. Increased blood viscosity often tends to reduce the blood flow, and it will also increase shear stresses to the endothelium at any given shear rate. The contribution of blood rheology as a prediction of some pathological states has been increasingly recognized in recent years [24].

Platelets, also called thrombocytes, play a vital role in the prevention of blood loss. They form a temporary plug that covers the break in the endothelial lining. Once the plug is formed, the platelet membrane provides a phospholipid surface on which the activated coagulation proteins bind and form a stable fibrin clot. Platelet disorders may cause defective formation of hemostatic plugs and bleeding because of decreased function despite adequate platelet numbers (platelet dysfunction) or because of decreased platelet counts (thrombocytopenia). The Bernard-Soulier syndrome is a rare disorder in which a platelet surface membrane glycoprotein GpIb, a receptor for vWf, is missing or not functional. Unusually large platelets are found in this disease, and they do not agglutinate with ristocetin but aggregate normally with the physiologic aggregating agents adenosine diphosphate (ADP), collagen, and epinephrine. Persons with

Glanzmann thrombasthenia may experience severe mucosal bleeding. Their platelets fail to bind fibrinogen during activation and thus fail to aggregate because of qualitative or quantitative abnormalities of the platelet surface membrane glycoprotein GpIIb and/or GpIIIa. Drugs may also induce platelet dysfunction. For example, aspirin irreversibly inactivates the enzyme cyclooxygenase, thereby suppressing platelet synthesis of thromboxane $A_2$ ($TXA_2$), a labile inducer of platelet aggregation and a potent vasoconstrictor. Thrombocytopenia may stem from failure of platelet production, sequestration of platelets in an enlarged spleen, increased platelet destruction and utilization, or dilution of platelets with massive transfusion. About 5% of those receiving heparin may develop heparin-induced thrombocytopenia. This is the most important of the thrombocytopenias resulting from drug-related antibodies. Heparin appears to alter the platelet surface, facilitating the binding of antibody to platelet antigens and antigen-antibody complexes to platelet Fc receptors, thus enhancing platelet destruction.

Besides platelet disorders, hemorrhagic diseases may result from abnormalities of plasma coagulation factors. Hemophilia A (classic hemophilia, factor VIII deficiency) and hemophilia B (Christmas disease, factor IX deficiency) are the most common bleeding disorders due to hereditary clotting factor deficiencies. Both types of hemophilia are inherited as sex-linked recessive disorders occurring almost solely in males. Disseminated intravascular coagulation (DIC) is the term commonly used for the generation of fibrin in the circulating blood. In most instances, the intravascular generation of substantial amounts of thrombin via the extrinsic or intrinsic coagulation

cascades, combined with the failure of the natural anticoagulant mechanisms to neutralize thrombin, initiates DIC. The widespread deposition of fibrin causes tissue ischemia from occlusive microthrombi and consumption of essential hemostatic components such as platelets, fibrinogen, prothrombin, and factors V and VIII, all of which may, in turn, lead to bleeding.

The von Willebrand disease is the most common hereditary hemorrhagic disease. It results from a quantitative (type I) or qualitative (type II variants) abnormality of vWf or its platelet receptor GpIb. Both endothelial cells and megakaryocytes, from which blood platelets are derived, can synthesize vWf. Purified vWf preparations from plasma are polydisperse, with molecular weights ranging from 500,000 to at least 20,000,000 Daltons. Newly synthesized vWf by endothelial cells is constitutively released to the plasma and to the abluminal surface of the endothelial cell. However, stored vWf in the Weibel-Palade bodies can be induced to secrete, primarily to the abluminal surface by the agonist stimulation [25,26]. The platelet vWf is located primarily in the $\alpha$ granules and can be released or induced to be expressed on the surface after platelet activation [27,28]. vWf is a large multivalent adhesive protein that plays an important role in platelet attachment to subendothelium, platelet spreading, and in platelet-platelet interaction (aggregation) at sites of vessel wall injury, especially at moderate to high shear forces. The vWf multimers of all sizes form complexes with clotting factor VIII in plasma and the formation of such complexes is required to maintain normal plasma factor VIII levels.

**Vessel Walls**

The endothelium, a monolayer of cells that lines blood vessels and the heart, normally maintains a surface resistant to thrombosis. Normal endothelium synthesizes and releases prostacyclin (prostaglandin $I_2$), which inhibits platelet activation by increasing cyclic AMP. It also produces endothelium derived relaxing factor (EDRF) or nitric oxide (NO), which inhibits platelet activation by increasing cyclic GMP. Under normal circumstances, the endothelium facilitates vascular uptake and degradation of prothrombotic vasoactive amines such as serotonin. This cell layer can bind, inactivate, and cleave thrombin. In addition, it expresses thrombomodulin on the surface that facilitates thrombin-dependent activation of the naturally occurring anticoagulant protein C. Plasminogen activators are also synthesized by the endothelium. On stimulation by a variety of physiologically relevant agonists, these profibrinolytic molecules are released and bind to their respective endothelial surface receptors, where the catalytic efficiency of plasminogen activation is enhanced.

Endothelial injury or dysfunction brings about a variety of acute or chronic pathologic states. In addition to the direct loss of their normal, protective antithrombotic mechanisms, dysfunctional endothelial cells also manifest prothrombotic properties. Endothelial cells express tissue factor when exposed to endotoxin, interleukin-1, or tissue necrosis factor, and activate the coagulation cascades as the result. On exposure to thrombin, they can synthesize and secrete vWf and plasminogen activator inhibitor-1. Endothelial denudation can also promote thrombosis by the exposure of platelet-reactive

components in the subendothelium. The depth of injury probably controls the platelet responses, with deeper damage exposing more platelet-reactive materials and tissue factor. The blood vessel wall consists of three layers: the intima, media, and adventitia. The intima is the innermost layer and contains the endothelial cells. Normal subendothelium has vWf, collagen types IV, V, and VI, fibronectin, vitronectin, thrombospondin, laminin, fibrinogen (fibrin), and trace amounts of tissue factor. Media, the middle layer of a blood vessel wall, contains the smooth muscle cells and collagen types I and III. The adventitia is the outermost layer and has mainly collagen types I and III and tissue factor [29].

Many studies on platelet adhesion to extracellular matrix proteins have been done [30-37]. On fibrinogen-, fibrin-, or vWf-coated surfaces, adherent platelets are basically non-overlapping or a few small platelet aggregates are formed. In contrast, platelets adhere to the immobilized type I fibrillar collagen with high turnover rates at the initial stage, and these adherent platelets serve as the "seeds" for incoming platelets to form multiplatelet thrombi. Unlike collagen I surfaces on which larger thrombi form at higher shear rates, collagen VI surfaces appear more reactive to platelets at low shear rates but are not capable of supporting mural platelet adhesion and subsequent aggregation at high shear rates [32]. The thrombogenic roles of different types of collagen in the vessel wall may vary, depending on the extent of damage to the blood vessel. The extracellular matrix of cultured cells from vessel walls has been used as a model of the vessel wall [38,39]. The platelet deposition on the endothelial cell matrix is uniform and consists of

single and spreading platelets. The deposition rate is strongly dependent on the wall shear rate, with increasing adhesion up to a shear rate of 800 $sec^{-1}$ and leveling off above this shear rate. The platelet deposition to the fibroblast matrix is in general more patchy than on the endothelial cell matrix, consisting of single platelets as well as small aggregates. On the matrix derived from smooth muscle cells, platelets show decreased adhesion compared to the endothelial cell matrix, and there is a lack of spreading of the platelets.

When blood comes in contact with a foreign surface such as an implanted artificial device, protein adsorption occurs within seconds and precedes the deposition of blood cells. Because a layer of plasma proteins is laid down on the surface in contact with blood before platelets arrive, differences in the platelet reactivity with the surface must result from variations in the nature of the protein-surface interactions. These interactions may vary in terms of which proteins bind to the surface, the amounts bound, and the various changes in protein conformation induced by surface contact.

## 1.2 Protocols for Studying Thrombosis under Flow Conditions

According to Virchow's paradigm, blood flow, blood components, and the vessel wall are intertwined in causing thrombosis. To identify these mechanisms and their interactions, the dynamics of the vascular system must be incorporated into experimental models. Engineering principles have been used to design model systems that simulate flowing conditions physiologically relevant to the vascular system. These protocols can

generate controlled mechanical forces *in vitro* for study, similar to hemodynamic forces produced *in vivo* [40].

**Turbidometric Platelet Aggregometry**

The turbidometric platelet aggregometry is one of the early experimental systems developed for the clinical evaluation of platelet functions. It is performed in a modified spectrophotometer, termed an aggregometer, to monitor the light transmittance of stirred platelet-rich plasma (PRP) over time. Agonists such as ADP, collagen, thrombin, and epinephrine that induce platelet aggregation are added to PRP, and the rate or extent of the increase in light transmittance is used as an index of the platelet aggregation. Agitation is required for platelet aggregation to occur in this system, so it can be described as shear-dependent. However, the shear forces in the aggregometer are usually generated by a stir bar with variable flow patterns and are thus hard to quantify. This technique is insensitive to the formation of small platelet aggregates and therefore does not record the early stages of aggregation, where other methods such as the single platelet counting in the flow cytometry have an advantage. Because the turbidometric platelet aggregometry is based on optical transmittance, it cannot be used to measure platelet aggregation in whole blood.

The tracings recorded during platelet aggregation in an aggregometer vary due to the nature and concentration of the agonists used. These differences indicate that the platelet activation by various soluble agonists goes through different signal transduction

pathways. Instead of conventionally used soluble agonists, some alternative methods have been developed to study the responses of platelets to immobilized agonists by using protein-coated microbeads [41-43].

**Cone-and-Plate Viscometer**

In order to understand cellular responses to shear forces, the exact features of the hemodynamic environment need to be quantitatively defined. Some devices designed with well-defined flow patterns, originally for measuring the viscosity of fluids, have been adapted to study thrombosis under shear conditions. The cone-and-plate device, consisting of a rotating cone and a stationary plate, generates a nearly constant shear rate throughout the gap for small cone angles (commercial cone-and-plate viscometers usually range from 0.5 to 8 degrees). The shear stress that suspended particles experience depends on the cone angle, the rotation rate, and the fluid viscosity. The flow profile in this device is well characterized and can be varied widely to match a number of physiologic and pathologic vascular conditions.

The cone-and-plate viscometer provides researchers with a reliable *in vitro* system to apply shear stresses to cell suspensions for the analysis of bulk phase platelet responses. This device is used to study the mechanisms of platelet responses to shear stresses and to explore the physiologic or pathologic significance of the shear-induced platelet activation and aggregation. Besides platelet-rich plasma and washed platelet suspensions, whole blood can also be used in this system to investigate different aspects

of thrombosis, with a situation that reflects more closely the physiologic status of platelets circulating *in vivo* [21,44,45]. The cone-and-plate device can be modified optically to simultaneously measure platelet aggregation and $[Ca^{2+}]_i$ [19,20,46-48]. It can also be used to study blood cell and surface interactions by employing immobilized vascular cells or subendothelial matrix proteins on the stationary plate [49,50].

**Couette System**

Another rotational device that has been adapted to investigate the effects of physical forces on thrombosis is the Couette type, using flow between two coaxial cylinders [51,52]. The cell suspension to be studied fills the annular space between the cylinders, and rotating the outer, the inner, or both cylinders can generate controlled shear forces on cells. The shear rate is not constant across the gap, but the variation is small if the gap/cylinder radius ratio is small.

**Parallel-Plate Flow Chambers**

In addition to the cone-and-plate viscometer, engineering designed flow chambers are also useful devices that generate controlled shear environments *in vitro*. The parallel-plate flow chamber is the most widely used instrument for studying the cell and surface interactions [38,53,54]. A common parallel-plate flow chamber consists of a rectangular polycarbonate distributor, a silicon gasket, and a glass slide. The distributor, forming one side of the parallel-plate flow chamber, includes inlet port, outlet port, and vacuum slot.

The thickness of the gasket determines the height of the flow chamber. The glass coverslip forms the bottom side of the parallel-plate flow chamber, and proteins or vascular cells may be immobilized on this surface. A vacuum forms a seal to hold these three parts and ensures a uniform channel height. Blood or cell suspensions are drawn from a reservoir through the flow chamber by a syringe pump, providing a well characterized and controlled fluid dynamic environment. The shear rate generated at the surface of the flow chamber can cover the full range of physiologic interest. The parallel-plate flow chamber may be mounted on an inverted-stage microscope connected to a video camera to perform the real-time, local visualization.

The flow in a parallel-plate flow chamber mimics the hemodynamic patterns in blood vessels more closely than that in an aggregometer or a viscometer. To investigate platelet-mediated events in mural thrombosis, whole blood is generally perfused through the chamber with the glass coverslip coated with thrombogenic components of the subendothelial matrix, such as vWf and collagen. The platelet deposition over time can be determined by the combination of the epifluorescence video microscopy and the digital image processing. The interactions between fluorescent labeled platelets and the protein-coated surface can be recorded on videotape. The video recording then is analyzed off-line using digital image processing to obtain quantitative values for the total surface coverage and the number of deposited platelets over time. Distinct pathways in mural thrombosis are usually studied by adding specific blocking antibodies or by using patient blood deficient in a particular component [31,37,55-57]. Many important insights

into the molecular mechanisms supporting the thrombotic process have been gained in this way. Specific interactions between a platelet receptor of interest and its immobilized ligand may also be examined by using mammalian cells transfected with this receptor and the glass slide coated with the particular protein [58-60].

Based on the parallel-plate flow chamber design, many modifications have been employed for different applications. Parallel-plate flow chambers constructed with an eccentric stenosis are used to quantify the effects of stenosis-related disturbances on thrombus formation in native blood and to compare these influences with the local fluid dynamics [61-65]. The linear-shear-stress or tapered parallel-plate flow chamber, with different gasket geometry, has been designed to generate a linear variation of shear stresses within the same flow field without changing the flow rate or the gap height [66]. A side-view chamber has been developed to permit observations from the side of the cell that contacts with the adhesive surface under dynamic flow conditions [67]. Besides the rectangular geometry of the parallel-plate flow chamber, tubular and annular flow chambers have also been used to study mural thrombosis *in vitro* [68,69].

## 1.3 Current Understandings of Mural Thrombosis

Both chemical and physical factors can influence the activity of platelets and coagulation factors responsible for the thrombus formation in the vicinity of an injured vessel wall. Studies performed in controlled shear devices have indicated that flow patterns, blood components, and surface reactions are mutually involved in affecting the

blood clot forming process. The current understanding of these thrombogenic determinants and their intertwined relationships are summarized and discussed in the following.

There are several steps involved in blood clot formation. First, thrombogenic surfaces, such as the damaged vessel wall or implanted artificial materials, are exposed to the circulating blood. Platelets and plasma coagulation factors are transported to and contact with the surfaces. This process is highly dependent on not only the flow patterns but also the concentration of red blood cells. High blood flow rates increase the mass transport of platelets and coagulation factors, and platelets may be activated by high shear stresses. In addition, at the low flow regions with lengthened residence times, such as a vortex and a stagnant point occurring at a sudden expanded flow channel, thrombogenic components can accumulate and form blood clots. The presence of red blood cells in flowing blood enhances the effective diffusivities of platelets and large molecular weight plasma proteins [70-74], and it is responsible for the near-wall excess of platelets [2-4,6,7]. Red blood cells may also contribute to activate platelets by releasing ADP [45,75]. After platelets contact with the thrombogenic surface, the platelet receptors interact with their ligands and result in the platelet firm adhesion. Under arterial conditions, this reaction is usually initiated by the GpIb-IX-V and vWf binding to tether platelets, and integrin molecules such as GpIIb-IIIa and GpIa-IIa then bind to adhesive proteins such as fibrinogen, vWf, and collagen to stabilize the adhesion. Moreover, adherent platelets will spread out on the surface and release granule contents that can activate other platelets in

the vicinity and promote coagulation cascades. Finally, the activated platelet GpIIb-IIIa receptors with high affinity can bind soluble fibrinogen and vWf molecules in the plasma, and nearby flowing platelets that may have been activated by released agonists can aggregate on top of those adherent platelets to form thrombi. A platelet plug formed on the thrombogenic surface is only temporary. Coagulation proteins then take up their role to ensure hemostasis by forming a stable fibrin clot.

The chemical mediators for mural thrombosis are different in various flow environments. Under high shear conditions, vWf involves in both the initial platelet adhesion to the thrombogenic surface and the subsequent platelet aggregation. In addition to vWf directly secreted into the subendothelium by endothelial cells, vWf in plasma can rapidly bind on thrombogenic components of the exposed subendothelium, such as collagen. The vWf molecule is well suited to support the platelet adhesion because a single platelet can form multiple bonds to the repeating subunits within this multimeric protein. Platelets have two distinct receptors for vWf, GpIb-IX-V and GpIIb-IIIa. The GpIb-IX-V is involved in the establishment of the initial contact between platelets and immobilized vWf as well as the generation of activation signals [19,20,76-79]. The GpIIb-IIIa can bind vWf after platelet activation, mediating the spreading of platelets on the surface and the aggregation [31,80,81]. In contrast to the thrombus formation at high shear conditions, fibrinogen rather than vWf is the principal mediator of mural thrombosis under low shear conditions, and this event mainly depends on GpIIb-IIIa receptors. In addition to fibrinogen, other adhesive proteins such as collagen,

fibronectin, and vitronectin whose interactions with their platelet integrin receptors are strong enough to resist the low shear forces can support the platelet adhesion at low shear conditions. Platelets are able to adhere to fibrinogen-coated surfaces under moderate wall shear rates mediated by the interaction between GpIIb-IIIa and the fibrinogen sequence at the carboxyl-terminus of the gamma chain, and this interaction is independent of platelet activation [33]. Fibrinogen has also been found on the surface of vascular endothelium and in atherosclerotic plaques, and it deposits on vascular prostheses [82-85]. Due to the great excess of fibrinogen over vWf in the plasma (~3,000 μg/ml and ~10 μg/ml respectively), fibrinogen is the relevant physiologic ligand likely to occupy the GpIIb-IIIa receptor. Therefore, vWf and fibrinogen perform physiologically important roles at high and low shear conditions respectively.

In addition to the chemical composition of the thrombogenic surface and platelet surface receptors, the shear dependency of mural thrombosis is related to the magnitude of the shear stress, the duration of the applied physical force, and the local geometry. It has been well established that at physiological shear conditions, the increase in the local shear rate enhances the rate of attachment of platelets to the vessel wall and the rate of growth of thrombi. In contrast, increases in local shear conditions inhibit the formation of fibrin networks on surfaces where the tissue factor is exposed. At the apex of severely stenosed vessels, platelet aggregate formation is dependent on the duration of the exposure time and the thrombogenic properties of the surface. In an *in vitro* well-defined stenosis model, collagen-induced thrombus formation at the apex is extensive, and

reduced thrombus growth at the most occlusive stenosis is probably due to the high shear stresses and short exposure times that reduce the rate of the platelet incorporation in to the thrombus [62,63]. On the other hand, in a stenosis model with non-thrombogenic Lexan artificial surfaces, platelets deposit on the proximal and distal regions to the stenosis apex, where the convective transport of platelets is enhanced because of velocity components perpendicular to the wall or the residence time of platelets is greatly lengthened due to vortex formation [64,65]. The shear dependency of the thrombus formation can affect antithrombotic drug efficacy. For example, anticoagulant effects may be more pronounced on a tissue factor-rich surface than on a collagen-rich surface, particularly at venous or low arterial shear rates, whereas inhibitors of vWf-platelet interactions are more efficient at high shear rates. Therefore, the insights about how blood flow patterns, blood components, and surface reactions are intertwined in mural thrombosis can help in developing more effective drugs and therapeutic strategies.

## 1.4 Thesis Overview

Mural thrombosis is a complicated dynamic process that involves blood flows, blood components, and surface reactions. Because of its complexity, some fundamental mechanisms of this blood clotting process are still difficult to resolve, and there are many apparently contradicting experimental observations. The work presented in this thesis has three key objectives, each of which contributes to the understanding of flow effects and platelet-surface interactions in mural thrombosis.

The near-wall excess of platelets is an important feature in blood transport, but the basic mechanisms and mathematical considerations of this phenomenon have not been completely understood despite considerable work. In Chapter 2, I propose a mathematical model that simulates steady-state cell distributions and velocity profiles in a parallel-plate flow chamber. Based on a constitutive equation that accounts for the lateral motions of red blood cells by collision and viscosity effects, this mathematical model is able to predict the red blood cell distributions under different shear rates and average hematocrits. The simulated blood velocity profiles show the characteristics of a non-Newtonian fluid. The platelet drift velocity toward the wall resulting from the plasma counter flow is calculated directly from the concentration profiles of red blood cells, and higher wall concentrations of platelets are predicted at higher shear rates and larger hematocrits, as these phenomena have been observed experimentally.

Various platelet deposition patterns on different extracellular matrix protein surfaces have been shown in the *in vitro* flow chamber experiments. However, the current belief that platelet-vWf interaction induces the activation of GpIIb-IIIa receptors, which then mediate platelet aggregation, has difficulty explaining why the platelets adhere separately but not form aggregates on a vWf-coated surface. In order to measure platelet activation status after platelets interact with different immobilized proteins, I develop a novel flow cytometric analysis, incorporating the protein-coated microspheres, and present it in Chapter 3. Platelets adhering on immobilized fibrillar collagen express a greater percentage of activated GpIIb-IIIa receptors and more P-selectin than those on

vWf- and soluble collagen-coated microspheres do. This finding can explain why platelets form aggregates on fibrillar collagen-coated surfaces but adhere separately on vWf-coated surfaces in flow chamber experiments. In addition, this result indicates that the structures of immobilized collagen affect the thromogenicity of the surfaces. Further studies using this novel flow cytometric method reveal that the $Ca^{2+}$ released from intracellular pools is involved in the signal transduction pathway that leads to the conformation change of GpIIb-IIIa and the surface expression of P-selectin after platelets interact with collagen.

Because the binding between GpIb-IX-V and immobilized vWf plays an important role in the initial stage of the platelet tethering and deposition unto a thrombogenic surface, especially at high shear conditions, this interaction was investigated by using a viscometric-flow cytometric method in Chapter 4. This viscometric-flow cytometric protocol was originally designed to study receptor-ligand binding forces, but an unexpected binding behavior between the platelet receptor GpIb-IX-V and immobilized vWf at high shear conditions was observed. Instead of less effective platelet adhesion at high shear conditions resulting from shorter contacting times and stronger forces on receptor-ligand bonds, the platelet association via GpIb-IX-V to microspheres with high vWf coating density was enhanced as the shear rate increased. I have examined some possible mechanisms that may cause this phenomenon. However, this enhancement does not result from shear-induced platelet activation in

suspensions, the platelet cytoskeletal rearrangement by calpains, or secondary flows in the cone-and-plate viscometer at high shear rates.

Finally, several suggestions for the extension of this work are presented in Chapter 5.

# Chapter 2

## A Predictive Model for Blood Cell Distributions under Shear Conditions

The life-supporting function of blood is to transport materials to or from the tissue cells, to prevent fluid loss by healing wounds, and to act as the primary carrier for immune surveillance. Blood delivers oxygen, hormones, nutrients, and minerals to tissues and picks up cellular waste products. Platelets and coagulation factors in blood play a vital role in hemostasis, the prevention of fluid loss through processes that inhibit the blood flow from a ruptured vessel. The immune system protects the body from microorganisms and foreign substances by attacking them and rendering them harmless, mainly through blood white cells, antibodies and complement proteins in the blood. All these processes involve mass transport. If there is an abnormal regulation of the mass transport, it may augment pathologic states such as thrombosis, atherosclerosis, and infection.

Some cardiovascular diseases occur in predisposed areas in the vascular system due to local shear forces and mass transport problems. Atherosclerosis is a chronic disease attributed to risk factors that are systemic in nature, yet the lesions involved do not occur in random fashion. The atherosclerotic plaques are preferentially located at the outer walls of vessel bifurcations and the points of blood flow separation, recirculation and stasis. These areas have been identified with low shear stresses and longer residence

times, which stimulate the endothelial atherogenic phenotype and accumulate atherogenic cholesterol and leukocytes. In coronary thrombosis, the majority of coronary thrombi are precipitated by a sudden rupture of the surface of an atherosclerotic plaque, causing platelets to deposit on the thrombogenic subendothelial tissue that has been exposed. The risk of occlusive thrombosis increases with increasing degree of preexisting stenoses, and the high blood velocity within the stenosis is responsible for this association by activating and delivering more platelets locally. As the thrombus forms within the stenosis, its freely floating tail progressively grows downstream where flow separation, recirculation, and turbulence take place, an area prone to platelet aggregation. Therefore, hydrodynamic forces and the mass transport in blood influence the pathogenesis of many cardiovascular diseases.

The mass transport in blood becomes more complicated than that in a simple fluid because blood contains particulate elements. Red blood cells are about 40%-50% of the total volume of whole blood, thus strongly influencing the transport properties of the blood. The viscosity of blood, for example, increases nonlinearly with increasing the volume percentage of red blood cells (hematocrit) in the blood. The large rise in the blood viscosity as the shear rate decreases is believed to result from formation of "rouleaux," the aggregates of red blood cells, under low shear conditions. Platelets, which play an important role in the processes of blood coagulation and clotting, are not uniformly distributed in the blood stream. An excess of platelets near the vessel wall may provide quick hemostatic responses to the injury of the vessel wall. The phenomena

and mechanisms of mass transport in a particulate fluid are not well understood. This chapter will focus on the theoretical considerations of mass transport for blood cells in flowing blood and implement a predictive mathematical model for blood cell distributions under shear conditions.

## 2.1 Background

Red blood cells play an important role in mural thrombosis even though the primary function of them is considered to be the transport of oxygen. For the most part, this thrombogenic role is probably physical, but a biochemical effect has also been proposed [45,75]. The physical effect is manifested in two ways. The presence of red blood cells in flowing blood enhances the effective diffusivities of platelets and large molecular weight species [70-74]; it is also responsible for the non-uniform radial distribution of platelets across the blood vessel [2-4,6,7]. Moreover, flowing blood behaves as a non-Newtonian fluid with a non-parabolic and blunt velocity profile, mainly because of the presence of red blood cells [86]. Therefore, the transport of platelets to the vessel wall is complicated, and the results obtained from mathematical models using classical transport theory often fail to agree with the experimental observations [53,87].

When mass transport theory is applied to platelets in flowing blood, the blood is usually considered to be a fluid with platelet and red blood cell wall concentrations similar to the average concentration of a flow channel, but this assumption is not true. Several groups have observed concentration profiles with near-wall excesses of platelets

or of platelet-sized latex beads. Using epifluorescence video microscopy alone or combined with the freeze-capture method, Eckstein's group demonstrated the effects of wall shear rates and hematocrits on the number of platelet-sized beads near the surface [3-5]. In general, the large near-wall excess of platelets occurred only for elevated wall shear rates and for significant levels of hematocrit. At 15% hematocrit, they observed that near-wall excesses were large only for wall shear rates of 430 $sec^{-1}$ and above. In addition, while a slight effect was seen for 7% hematocrit, a significant effect appeared for 15% and 30%. This group also investigated the effects of other parameters such as bead size, channel height, suspending fluid viscosity, and red blood cell deformability, on the occurrence of the near-wall excess of platelet analogues [5]. Sixma's group studied platelet and red blood cell distributions in flowing blood for various hematocrits and shear rates using the laser-Doppler technique [6]. Their data were qualitatively similar to those observed by Eckstein's group. The results showed that red blood cell ghosts were crowded near the axis of the tube, with a local hematocrit higher than the average tube hematocrit, and their concentrations decreased steadily toward the wall. In the presence of red blood cell ghosts, the platelets were expelled toward the wall region; and this high concentration at the wall increased with larger average tube hematocrits and higher wall shear rates.

Why blood cells move perpendicular to the flow direction and distribute non-uniformly is not yet completely known. The collisions between platelets and red blood cells may cause a preferred platelet convective flux toward the wall. Eckstein and

coworkers have tried to explain their experimental results in terms of the biased random walk model [3]. That is, the probabilities describing the turns of the random walk due to particle collisions in the flow are altered so that the outcomes for motion are not the same in all directions. It seems reasonable to expect the probabilities describing the lateral displacement of a relatively rigid platelet after colliding with a deformable red blood cell to be unequal because of the difference in cell rigidities and the shear-induced transitions of red blood cell orientations [88]. In fact, rigid particles interacting in dilute suspensions show little or no net motion across streamlines, while flexible particles have directed lateral movements. In addition, the red blood cells in dilute suspensions are known to deform and become aligned with the flow at higher shear rates, and the microenvironments in the suspensions are not random any more. The major effect of using random walk biased to account for non-uniform interactions among the platelets and red blood cells is that the lateral platelet motion is no longer purely diffusive but has a convective nature.

Later in the studies of Eckstein's group, they added a drift term (a lateral velocity) to the convective diffusion equation for the platelet transport so that the near-wall excesses of platelets could be simulated [89,90]. A mathematical relationship between the drift and the fully developed, steady-state platelet concentration profile was also shown. This approach was used to determine the platelet distribution in the developing region of a tube flow. In addition, their numerical simulations with the stochastic differential equations that were equivalent to the convective diffusion transport equation with a

surface reaction boundary condition could illustrate the transient platelet concentration profiles and the platelet deposition in a tube flow. However, the arguments of this paper had a circular nature: a drift function was determined from the experimental estimate of a fully developed concentration profile to calculate a concentration profile. To avoid this problem, it is better to estimate the drift velocity in a straightforward way from the fundamental transport mechanisms.

As mentioned earlier, red blood cells are dominant in determining the transport phenomena of the blood because of their large volume percentage and effects on blood viscosity. In contrast, platelets comprise only about 0.1% of the total volume of whole blood and are significantly smaller in size than red blood cells. Therefore, in order to simulate the near-wall excess of platelets, the transport of red blood cells needs to be solved first. In this study, I propose a mathematical model that uses a constitutive equation for concentrated suspensions, accounting for shear-induced migration and viscosity-induced resistance, to determine the red blood cell distribution in a parallel-plate flow chamber and then calculate the platelet distribution. Red blood cells are predicted to move laterally to the center of the flow channel, and the plasma flows in an opposite direction so that the mass balance is maintained. As a result, this plasma flow causes platelets to move toward the wall. This mathematical model is able to describe at least qualitatively the experimental observations that have been presented in the literature.

## 2.2 Model Development

There is a wide array of potentially important types of interparticle interactions in concentrated suspensions such as blood. These include hydrodynamic, electrostatic, and other surface interactions. Dynamic simulations of such many-particle systems that account rigorously for all these effects would be too computationally expensive to be applied to the real situation that is usually more complex than the ideal model system. Therefore, a constitutive model that is based on the essential physics of the suspension but is simple enough to be used in flow simulations would be very helpful. For this purpose, Leighton and Acrivos have proposed such a mechanism for the particle migration in non-homogeneous shear flows [91,92]. Their explanation is based on the spatially varying effects of an interparticle interaction frequency and an effective viscosity. Later, Phillips et al. used a modified version of Leighton and Acrivos' flux expressions to develop a diffusion equation that described the evolution of particle concentration profiles over time [93]. Their simulation results agreed remarkably well with the measurements for both transient and steady state experiments in a Couette apparatus. Based on the constitutive equation for concentrated suspensions that Phillips et al. developed and the formulation of viscosity that was derived by Quemada [94-96] and was correlated with the blood data by Cokelet [97], I developed a mathematical model that can predict red blood cell distributions and velocity profiles for steady flows in a parallel-plate flow chamber.

**Red blood cell distribution and velocity profile**

Like traditional mass transport problems, the analyses of velocities (v) and red blood cell concentrations (ϕ) in a parallel-plate flow chamber require solutions of the equation of continuity

$$\frac{D\rho}{Dt} = -\rho(\nabla \cdot v),$$

the equation of motion,

$$\rho\frac{Dv}{Dt} = -\nabla P - \nabla \cdot \tau,$$

and the mass transport equation of red blood cells

$$\frac{D\phi}{Dt} = -\nabla \cdot (N_\eta + N_c + N_b).$$

In these equations, $D/Dt \equiv \partial/\partial t + v \cdot \nabla$ is the substantial time derivative. The blood density ρ is assumed to be constant because blood is incompressible in physiological conditions. The blood pressure gradient $\nabla P$ is the driving force for the blood flow. To describe the stress tensor term $\tau = -\eta(\phi,\gamma)\cdot\gamma$, the blood viscosity $\eta(\phi,\gamma)$ that depends on the local hematocrit $\phi$ and the shear rate $\gamma$ is used.

The core of the red blood cell transport is based upon the effects of two-body, irreversible interactions, as Leighton and Acrivos have suggested [91,92]. The mass flux of red blood cells can be separated as $N_b$, $N_c$, and $N_\eta$. $N_b$ accounts for the Brownian diffusion of red blood cells and is negligible compared to the convective flux. $N_c$ describes the irreversible cell movement from the original streamline because a red blood cell that experiences a higher frequency of collisions from one direction than from the opposite direction will migrate normal to its shearing surface and in the direction of the

lower collision frequency (Figure 2.1(a)). The number of collisions experienced by a red blood cell will scale as $\gamma\phi$, and the variation in the collision frequency over a distance in the order of a cell radius $a$ (O($a$)) is then given by $a\nabla(\phi\gamma)$. Assuming that the cell migration velocity is linear proportional to this variation in the collision frequency and the displacement of O($a$) given rise by each of these two-body interactions, the flux $N_c$ due to the spatially varying collision frequency can be expressed as

$$N_c = -K_c \cdot \phi \cdot a \cdot a\nabla(\phi\gamma) = -K_c a^2(\phi^2\nabla\gamma + \phi\gamma\nabla\phi),$$

where $K_c$ is an adjustable constant that may be determined from experimental data.

Besides the mass flux is caused by the varying collision frequency, the interaction between two red blood cells is possibly affected by the spatially varying viscosity resulting from the existence of red blood cell concentration gradients. Based on Leighton and Acrivos' reasoning, a quantitative flux expression of this effect is derived. A gradient in viscosity results in resistances to motion so that two touching cells in a shear field will no longer rotate about their center of mass and the cells will be displaced during an interaction from regions of high to low viscosity (Figure 2.1(b)). The drift velocity is assumed to be proportional to the change in viscosity over a distance of O($a$) relative to the overall magnitude of the viscosity, $(a/\eta)\nabla\eta$. If the collision frequency scales as $\gamma\phi$ and each interaction leads to a displacement of O($a$), the flux $N_\eta$ due to the spatially varying viscosity can be expressed as

$$N_\eta = -K_\eta \cdot \phi \cdot a\phi\gamma \cdot a\frac{\nabla\eta}{\eta} = -K_\eta a^2\phi^2\gamma\frac{d\eta}{\eta d\phi}\nabla\phi,$$

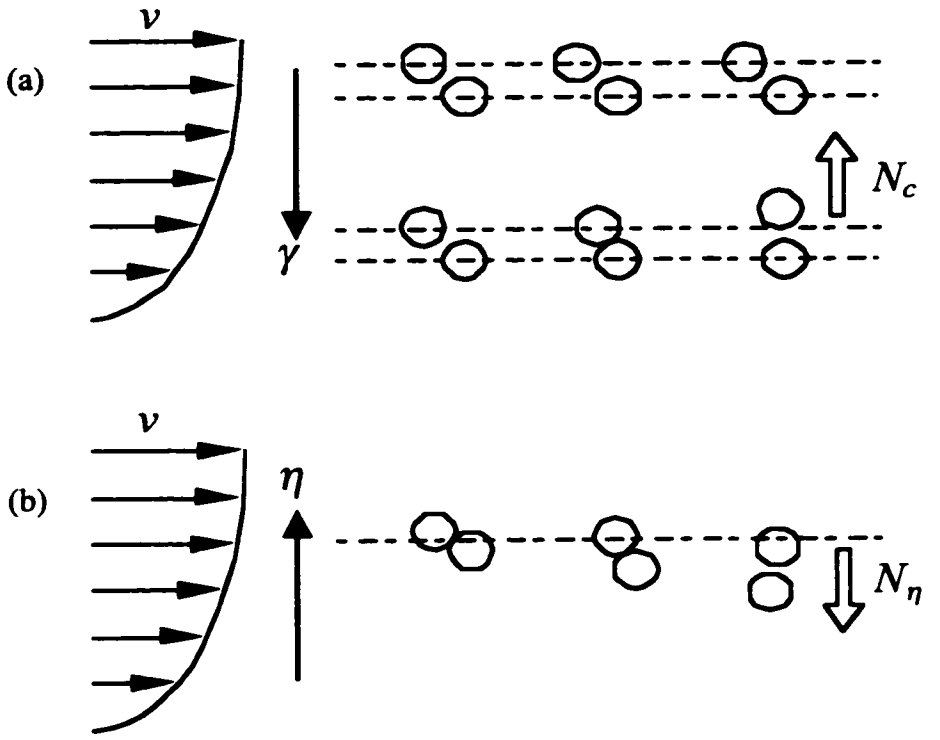


Figure 2.1 Schematic diagrams of irreversible, two-body collisions with (a) spatially varying shear rate γ and (b) spatially varying viscosity η.

where $K_\eta$ is an adjustable constant that needs to be determined from experimental data. As a result, the mass transport equation of red blood cells can be written as

$$\frac{D\phi}{Dt} = a^2 K_c \nabla \cdot (\phi^2 \nabla \gamma + \phi\gamma \nabla \phi) + a^2 K_\eta \nabla \cdot (\phi^2 \gamma \frac{d\eta}{\eta d\phi} \nabla \phi).$$

In this study, a parallel-platelet flow chamber with the height of $2B$ is used as a model system. Assuming the blood density is constant and the system has reached the steady state, the above equations can be simplified as

$$-\frac{dP}{dx} - \frac{d\tau}{dy} = 0, \text{ and} \tag{1}$$

$$K_c \frac{d}{dy}(\phi^2 \frac{d\gamma}{dy} + \phi\gamma \frac{d\phi}{dy}) + K_\eta \frac{d}{dy}(\phi^2 \gamma \frac{d\eta}{\eta dy}) = 0, \tag{2}$$

where $x$-axis indicates the flow direction and $y$ is the distance perpendicular to the flow from the center plane.

This model system is symmetric to the center plane of the flow chamber so the half of the system $y=[0,B]$ can be solved with symmetric boundary conditions at $y=0$; that is, there is no variation in velocity and hematocrit. In addition, there is no velocity slip on the wall ($y=B$) and the wall is impermeable and non-reactive. Therefore, the boundary conditions are

at $y=B$, $v=0$, and (B1)

$$K_c(\phi^2\frac{d\gamma}{dy}+\phi\gamma\frac{d\phi}{dy})+K_\eta(\phi^2\gamma\frac{d\eta}{\eta dy})=0; \quad \text{(B2)}$$

at $y=0$, $\frac{dv}{dy}=\gamma=0$, and (B3)

$$\frac{d\phi}{dy}=0. \quad \text{(B4)}$$

Because blood is a rather complex fluid, its deformation and flow behaviors are not simple. The apparent viscosity of blood depends on shear rate, hematocrit, temperature, and chemical composition of the blood. Because of their importance, shear rate and hematocrit are the primary variables for describing the apparent viscosity of blood. Other independent variables, such as temperature and concentrations of plasma macromolecules that can cause red blood cell aggregation at low shear rates, are usually of less practical importance in a descriptive equation because they are constant in a given problem. Many descriptive equations have been used in the literature to represent the rheological behavior of blood [98]. In this study, a non-Newtonian viscosity equation derived by Quemada [94-96], using a semi-phenomenological approach, is employed to

describe the dependence of blood viscosity $\eta(\phi,\gamma)$ on shear rates and hematocrits. Quemada's equation is

$$\eta = \eta_0(1-0.5k(\phi,\gamma)\phi)^{-2},$$

$$\text{where } k(\phi,\gamma) = \frac{k_0 + k_\infty(\gamma/\gamma_c)^{1/2}}{1+(\gamma/\gamma_c)^{1/2}}. \qquad (3)$$

In this equation, $\eta_0$ is the viscosity of plasma and other three coefficients reflect the suspension properties. The terms $k_0$ and $k_\infty$ are the intrinsic viscosities at zero and infinite shear rates respectively. The critical shear rate $\gamma_c$ is related to the critical shear stress under which the particle aggregate structure is broken. These three coefficients are functions of hematocrit, suspending medium composition, etcetera. Quemada's equation can represent blood rheology over a wide range of conditions and its coefficients have physical interpretations, thus being useful. Cokelet used data for blood at various hematocrits to fit to Quemada's equation and the coefficients were correlated as [97]

$$k_0 = \exp(3.874 - 10.41\phi + 13.80\phi^2 - 6.738\phi^3),$$

$$k_\infty = \exp(1.3435 - 2.803\phi + 2.711\phi^2 - 0.6479\phi^3), \text{ and}$$

$$\gamma_c = \exp(-6.1508 + 27.923\phi - 25.60\phi^2 + 3.697\phi^3).$$

Because the empirical expression for $k_0$ yields a non-monotonic zero-shear-rate viscosity, which also becomes infinity at $\phi = 0.122$, 0.18, 0.731, and 0.856, the modified expression for $k_0$ given by Das et al. [99] is used; that is,

$$k_0 = 0.275363 + 2/(0.100158 + \phi).$$

To solve the equations of motion, I integrated Equation (1) with the boundary condition (B3) to get

$$\eta(\phi,\gamma)\gamma = (\frac{dP}{dx})y. \tag{4}$$

Steady-state concentration profiles are determined by the direct solution of Equation (2). This equation can be trivially integrated with the no-flux boundary condition (B2). The result shows that the net mass flux is zero everywhere in the blood:

$$K_c(\phi^2 \frac{d\gamma}{dy} + \phi\gamma\frac{d\phi}{dy}) + K_\eta(\phi^2\gamma\frac{d\eta}{\eta dy}) = 0. \tag{5a}$$

Rearranging Equation (5a) to the form (divided by $\phi^2\gamma$, for the region $0 < y \le B$)

$$K_c\frac{1}{\phi\gamma}\frac{d(\phi\gamma)}{dy} + K_\eta\frac{1}{\eta}\frac{d\eta}{dy} = 0, \tag{5b}$$

and integrating Equation (5b) with $\phi = \phi_w$, $\gamma = \gamma_w$, and $\eta = \eta_w$ at the wall yields

$$\frac{\phi\gamma}{\phi_w\gamma_w} = (\frac{\eta}{\eta_w})^{-K_\eta/K_c}. \tag{5}$$

As a result, two differential equations (1) and (2) can be reduced to two non-linear algebraic equations (4) and (5), which must be solved simultaneously to obtain the local shear rate $\gamma$ and hematocrit $\phi$.

In this study, the effects of model parameters, including $K_\eta/K_c$ (defined as $K$), $\frac{dP}{dx}$, and average hematocrit $\bar{\phi}$, on the red blood cell distribution and the velocity profile are analyzed by numerical simulations. The constants $K_c$ and $K_\eta$ are phenomenological parameters that need to be determined by fitting the predictions of the model to experimental measurements of the red blood cell distribution. However, at steady state, only the ratio $K_\eta/K_c$ ($K$) appears in the diffusion equation and it is an adjustable parameter in the numerical simulations. The flow driving force $\frac{dP}{dx}$ can be estimated from experimental settings with a Newtonian fluid flowing in the flow system. For instance, the pressure gradient $\frac{dP}{dx}$, which pushes a "Newtonian" blood with the viscosity

$\eta_0=3.8$ cP to flow in a parallel flow chamber with the height ($=2B$) of 76 μm and generates a wall shear rate of 1,500 $sec^{-1}$, is estimated to be 15,000 $dyne/cm^3$ from Equation (4). The average red blood cell volume fraction $\bar{\phi}$ is determined by the value chosen for the wall hematocrit $\phi_w$. Other model parameters such as the half height of the flow channel B and the plasma viscosity $\eta_0$ are known for the parallel-plate flow chamber system.

In order to solve Equations (4) and (5) and satisfy the criterion of a given average red blood cell volume fraction $\bar{\phi}$, the value chosen for the wall hematocrit $\phi_w$ is set by trial and error. Assuming a value of wall hematocrit $\phi_w$ at $y=B$ with given $\frac{dP}{dx}$ and $\eta_0$, the wall shear rate $\gamma_w$ is solved by using the van Wijngaarden-Dekker-Brent method [100] to find the root of Equation (4). Next, with a given parameter $K$, the local hematocrit $\phi_i$ and the local shear rate $\gamma_i$ at $y = y_i$, starting from the wall ($y=y_0=B$) to the center plane ($y=0$) of the flow channel, are solved from Equations (4) and (5) simultaneously by the Newton-Raphson method [100]. The root pair ($\phi_i$, $\gamma_i$) at $y_i$ is used as an initial guess to find the root pair ($\phi_{i+1}$, $\gamma_{i+1}$) for the next position $y= y_{i+1}$; this procedure is continued until the local shear rate equals the critical shear rate $\gamma_c$ at $y=y_c$ (the local hematocrit $\phi_c$ is also obtained). The critical shear rate $\gamma_c$ is related to the critical shear stress under which the red blood cell aggregate structure is broken. Therefore, from $y=y_c$ to the center plane ($y=0$) of the flow channel, the local shear rates are smaller than $\gamma_c$; and the red blood cell aggregate structure is not disturbed so the hematocrit keeps constant. The local shear rates from $y=y_c$ to $y=0$ then are solved from Equation (4) with this constant hematocrit

$\phi_c$. When all root pairs ($\phi_i$, $\gamma_i$) have been obtained, the average red blood cell volume fraction $\bar{\phi} = \frac{1}{B}\int_0^B \phi dy$ is calculated by numerical integration. If the result is not equal to the certain value of the average hematocrit specified, a new guess of the wall hematocrit $\phi_w$ is assigned and the root pairs ($\phi_i$, $\gamma_i$) are solved again until the specific average hematocrit is reached. The velocity profile $v(y) = \int_B^y \gamma dy$ then can be calculated by numerical integration.

**Platelet distribution**

After the red blood cell distributions at different shear rates and average hematocrits are solved by the constitutive equation for concentrated suspensions, the platelet distributions can be calculated. Because red blood cells transport laterally, there will be a counter flow of the plasma to maintain the mass balance. This counter flow may cause the lateral movement of platelets.

In traditional mass transport analysis, the net red blood cell flux $N_y^\phi$ can be written as

$$N_y^\phi = u_y^\phi \phi - D^\phi \frac{d\phi}{dy},$$

where $u_y^\phi$ is the lateral drift velocity of red blood cells and $D^\phi$ is the apparent diffusivity of red blood cells. For an impermeable and non-reactive wall, $N_y^\phi$ equals zero in the case that the velocity and concentration profiles are fully developed and at steady state. Therefore, the drift velocity can be rearranged as

$$u_y^\phi = \frac{D^\phi}{\phi}\frac{d\phi}{dy}.$$

Because the main components of the blood are red blood cells and the plasma, there is a flow of the plasma in an opposite direction to the lateral movement of red blood cells so that the mass balance is preserved. That is,

$$u_y^{\phi}\phi + u_y^{plasma}(1-\phi) = 0.$$

In addition, this counter flow results in the drift movement of platelets:

$$u_y^{plasma} = -\frac{\phi}{1-\phi}u_y^{\phi} = -\frac{D^{\phi}}{1-\phi}\frac{d\phi}{dy} \approx u_y^{plt}. \qquad (6)$$

As a result, the drift velocity of platelets $u_y^{plt}$ can be estimated from the red blood cell distribution.

Based on the same argument for red blood cells in a system that has an impermeable non-reactive wall and at steady state, the mass flux of platelets $N_y^{plt}$ is equal to zero. That is,

$$N_y^{plt} = u_y^{plt}x_{plt} - D^{plt}\frac{dx_{plt}}{dy} = 0, \qquad (7)$$

where $x_{plt}$ is the volume fraction of platelets and $D^{plt}$ is the apparent diffusivity of platelets. After rearranging Equations (6) and (7), the platelet distribution can be expressed as

$$\frac{dx_{plt}}{dy} = \frac{u_y^{plt}x_{plt}}{D^{plt}} = -(\frac{D^{\phi}}{D^{plt}})\frac{1}{1-\phi}\frac{d\phi}{dy}x_{plt}. \qquad (8)$$

If the term $\frac{D^{\phi}}{D^{plt}}$ in Equation (8) can be formulated explicitly, the steady-state platelet distribution $x_{plt}$ can be calculated directly from this equation and the known concentration profile of red blood cells. Because red blood cells tend to align with the flow at high shear rates, platelets have to wiggle along the tortuous openings in the red blood cell arrays when they move laterally. This phenomenon is similar to the situation

in which a mass diffuses through a film composed of periodically spaced "flake" arrays; the term "flakes" means that impermeable bodies have one short dimension and two long dimensions. When the flakes are arranged perpendicular to the diffusion and parallel to the surface of the film (Figure 2.2), the ratio of the effective diffusion coefficient $D_{eff}$ to the diffusion coefficient in suspension fluid $D_0$ is given by [101]:

$$\frac{D_{eff}}{D_0} = \frac{1}{1+\alpha^2\phi_F^2/(1-\phi_F)},$$

where $\phi_F$ is the volume fraction of flakes and $\alpha$ is the aspect ratio of a flake, which is defined as the ratio of its long dimension to its short dimension. Therefore, I assume the expression of $\frac{D^{\phi}}{D^{plt}}$ as

$$(\frac{D^{\phi}}{D^{plt}}) = (\frac{D^{\phi}}{D^{plt}})_0 \frac{1-\phi+\alpha^2\phi^2}{1-\phi}. \qquad (9)$$

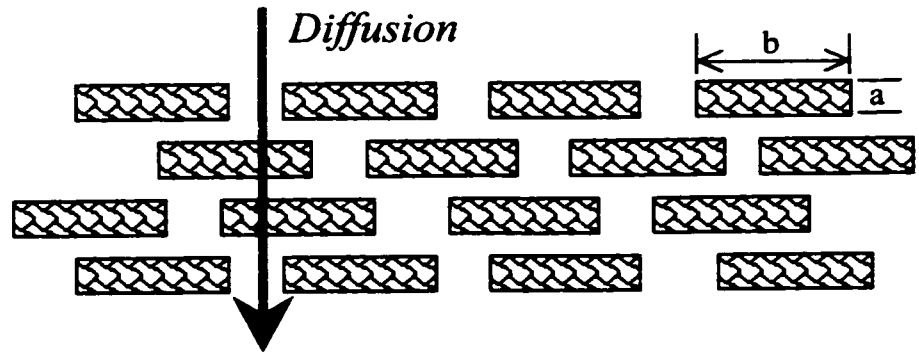


Figure 2.2 A schematic diagram of the diffusion through a suspension of impermeable flakes. The aspect ratio is defined as $\alpha=b/a$.

In this formulation, when the hematocrit is very low, the term $\frac{D^{\phi}}{D^{plt}}$ reduces to the ratio of Brownian diffusivities of red blood cells and platelets $(\frac{D^{\phi}}{D^{plt}})_0$. Moreover, as the hematocrit approaches 1, the platelet may be trapped in the red blood cell aggregate and $\frac{D^{\phi}}{D^{plt}}$ becomes infinity. That is,

$$(\frac{D^{\phi}}{D^{plt}}) \to (\frac{D^{\phi}}{D^{plt}})_0 \quad \text{as } \phi \to 0, \text{ and}$$

$$(\frac{D^{\phi}}{D^{plt}}) \to \infty \quad \text{as } \phi \to 1.$$

Finally, by combining Equations (8) and (9), the relationship between the steady-state red blood cell and platelet distributions is

$$\frac{dx_{plt}}{x_{plt}dy} = -(\frac{D^{\phi}}{D^{plt}})_0 \frac{1-\phi+\alpha^2\phi^2}{(1-\phi)^2}\frac{d\phi}{dy}. \qquad (10)$$

From the equation (10), the platelet profile can be calculated numerically from the predominant red blood cell distribution, adjusting the average platelet volume fraction to a given value by trial and error. The parameter $(\frac{D^{\phi}}{D^{plt}})_0$ is the ratio of Brownian diffusion coefficients of red blood cells and platelets, and it can be estimated from the dimensions of cells. Theoretically the Brownian diffusivity is inversely proportional to the size of the solute; because the long dimensions of a red blood cell and a platelet are 8 μm and 2 μm respectively, $(\frac{D^{\phi}}{D^{plt}})_0$ is about 0.25. The aspect ratio α can be estimated from the ratio of the long dimension to the short dimension of a red blood cell, and it is about 4-5. However, the values may vary because of the complicated flow conditions. Even though the parameters $(\frac{D^{\phi}}{D^{plt}})_0$ and α have their physical interpretations, they are adjustable in numerical simulations.

## 2.3 Results

The numerical simulations of cell distributions and velocity profiles from the phenomenological constitutive equations at steady state are made with various driving forces $\frac{dP}{dx}$, average hematocrits $\bar{\phi}$, parameters $K$, $(\frac{D^{\phi}}{D^{plt}})_0$ and $\alpha$. In general, this mathematical model predicts that local hematocrits increase from the wall to the center plane, velocity profiles show the non-Newtonian properties, and wall concentrations of platelets are higher at higher shear rates and larger hematocrits. These results are consistent with the experimental observations that have been presented in the literature.

**The effect of the driving force $\frac{dP}{dx}$ on cell distributions and velocity profiles:**

The predictions of red blood cell distributions, velocity profiles, and platelet distributions at different driving forces are shown in Figures 2.3, 2.4, and 2.5 respectively. These simulations are done at the average hematocrit $\bar{\phi} = 0.4$ and $K(\equiv K_\eta / K_c) = 2$. The driving forces used here are 15,000, 8,000, and 1,000 dynes/cm$^3$, which generate the wall shear rates of 1,500, 800, and 100 sec$^{-1}$ respectively for a "Newtonian" blood with the viscosity of 3.8 cP in a parallel-plate flow chamber with the height of 76 μm. These wall shear rates are chosen because they are relevant in arterioles (1,500 sec$^{-1}$), large arteries (800 sec$^{-1}$), and veins (100 sec$^{-1}$). As indicated in Figure 2.3, red blood cells are transported from high shear conditions at the wall to low shear conditions at the center plane of the parallel flow chamber where they are concentrated. This phenomenon is more significant at higher driving forces. In Figure 2.4, these

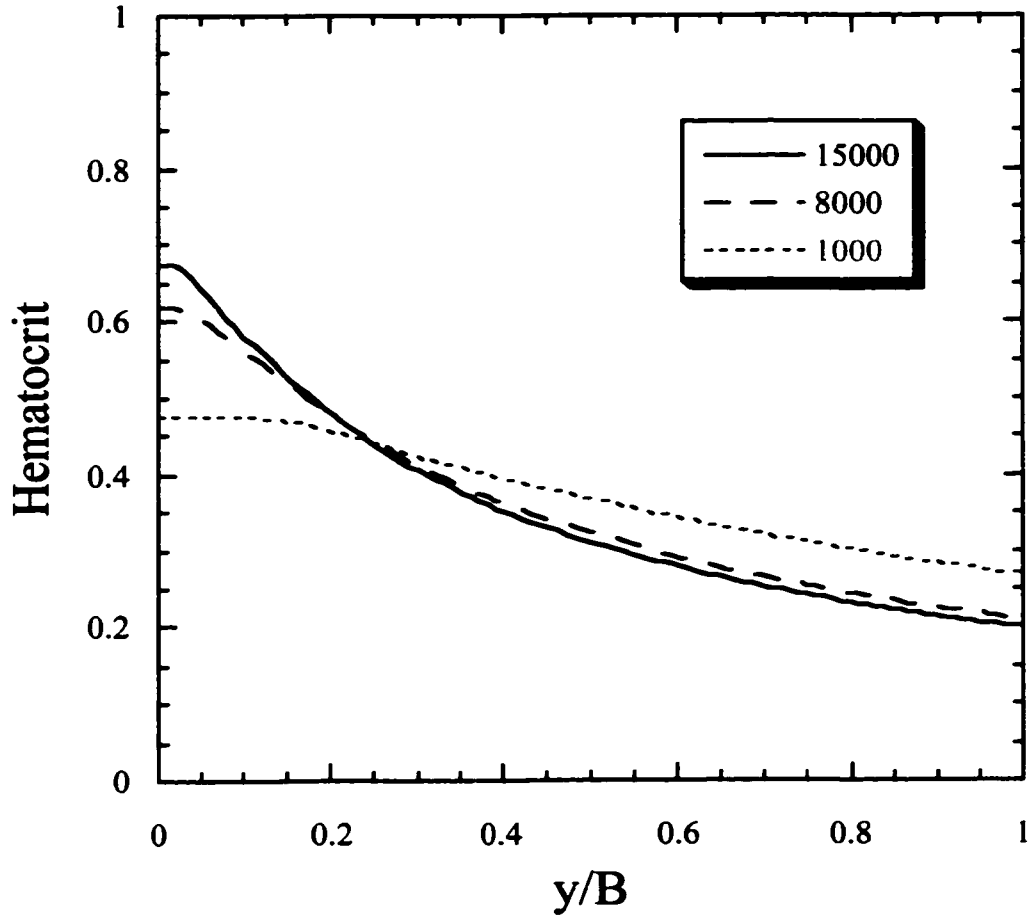


Figure 2.3 The effect of the driving force *dP/dx* on red blood cell distributions. These simulations are done with parameters $\bar{\phi} = 0.4$ and $K(\equiv K_\eta / K_c) = 2$. The driving forces are 15,000, 8,000, and 1,000 dynes/cm$^3$, generating the wall shear rates of 1,500, 800, and 100 sec$^{-1}$ respectively for a "Newtonian" blood with the viscosity of 3.8 cP in a parallel-plate flow chamber with the height of 76 μm.

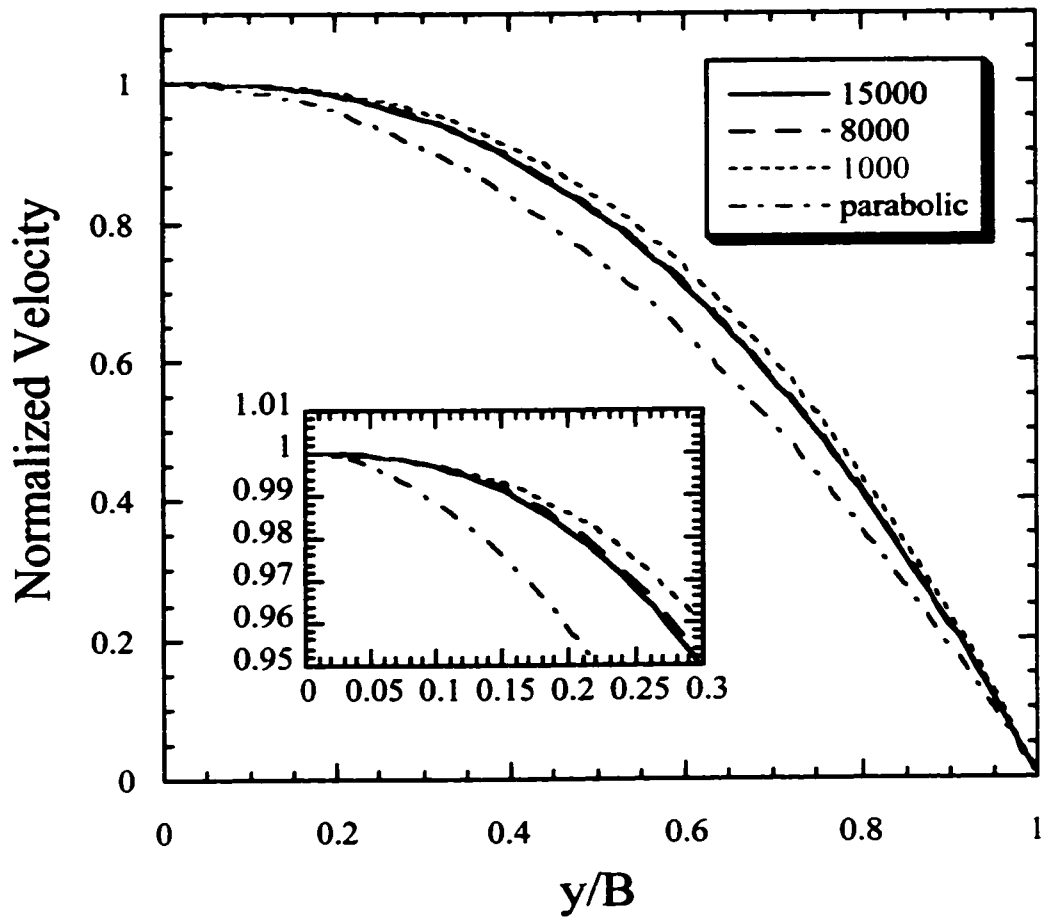


Figure 2.4 The effect of the driving force *dP/dx* on velocity profiles. These simulations are done with the parameters described in Figure 2.3. For each curve, the velocities are normalized with the maximum velocity at the center plane (*y=0*) of the parallel-plate flow chamber. The theoretical parabolic velocity profile for a Newtonian fluid is also shown for comparison. The inset zooms in the velocity profiles close to the center plane for better distinction.

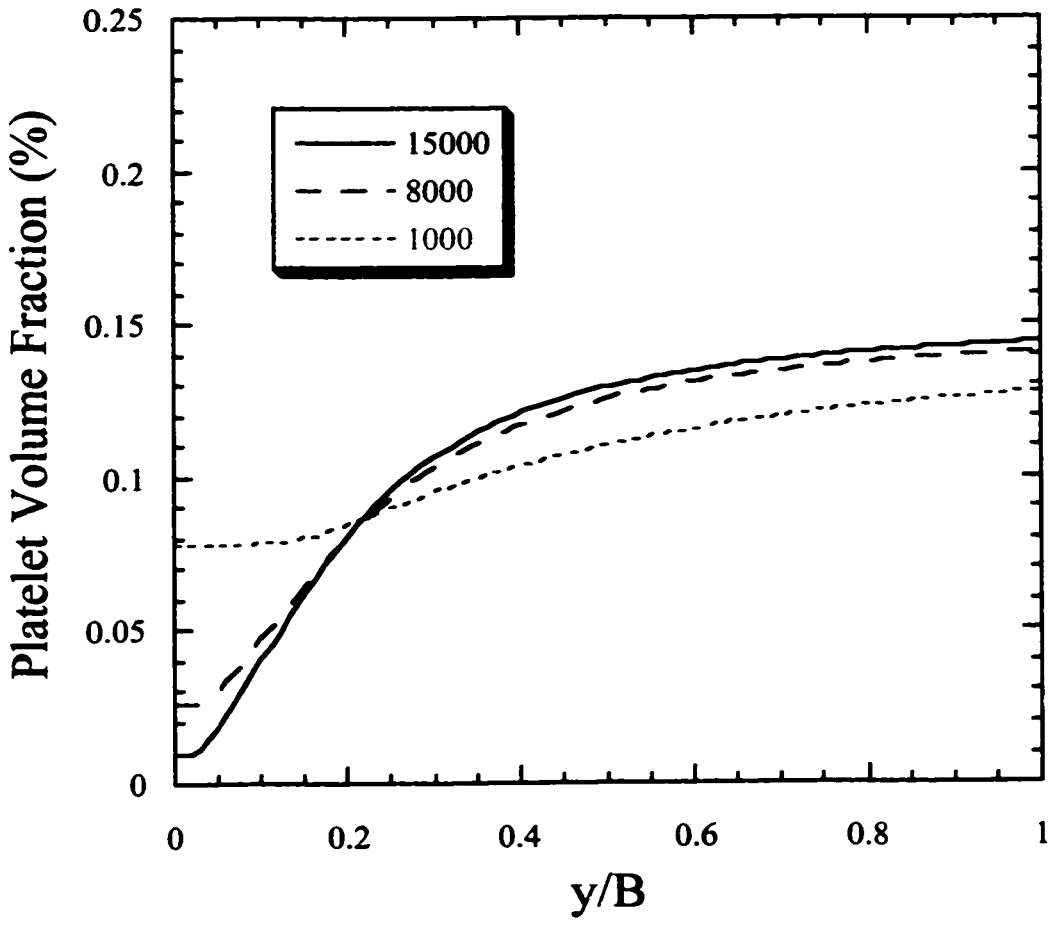


Figure 2.5 The effect of the driving force *dP/dx* on platelet distributions. These platelet concentration profiles are calculated from the red blood cell distributions shown in Figure 2.3 with parameters $(D^{\phi}/D^{plt})_0 = 0.25$, $\alpha^2$=20, and the average platelet volume fraction of 0.1%.

simulated velocity profiles are blunted from the parabolic, indicating the characteristic of a non-Newtonian fluid. The degree of blunting of the velocity profile decreases with increasing driving force. To predict the platelet distribution, parameters $(\frac{D^{\phi}}{D^{plt}})_0 = 0.25$ and $\alpha^2$=20 are used, which are estimated from the dimensions of the red blood cell and the platelet. As shown in Figure 2.5, platelets distribute in the flow chamber non-uniformly. The wall concentration of platelets increases as the driving force increases.

**The effect of the average hematocrit $\bar{\phi}$ on cell distributions and velocity profiles:**

The simulation results of red blood cell distributions, velocity profiles, and platelet distributions at average hematocrits are shown in Figures 2.6, 2.7, and 2.8 respectively. These simulations are done at the driving force $\frac{dP}{dx} = 8{,}000$ dynes/cm$^3$ and $K$=2. Red blood cells are concentrated at the center plane of the parallel flow chamber as shown in Figure 2.6. These velocity profiles are blunted from the parabolic and the degree of blunting of the velocity profile increases as the average hematocrit increases (Figure 2.7). Parameters $(\frac{D^{\phi}}{D^{plt}})_0 = 0.25$ and $\alpha^2$=20 are again used to calculate the platelet distributions. In Figure 2.8, platelets show the non-uniform distribution in the flow chamber. The wall concentration of platelets increases as the average hematocrit increases.

**The effect of the parameter $K(\equiv K_\eta / K_c)$ on red blood cell distributions:**

Because the parameter $K$ is related to the ratio of two mechanisms resulting in the

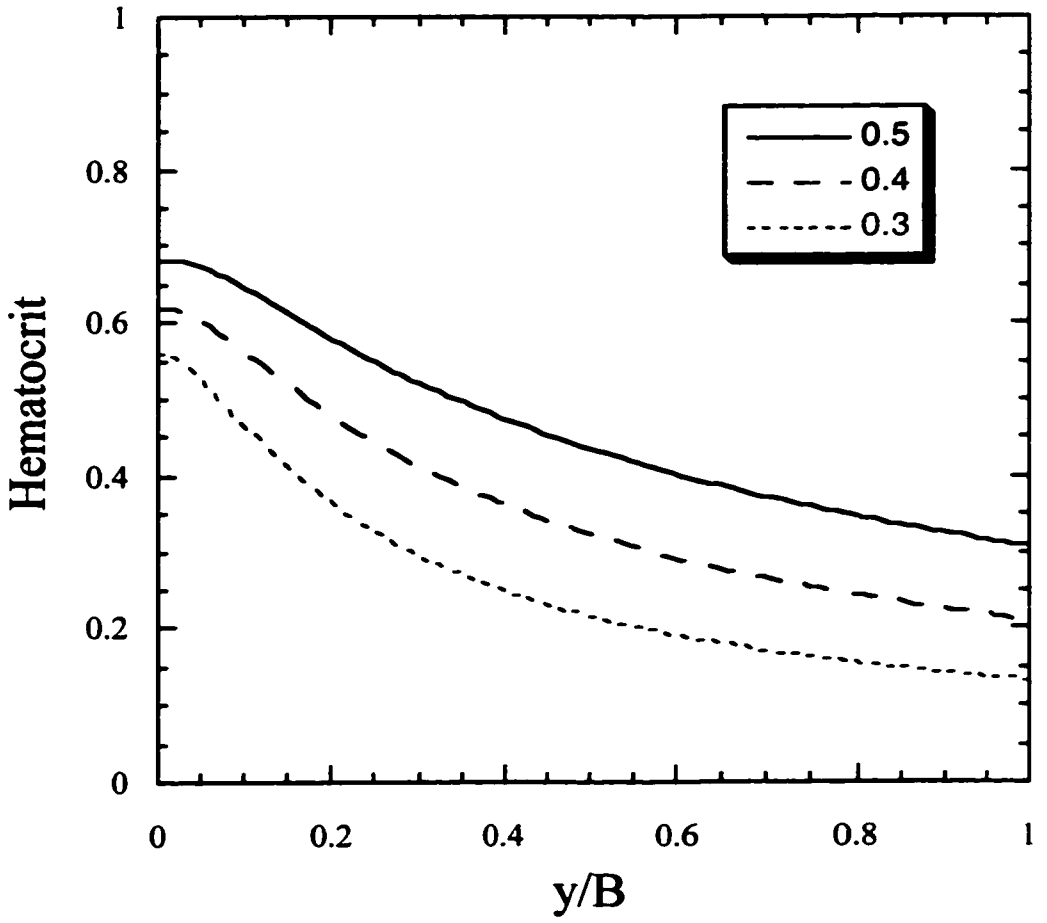


Figure 2.6 The effect of the average hematocrit $\bar{\phi}$ on red blood cell distributions. These simulations are done with parameters $dP/dx$=8,000 dynes/cm$^3$ and $K(\equiv K_\eta / K_c) = 2$. The average hematocrits shown are 0.5, 0.4, and 0.3.

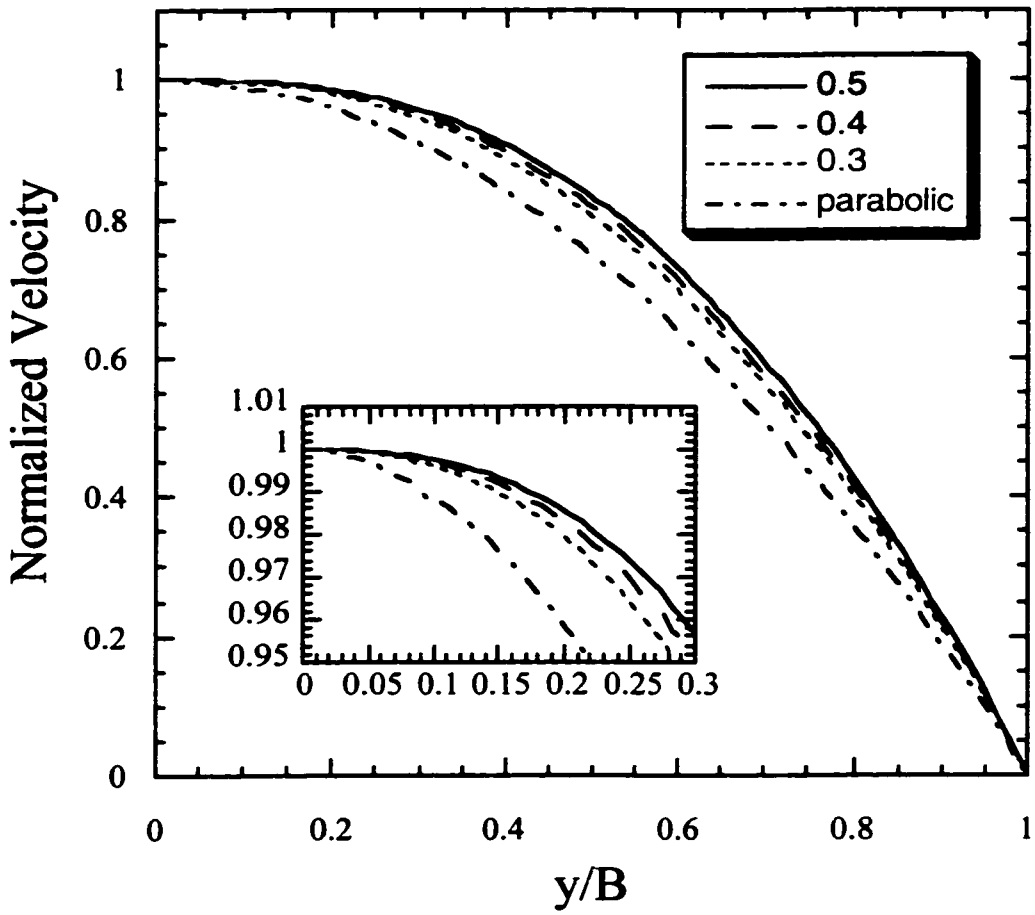


Figure 2.7 The effect of the average hematocrit $\bar{\phi}$ on velocity profiles. These simulations are done with the parameters described in Figure 2.6. For each curve, the velocities are normalized with the maximum velocity at the center plane ($y=0$) of the parallel-plate flow chamber. The theoretical parabolic velocity profile for a Newtonian fluid is also shown for comparison. The inset zooms in the velocity profiles close to the center plane for better distinction.

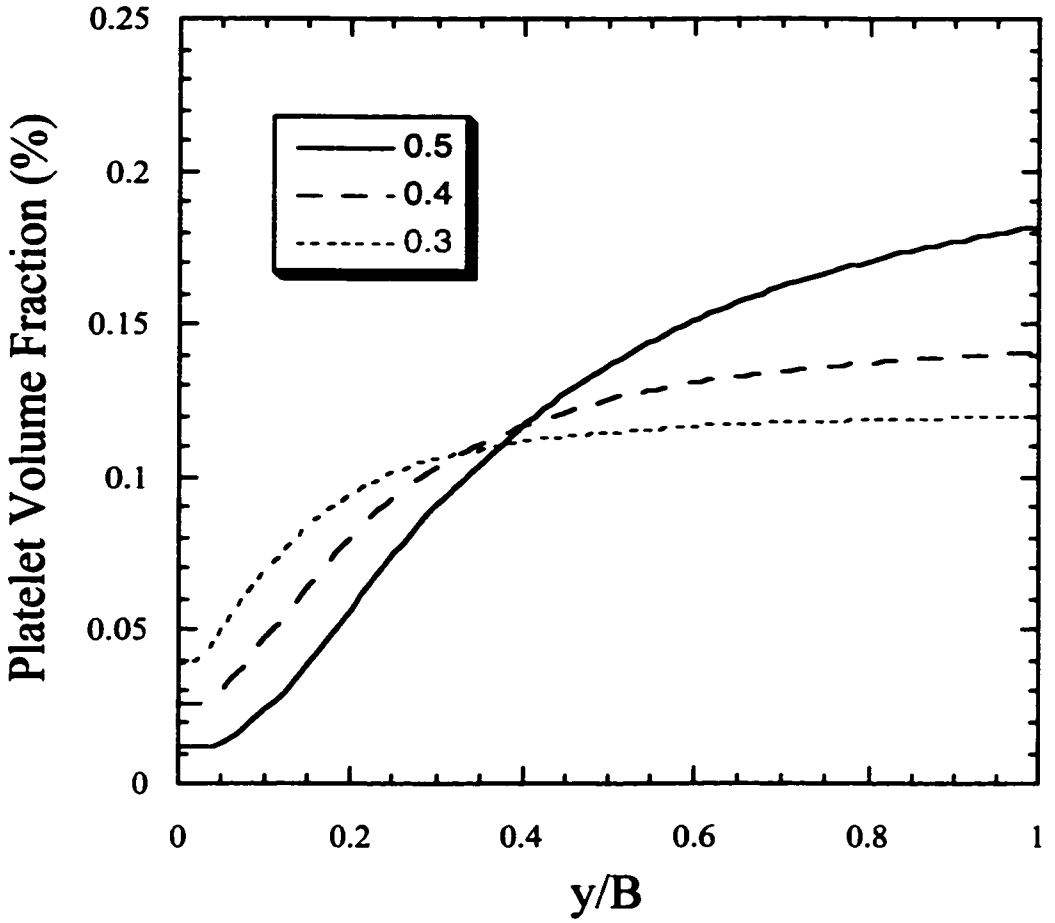


Figure 2.8 The effect of the average hematocrit $\bar{\phi}$ on platelet distributions. These platelet concentration profiles are calculated from the red blood cell distributions shown in Figure 2.6 with parameters $(D^{\phi}/D^{plt})_0 = 0.25$, $\alpha^2$=20, and the average platelet volume fraction of 0.1%.

lateral flux of red blood cells, the effect of viscosity-induced resistances to the effect of shear-induced collisions, $K$ can significantly affect the red blood cell distribution. The simulation results shown in Figure 2.9 are done with the average hematocrit $\bar{\phi} = 0.4$ and the driving force $\frac{dP}{dx} = 8{,}000$ dynes/cm$^3$. When $K$ is large, red blood cells distribute more uniformly; on the other hand, when $K$ is small, hematocrit will increase rapidly from the wall to the center. In some simulated red blood cell distributions such as, for example, the result with $K$=4 in Figure 2.9, the maximum hematocrit occurs at about $y/B$=0.05 but not the center plane of the flow chamber. This prediction may represent the "pinch effect" that has been shown in the literature [102,103].

**The effects of the parameters $(\frac{D^{\phi}}{D^{plt}})_0$ and $\alpha^2$ on platelet distributions:**

The platelet lateral movements in a parallel-platelet flow chamber depend mainly on the dominant red blood cell distribution. Nevertheless, the relative diffusivities between red blood cells and platelets as well as the aligned red blood cell structure at high shear conditions can also affect the platelet distribution. The effects of the parameters $(\frac{D^{\phi}}{D^{plt}})_0$ and $\alpha^2$ on platelet distributions are shown in Figure 2.10. These platelet concentration profiles are calculated from the red blood cell distribution that is simulated with $\frac{dP}{dx} = 8{,}000$ dynes/cm$^3$, $\bar{\phi} = 0.4$, and $K$=2. When $(\frac{D^{\phi}}{D^{plt}})_0$ is smaller, that is, the diffusive movement of platelets is much faster than that of red blood cells, platelets can distribute more uniformly in the flow channel. Because red blood cells will deform at high shear rates and they move with the flow, the aspect ratio $\alpha$ may no longer depend

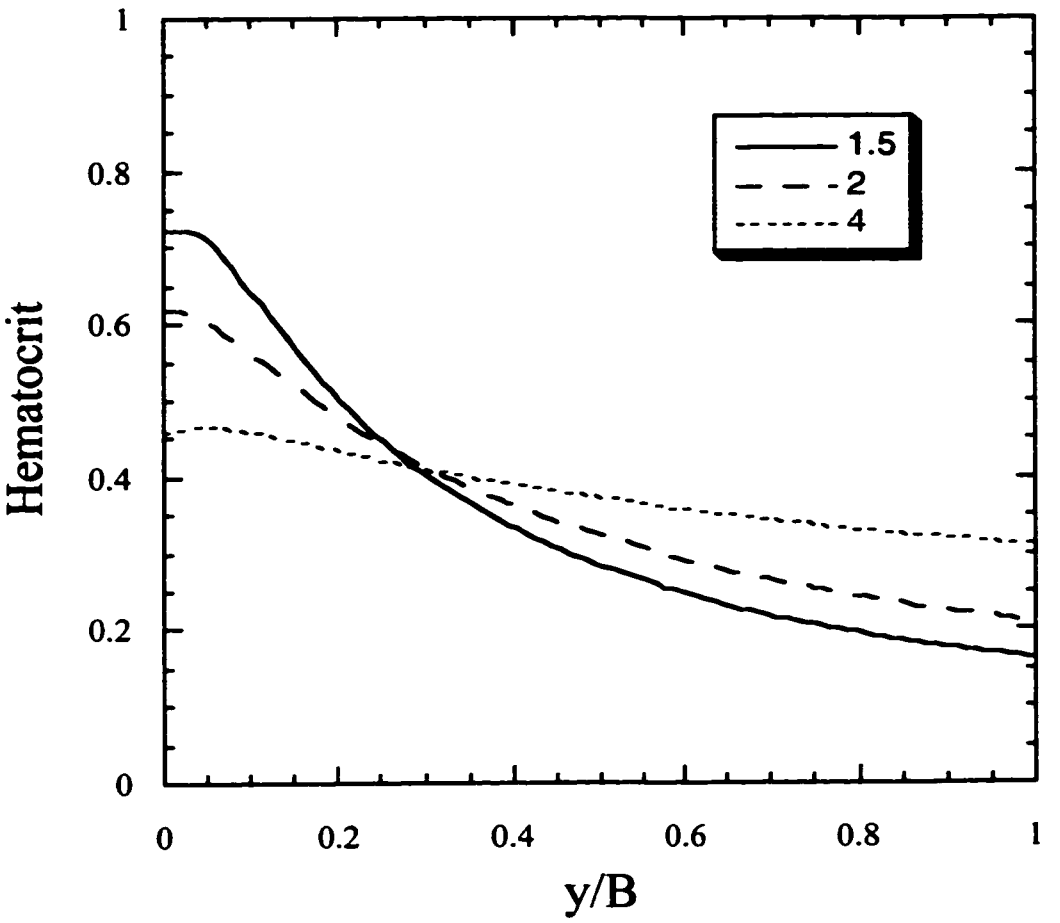


Figure 2.9 The effect of the parameter $K(\equiv K_\eta/K_c)$ on red blood cell distributions. These simulations are done with the driving force $dP/dx$=8,000 dynes/cm$^3$ and the average hematocrit $\bar{\phi} = 0.4$. The $K$ values used are 1.5, 2, and 4.

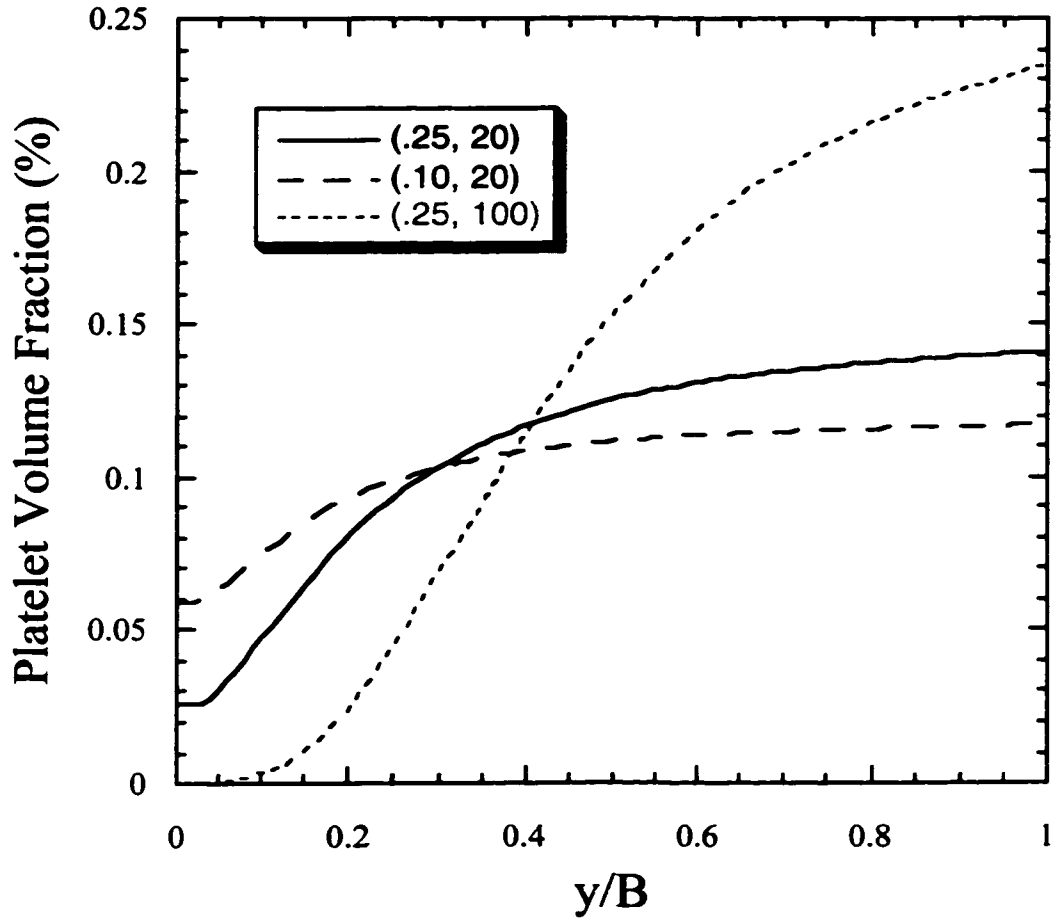


Figure 2.10 The effects of parameters $(D^{\phi}/D^{plt})_0$ and $\alpha^2$ on platelet distributions. These simulations are done with the driving force $dP/dx$=8,000 dynes/cm$^3$, the average hematocrit $\bar{\phi} = 0.4$, $K(\equiv K_\eta/K_c) = 2$, and the average platelet volume fraction of 0.1%. The parameter pairs $((D^{\phi}/D^{plt})_0, \alpha^2)$ used are (0.25, 20), (0.10, 20), and (0.25, 100).

only on the dimensions of a red blood cell in the stagnant condition. When $\alpha$ increases, the non-uniform distribution of platelets is more significant and the wall concentration of platelets is higher.

## 2.4 Discussion

The mathematical model presented in this study is able to predict at least qualitatively many phenomena that have been observed experimentally. The simulated red blood cell distribution has the minimum at the wall and usually attains the maximum at the center of the flow channel. The velocity profile is blunted from the parabolic, showing the characteristics of a non-Newtonian fluid. The degree of the blunting increases with increasing average hematocrits and decreasing driving forces. In addition, the higher wall concentrations of platelets at higher wall shear rates and larger average hematocrits are predicted. The ability of this mathematical model to predict those important features in blood transport indicates a good start in getting insight into mural thrombosis from an engineer's point of view. However, the detailed experimental estimation of model parameters, not yet accomplished in this work, must be done before applying this model to simulate real physiological systems. There are also some intrinsic limitations in this method, and further improvement is needed. I will discuss both advantages and disadvantages of this mathematical model in the following.

This mathematical model, based on a phenomenological constitutive equation for concentrated suspensions that accounts for shear-induced particle migration, can

represent the lateral movements of both red blood cells and platelets. The red blood cells move perpendicular to the flow direction because of shear-induced collisions and viscosity-induced resistance, and the plasma counter flows to maintain the mass balance, leading to the lateral drift of platelets. Therefore, this model is able to estimate the drift velocity straightforwardly. This approach avoids the circular nature in the method proposed by Eckstein's group; that is, a drift function is determined from a fully developed platelet distribution and this function is then used to calculate a platelet distribution.

Even though this phenomenological model can make straightforward predictions of cell distributions and velocity profiles, the parameters in this model such as $K$, $(\frac{D^{\bullet}}{D^{plt}})_0$, and $\alpha$ must be determined from experimental data in order to apply the model to real physiological conditions. By statistically best fitting the steady-state distributions of red blood cells and platelets at various flow rates and average hematocrits in a parallel-plate flow chamber, these parameters can be estimated. In order to determine the individual values of $K_\eta$ and $K_c$, the predictions for the transient flow must be fitted to experimentally measured profiles. It is not an easy task to measure accurately both red blood cell and platelet distributions in a flow channel. A new experimental protocol, for instance, epifluorescence video microscopy combined with the freeze-capture method or the laser-Doppler technique, must be set up to obtain these concentration profiles of red blood cells and platelets at different shear conditions. After all parameters have been determined, this mathematical model can be applied to the flow system with more complicated

geometry and predict platelet concentrations near the wall. The near-wall region usually has complicated flow patterns and concentrated platelets, thus being prone to thrombosis. The mathematical predictions of the flow field and cell distributions can aid in understanding the intertwined relationships among these thrombogenic determinants.

The numerical simulations with this phenomenological constitutive model are relatively computational inexpensive. In the predictions of steady-state cell distributions done in this work, the local shear rate and hematocrit can be solved by finding roots of two non-linear algebraic equations (Equations 4 and 5) simultaneously. However, a trial-and-error method is inevitable to conserve the given average hematocrit and average platelet volume fraction. By solving the complete equations of motion and cell transport with suitable initial conditions, the mass conservation would be quantitatively taken into account, and the trial-and-error would no longer be needed. However, this approach requires the implementation of a much more complicated algorithm than root-finding methods to solve the non-linear partial differential equations of momentum and mass balances. Even though the algorithm for simulating the transient behaviors of cell distributions and velocity profiles for flowing blood is more difficult to implement than that for steady-state simulations, this phenomenological constitutive model is still less computationally expensive than the dynamic simulations of many-particle systems that account rigorously for all hydrodynamic, electrostatic, and surface interactions. In this work, the model system contains impermeable and non-reactive walls. Nevertheless, the

platelet-wall reaction can also be implemented in this mathematical model by incorporating boundary conditions with the reaction terms.

Although the mathematical model presented in this chapter can predict many important features in blood transport, there are intrinsic limitations to it, such as that the sizes of blood cells cannot be taken into account in the governing equations and the red blood cell depletion layer near the wall cannot be predicted. Comparing the relative size of a cell to a flow channel, we can expect that the flow patterns and distributions of red blood cells with their long dimension of 8 μm will be different in a large artery of 500 μm in diameter and an arteriole of 30 μm in diameter. In fact, *in vitro* evidence also shows that the degree of blunting in the velocity profile decreases with increasing tube radius [86]. In addition, because of the size of red blood cells and the flow-induced collisions that restrict motions of individual red blood cells near the wall, the concentration of red blood cell is relatively depleted and a peripheral plasma layer occurs in the near-wall region, typically 2-5 μm thick. This non-uniform distribution of red blood cells in the near-wall region may be also a source of the near-wall excess of platelets. After platelets drift with the plasma counter flow into this peripheral plasma layer, they accumulate in this near-wall region because fewer platelet-red blood cell collisions occur to cause further lateral movements. Eckstein's group observed experimentally that the concentration of platelet-sized beads peaked only at about 5 μm from the wall, where the red blood cell-free layer occurred, but the bead distribution was relatively uniform in the region 10 μm away from the wall to the center of the flow

channel [3,90]. The inability to predict the red blood cell depletion layer in this mathematical model may be the reason why the simulation results of platelet distributions (shown in Figures 2.5, 2.8, and 2.10) do not have the same quantitative shapes as those in the experimental observations. The parameters for predicting platelet distributions may be adjusted, such as increasing $\alpha$, to make the simulation results closer to the "near-wall excess" shapes. However, this adjustment cannot completely make up for the fundamental deficiency.

As a final remark, the dependence of shear or hematocrit in those simulated cell distributions and velocity profiles is determined by the choice of the viscosity formulation for blood. In the work of Phillips and colleagues [93], they used the Krieger equation $\eta = \eta_0(1-\phi/\phi_m)^{-1.82}$, which depends only on the local volume fraction of particles, and their predicted particle distributions and velocity profiles were not dependent on the driving force with the same average volume fraction of particles and the same value of $K$. Also in their simulations, the maximum particle concentrations in the center of the flow channel always reached the value of the parameter $\phi_m$. On the other hand, Quemada's equation is used in this study, and the shear rate and average hematocrit influence the predictions of cell distributions and velocity profiles due to the nature of this equation.

# Chapter 3

## Platelet Activation by Interacting with Immobilized Collagen or von Willebrand Factor

In addition to the cell transport that has been mathematically modeled in Chapter 2, the surface reaction between exposed subendothelial matrix and blood cells or plasma coagulation proteins is one of important thrombogenic determinants, as the traditional Virchow's triad (flow, blood components, and vessel) has discussed. After endothelial denudation, whether the thrombus remains mural and limited, just sealing the rupture, or evolves into occlusive thrombi depends on the amount and character of exposed thrombogenic material. In fact, in the case of atherosclerotic plaque rupture, thrombus formation on the atheromatous core with abundant cholesterol crystals was up to six fold greater than that on other plaque components [104]. Many *in vitro* experiments have shown that platelets respond differently, such as adhering separately or forming large aggregates (thrombi), on surfaces coated with different purified matrix proteins [30-37].

Even though platelets are small, enucleated cells, they can be activated to different extents by various stimuli; for example, platelet receptors can receive signals from outside by binding to subendothelial matrix proteins or to soluble agonists, and then send signals inside to initiate many kinds of biochemical reactions and changes. When platelets are stimulated, they will increase cytosolic calcium, change normal discoid shape to a spiny sphere, release contents in $\alpha$ and dense granules, form microparticles, or

switch their surface receptors from the rest state to the activated high affinity binding state. After activation, platelets may aggregate one with another by high affinity GpIIb-IIIa receptors, binding bridge plasma proteins such as vWf and fibrinogen. In addition, platelets provide released coagulation factor Va and an anionic phospholipid surface for clotting reactions that lead to thrombin generation. Those reactions are under elaborate control mechanisms naturally lest the response either be inadequate to meet the hemorrhagic challenge or result in inappropriate thrombosis in response to trivial provocation.

We have gained a lot of knowledge about those complicated phenomena of platelet responses during the past decades, yet many experimental observations conflict and specific activation mechanisms need to be clarified. This chapter will investigate the question of platelet activation status after interacting with immobilized vWf and collagen, evidenced by expressing activated GpIIb-IIIa and P-selectin, and demonstrate some of the mechanisms of inside-out signaling required for GpIIb-IIIa state change.

## 3.1 Background

The immediate hemostatic response to blood vessel injury is that platelets bind with many subendothelial matrix proteins and adsorbed plasma proteins on the injured sites to form a platelet plug. Many researchers used *in vitro* flow chamber experiments to study the interactions between platelets and purified proteins coated on the glass slides [30-37]. Different platelet deposition patterns were observed, including non-overlapping

singlet platelets and multi-platelet thrombi. In my preliminary flow chamber experiments, the patterns of platelet deposition on different protein-coated surfaces (Figure 3.1) were consistent with those findings. On the collagen I surface, platelets tended to attach to previously adherent platelets rather than to the collagen fibrils for blood-surface contact times longer than 30 seconds, forming large aggregates. In contrast, on the vWf surface, platelets adhered on the surface separately with only a few of small aggregates formed. Even though it is expected that the responses of platelets to various ligand-coated surfaces are different, the differential mechanisms underlying this observation have not been identified. If the detailed molecular mechanisms by which these different patterns occur can be obtained, the information will help with our understanding of pathologic mural thrombosis and with the development of novel therapeutics to prevent it.

Glycoprotein IIb-IIIa (GpIIb-IIIa), the most abundant adhesive receptor on the platelet surface, is important in platelet aggregation. GpIIb-IIIa is normally present at the level of 40,000 to 80,000 molecules on the surface of a resting platelet. Another 20,000 to 40,000 receptors are present inside platelets, primarily in the membranes lining the open canalicular system and in $\alpha$ granule membranes; these are able to be expressed on the cell surface when platelets are activated and undergo the release reaction. On resting platelets, GpIIb-IIIa has a low affinity for binding soluble ligands such as vWf and fibrinogen; however, when platelets are activated with ADP, epinephrine, thrombin, or other agonists, the GpIIb-IIIa complex undergoes a conformation change that results in

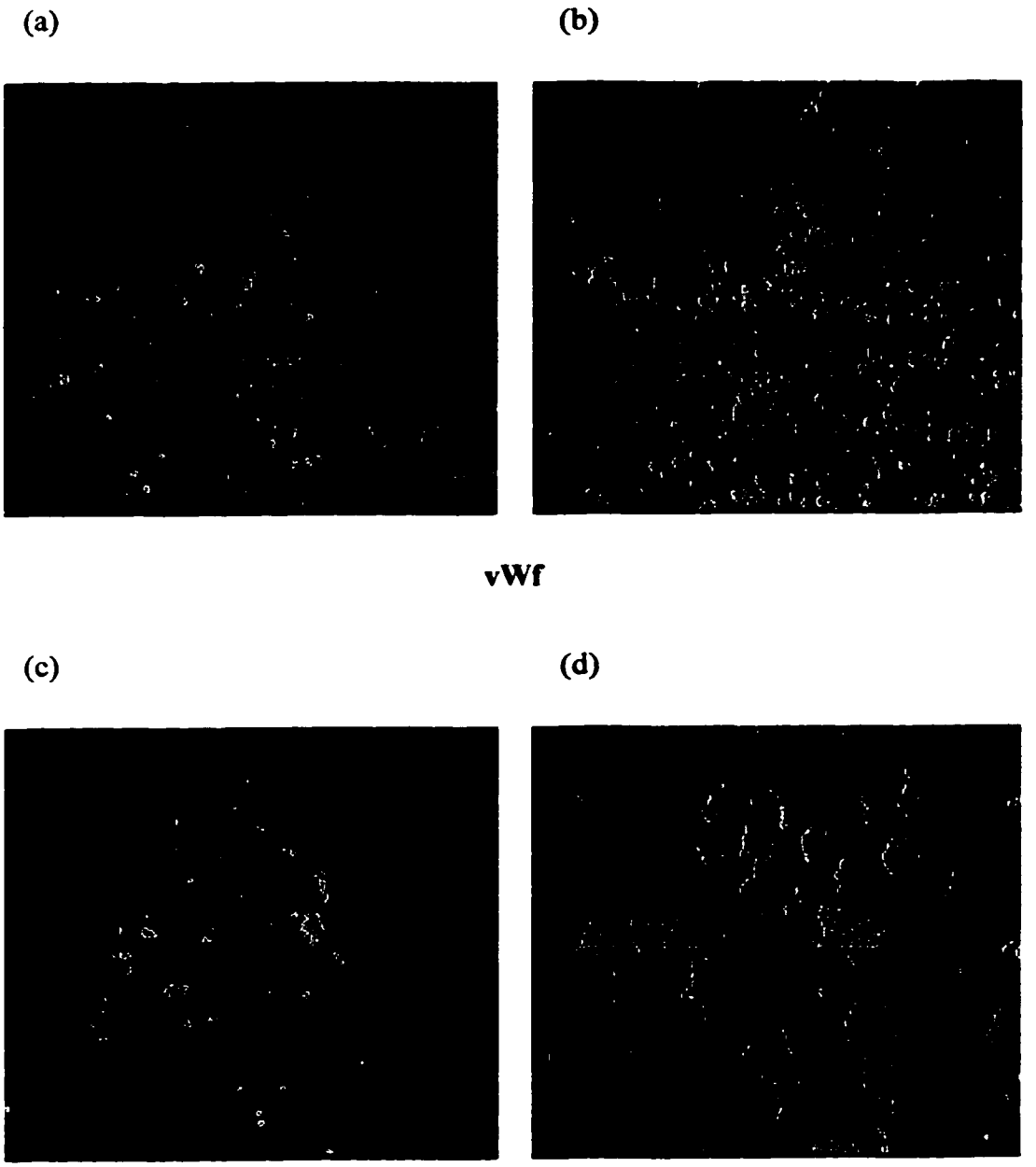


Figure 3.1 Fluorescent images of platelet deposition on immobilized proteins at a wall shear rate of 1000 $sec^{-1}$. (continue to next page)

(e) (f)

**Soluble VITROGEN 100® collagen**

Figure 3.1 (continued) Fluorescent images of platelet deposition on immobilized proteins at a wall shear rate of 1000 $sec^{-1}$. Whole blood incubated with 10 μM fluorescent dye mepacrine was pumped through a parallel-plate flow chamber mounted on an inverted-stage microscope equipped with an epifluorescent illumination attachment, a 100x oil objective, and a silicon-intensified target video camera. The dynamic of platelet deposition was recorded in real time to a videocassette. The video data was analyzed off-line using Inovision *ISee*™ imaging processing software. The glass coverslip, a side wall of the parallel plate flow chamber, was coated with either vWf (a, b), insoluble type I fibrillar collagen (c, d), or soluble VITROGEN 100® collagen (e, f). The images were taken at 30 (a, c, e) or 120 seconds (b, d, f).

the exposure of a ligand-binding pocket which permits the rapid binding of vWf or fibrinogen. The integrin cytoplasmic tails seem to play an important role in inside-out signaling for controlling the activation process, because an inherited point mutation in the $\beta_3$ (GpIIIa) cytoplasmic tail can abrogate ligand binding to this receptor in response to platelet agonists [105]. A murine monoclonal IgM antibody, PAC-1, has been developed to recognize specifically the activated form of GpIIb-IIIa [106]. Binding of vWf or fibrinogen to platelet GpIIb-IIIa leads to platelet aggregation, presumably via cross-linking or bridging of GpIIb-IIIa molecules on two different platelets by these ligands.

We hypothesize that the different platelet deposition patterns on vWf and collagen coated surface result from different amounts of activated GpIIb-IIIa molecules expressed on adherent platelets on the surfaces. Some experimental results from our laboratory or other groups indicated that the initial interaction between platelet receptor GpIb-IX-V and vWf would induce signals to cause GpIIb-IIIa activation [19,20]. Nevertheless, if platelets express more activated GpIIb-IIIa with high ligand-binding affinity after contacting with immobilized vWf surface, those activated receptors may bind soluble vWf from the bloodstream and then form another vWf surface to recruit other platelets, that is, initiate thrombus formation. If true, this would appear to contradict the observations in flow chamber experiments shown previously (Figure 3.1), so the premise of the reasoning might be wrong. Because the conclusions of GpIIb-IIIa activation induced by GpIb-IX-V and vWf were made mostly in soluble vWf systems and at abnormally high shear conditions, the possible discrepancy in whether GpIb-IX-V and

vWf interaction can cause GpIIb-IIIa activation may be also due to the different experimental settings. For this reason, the hypothesis of distinct platelet activation status after interacting with immobilized vWf or collagen has been investigated, focusing on the subsequent expression of activated GpIIb-IIIa.

An effective experimental protocol is needed to examine the expression and state of the adhesive receptors after platelets adhere onto the protein-coated surface. Most of the studies concerning platelet-surface interactions are done in flow chamber systems because of the nature of the method [30-39]. The flow chamber can mimic closely the physiological hemodynamic conditions, and thrombogenic properties of various subendothelial matrix proteins are studied by coating them on the wall of the chamber. Distinct functions of different platelet receptors are investigated by adding specific monoclonal antibodies to block the interactions. However, in order to check the receptor expression on the surface of adherent platelets, large amounts of fluorescent labeled antibody for immunofluorescence staining and image processing are required; it is costly and time-consuming. On the other hand, flow cytometry provides a useful and fast tool for the quantitative analysis of platelet surface glycoproteins since many monoclonal antibodies are readily available. Platelets can be easily distinguished from other blood cells by the forward and side light scattering due to their size and granularity, and the amount of a specific surface receptor is detected by using fluorescent labeled monoclonal antibodies to that receptor. However, most of the studies using flow cytometry have been related to the effects of soluble agonists or plasma proteins on the platelet activation.

Accordingly, developing a flow cytometry protocol possible to use with immobilized proteins will be an improved way to study the number and activation state of the platelet receptors after adhering onto a protein-coated surface.

Because only small particles (< 100 μm) can flow through the measuring apparatus of the flow cytometer, the supporting surface on which proteins are immobilized should be small. Many diagnostic tests and assays have used small uniform latex particles, also called microspheres, as substrates or supports for immunologically based reactions. Studies on the interaction between latex particles and blood have contributed to the basic information for explaining the mechanisms of cell reactions, including phagocytosis of latex particles by leukocytes, hemolysis of erythrocytes, and platelet aggregation associated with phagocytosis and release reaction [107-109]. The insights gained from those investigations have helped in design and synthesis of antithrombogenic polymers. Some assays have been developed to detect platelet adhesion and aggregation to immobilized proteins on microspheres by aggregometry or electron microscopy [41-43]. Other researches examined platelet adhesion onto artificial surfaces or ligand-coated microspheres as demonstrated by flow cytometric quantification [110,111]. Therefore, it would appear appropriate to study platelet interaction with immobilized proteins by introducing protein-coated microspheres. In this study, a protocol combining flow cytometry and microsphere technology was developed to investigate platelet activation status after interacting with immobilized vWf or collagen.

After platelet receptors bind to immobilized subendothelial matrix proteins or to soluble agonists, signals may be sent inside the platelet to initiate many different biochemical signal transduction pathways and subsequent responses. For instance, when platelets are stimulated by thrombin or other agonists in the presence of radiolabeled fibrinogen and divalent cations, ligand binding is observed within seconds and reaches steady state within several minutes [112]. Almost all the binding can be reversed by compounds that stimulate production of cAMP or cGMP and reverse the platelet activation process during this time [113]. Nevertheless, if allowed to proceed for more than 10 minutes, most of the fibrinogen binding becomes irreversible and the ligand can now be recovered in the Triton X-100 insoluble cytoskeleton pellet [114]. Binding studies with a fibrinogen mimetic monoclonal antibody, PAC-1, suggest that conformation change takes place in GpIIb-IIIa in the first few seconds after platelet activation to expose binding sites for ligands [115,116]. Moreover, the actin filament function inhibitors cytochalasin D and E prevent the later, irreversible phase of fibrinogen binding to platelets, but not the earlier, reversible phase [117,118]. These observations suggest that a conformation change mechanism is the primary one responsible for the initial reversible phase of fibrinogen binding to GpIIb-IIIa, and that subsequent cytoskeletal events may contribute to the later, irreversible phase of ligand binding. *In vivo*, the intracellular signal transduction is elaborately regulated to induce the transition of platelet receptors from one adhesive phenotype to another and allow progression through different stages of adhesion, spreading, and aggregation.

Even though we have known for a decade that a conformation change converts GpIIb-IIIa into a functional adhesion receptor, the signaling pathways responsible for modulation of GpIIb-IIIa activation state have not been worked out in complete detail. Inside-out signaling may involves reactions that initiate and propagate the flow of information from agonist receptor to proximal integrin effectors, or that directly effect integrin activation. Only a broad outline of these reactions can be provided currently. In the case of some of excitatory agonists, including thrombin, ADP, epinephrine, and thromboxane $A_2$, one important consequence is activation of phospholipase Cβ (PLCβ) by the activated α subunit of the heterotrimeric (αβγ) $G_q$ protein. This reaction results in hydrolysis of phosphatidylinositol and production of the second messengers, diacylglycerol (DAG) and inositol-1,4,5-triphosphate ($IP_3$). The former product then activates protein kinase C (PKC), and the latter mediator helps to mobilize calcium from intracellular stores, such as the dense tubular system. PKC activation and intracellular $Ca^{2+}$ elevation, which may be due to the influx from extracellular stores or transport from intracellular pools, seem to be major signal elements involved in inside-out signal for GpIIb-IIIa activation. The activation of PKC and the phosphorylation of its substrates correlate well with platelet activation [119,120]; furthermore, addition of selective PKC inhibitors to permeabilized platelets prevents the activation of GpIIb-IIIa [121]. The rise in the concentration of free intracellular calcium has been shown to accompany most, if not all, functional events of platelets, including initiation of the shape change, exposure of GpIIb-IIIa receptors, release of granule contents, and development of a procoagulant

surface [122-124]. Many intracellular proteins become phosphorylated on tyrosine residues during platelet activation. Recently, evidence was shown for the involvement of the Src-family tyrosine kinase $p59^{fyn}$ and $p53/56^{lyn}$ in platelet signaling via GpVI, a collagen receptor [125]. GpVI is non-covalently associated with the homodimer FcRγ-chain [126,127], and it has been demonstrated to be the crucial receptor mediating collagen-induced platelet activation [128]. Collagen can activated platelets through a pathway involving tyrosine phosphorylation of FcRγ-chain, tyrosine kinase Syk, and phospholipase Cγ2 (PLCγ2), a similar pathway as immune receptors. The activation of PLCγ2 again causes the formation of the two important secondary messengers, DAG and $IP_3$. Even though some collagen-induced intracellular signaling pathways, especially downstream of GpVI engagement, have been described [129], their involvement in causing GpIIb-IIIa activation is not elucidated. In order to gain more insights of the inside-out signal for GpIIb-IIIa activation, some possible signal pathways that lead the conformation change of GpIIb-IIIa after platelets adhered on collagen-coated surface were examined in this study.

## 3.2 Materials and Methods

### Microsphere preparation

Human vWf was purified from normal human cryoprecipitate by glycine and sodium chloride fractionation, followed by agarose 4B column chromatography. The concentration or the antigen level of the vWf solution, calibrated against the vWf

concentration found in normal pooled plasma according to the 3rd International Reference Standard established by World Health Organization, was measured by an enzyme-linked immunoassay SPECTRO vWf (Ramco Laboratories, Inc.). A suspension of type I insoluble fibrillar collagen from bovine achilles tendon (Sigma Chemical Company) was prepared by homogenizing 1 g of the collagen in 410 ml of 0.5 M acetic acid, pH 2.8. VITROGEN 100® collagen is a sterile solution of purified, pepsin-solubilized bovine dermal collagen dissolved in 0.012 N HCl with the concentration of 3.0 mg/ml (Collagen Aesthetics, Inc.). Polystyrene microspheres with 10.0 μm in diameter, packaged in an aqueous suspension of 2.5% solids, were purchased from Polysciences, Inc.. Storage buffer for protein-coated microspheres was prepared with Dulbecco's phosphate buffered salt solution (PBS), pH 7.4, containing 10 mg/ml bovine serum albumin (BSA), 1 mg/ml sodium azide, and 5% glycerol. Citrate-phosphate buffer for vWf dilution consisted of 0.0394 M citric acid and 0.1212 M dibasic sodium phosphate, pH 5.8. The 12x75 mm polystyrene tube with 35 μm strainer cap for filtering out large microsphere aggregates in insoluble collagen coating process was obtained from Becton Dickinson Immunocytometry Systems.

The method for attachment of proteins to polystyrene microspheres was passive adsorption. For coating vWf, 12 drops (~0.5 ml) of microsphere suspensions were added to an 1.5 ml Eppendorf tube with 1 ml of the vWf solution of 200% antigen level, diluted from stock solution to with citrate-phosphate buffer. Next the microspheres and vWf were incubated for 1 hour at room temperature with gentle end-to-end mixing by a

nutator mixer. The suspension was then spun for 2 minutes in an Eppendorf micro centrifuge (15,000 rpm) and the supernatant was removed. The pellet was resuspended by vortex and washed in 1 ml of storage buffer, incubated for 30 minutes and then centrifuged for 2 minutes. The final pellet was resuspended in the storage buffer and adjusted to $2x10^7$ microspheres/ml using an electronic particle counter (Multisizer; Coulter Electronics, Inc.). It was the same procedure for coating VITROGEN 100® collagen except for adding microsphere suspensions into the collagen solution that is not diluted. For immobilizing insoluble collagen onto the microspheres, a great caution should be taken because long fibrils of collagen would cause flocculation. Some preparation steps had been modified as the following. Only 8 drops of microsphere suspensions were added to every 1 ml of collagen solution to lower the chance that microspheres would collide and be flocculated by collagen fibers. The centrifugation was done at lower g-force (250 g) for 5 minutes at 10 °C in a tabletop centrifuge (Sorvall RT 6000D; DuPont) to get a loose pellet. After the first pellet was resuspended in the storage buffer and incubated for 30 minutes, large microsphere aggregates were removed by filtering the suspensions into 12x75 mm polystyrene tubes with 35 μm strainer cap before the centrifugation. The yield of collagen-coated singlet microspheres was about 40%. Those protein-coated microsphere suspensions were stored at 4 °C.

In order to check the protein coating, purified mouse anti-human vWf and fluorescein isothiocyanate (FITC) conjugated rat anti-mouse IgG monoclonal antibodies were purchased from PharMingen; affinity purified rabbit anti-collagen type I and FITC

conjugated affinity purified Goat anti-Rabbit IgG antibodies were obtained from Rockland, Inc.. FITC, with excitation wavelength of 488 nm and emission wavelength of 520 nm, could be quantified by the FL-1 detecting channel in the flow cytometry. HEPES buffer (10 mM N-2-hydroxyethylpiperazine-N'-2-ethanesulfonic acid (HEPES), 145 mM NaCl, 5 mM KCl, 0.5 mM $Na_2HPO_4$, 1 mM $MgSO_4$, 5.5 mM glucose, and 3.5 g/l BSA, pH 7.4), filtered through 0.22 μm syringe filter, was utilized for diluting antibody solutions. Fixing solution was made with formaldehyde (final concentration 1%) and filtered Dulbecco's PBS.

The protein coating was checked by flow cytometry. 10 μl of the protein-coated microsphere suspensions were added to 20 μl of primary antibody (mouse anti-human vWf or rabbit anti-collagen type I, concentration 1 μg/20 μl) or HEPES buffer as negative control, and incubated at room temperature for 30 minutes. After that, 20 μl of FITC-labeled secondary antibody (rat anti-mouse IgG or goat anti-rabbit IgG, concentration 2 μg/20 μl) were added and incubated for 30 more minutes in the dark. The final sample, after adding 2 ml of 1% formaldehyde fixing solution to the microsphere-antibodies mixture, was measured by the FITC (FL-1) fluorescent intensity in the FACScan® flow cytometer (Becton Dickinson Immunocytometry Systems).

**Platelet preparation**

Sodium citrate solution (3.8 g/100 ml) was used as the anticoagulant. HEPES washing buffer contained 10 mM N-2-hydroxyethylpiperazine-N'-2-ethanesulfonic acid

(HEPES), 145 mM NaCl, 5 mM KCl, 0.5 mM $Na_2HPO_4$, 1 mM $MgSO_4$, 5.5 mM glucose, 3.5 g/l BSA, and 0.1 mM $CaCl_2$, pH 6.8. HEPES resuspending buffer had the same compositions as HEPES washing buffer except containing 1 mM $CaCl_2$ and adjusting pH to 7.4. ADP scavenger apyrase and platelet activation inhibitor prostaglandin $I_2$ ($PGI_2$) were purchased from Sigma Chemical Company. PKH26 red fluorescent cell linker kit (1 mM PKH26 dye stock and diluent C), also obtained from Sigma Chemical Company, was used for platelet membrane labeling. This membrane dye can be excited by the 488 nm light and emit at 567 nm, compatible with r-phycoerythrin detection (FL-2) in the flow cytometry system. The PKH26 staining process was stopped by the stopping buffer, which is basically the HEPES washing buffer containing 10 g/l BSA, pH 6.8. The fibrinogen-related tetrapeptide Gly-Pro-Arg-Pro (GPRP), purchased from Sigma Chemical Company, can prevent fibrin polymerization and fibrinogen binding to platelet via its direct binding to the fibrinogen D domain [130,131]. This tetrapeptide was utilized to differentially inhibit platelet aggregation but not interaction with immobilized vWf or collagen.

Blood was obtained by venipuncture from healthy non-smoking volunteers who had not ingested any medications for at least 10 days before donation. The blood was anticoagulated with 1/10 volume of 3.8% sodium citrate solution. Platelet-rich plasma (PRP) was obtained by spinning whole blood at 150g for 15 minutes at 25 °C. An equal volume of the citrate anticoagulant was added to PRP and the platelets were loosely pelletized by further centrifugation at 250g for 15 minutes at 25 °C [132] in the presence of

2 units/ml apyrase and 5μM $PGI_2$ [133]. The pellet (about 9-12x$10^8$ platelets) was rested in 2 ml of diluent C with 5 μM $PGI_2$ for 15 minutes and then resuspended. Immediately prior to staining, 2 ml of 4 μM PKH26 dye in diluent C was freshly prepared. The platelet suspensions were rapidly added to the dye solution and mixed by gentle pipetting. The mixture was incubated at room temperature for 10 minutes and the incubating tube was periodically inverted gently to assure mixing during this staining period. After that, 4 ml of the BSA stopping buffer was added to stop the staining reaction and let the mixture incubate for 1 minute. The sample was diluted with 7 ml of the HEPES washing buffer, including apyrase (final concentration 2 units/ml) as well as $PGI_2$ (5μM), and spun at 250g for 15 minutes at 25 °C to get the platelet pellet. The pellet was rested in 2 ml of HEPES resuspending buffer for 15 minutes and then resuspended. The final platelet suspensions were adjusted to 1x$10^8$ cells/ml with 400 μM GPRP, and incubated in the 37 °C water bath for 30 minutes before using.

**Viscometric-flow cytometric experiments**

To characterize the activation status of platelets, such as amount of activated GpIIb-IIIa and P-selectin expression after platelets adhered onto protein-coated microspheres, monoclonal antibodies for those specific surface receptors were used. The monoclonal IgM antibody specific to high affinity GpIIb-IIIa, PAC-1, was purchased from Becton Dickinson Immunocytometry Systems. The total number of GpIIb-IIIa receptors on the platelet surface was detected by anti-human CD61 IgG, specific to

integrin $\beta_3$ chain (GpIIIa), and P-selectin expression after granule release was measured by anti-human CD62P IgG. Both antibodies were obtained from PharMingen. IgG and IgM isotype control antibodies were ordered from PharMingen and Sigma Chemical Company respectively. All those antibodies are conjugated with FITC, suitable for flow cytometry FL-1 detection. Human α-thrombin (Sigma Chemical Company) was used to stimulate the platelets as a positive control.

Some chemicals were used to check the inside-out signal transduction pathways for GpIIb-IIIa activation. Cytoskeleton disrupter cytochalasin D, inhibiting the agonist-induced polymerization of new actin filaments and depolymerizing the existing actin filaments at higher concentrations, was purchased from Sigma Chemical Company. PP1 is a potent and selective inhibitor of the Src family of protein tyrosine kinases; SKF-96365 inhibits receptor-mediated $Ca^{2+}$ entry in activated platelets at concentrations that do not affect internal $Ca^{2+}$ release; TMB-8 is an intracellular $Ca^{2+}$ antagonist that blocks the release from intracellular stores, used to discern dependence on intracellular versus extracellular $Ca^{2+}$ (Alexis Biochemicals). Staurosporine, a general protein kinase C inhibitor, was obtained from Calbiochem. Cytochalasin D, PP1 and staurosporine were first dissolved in dimethyl sulfoxide (DMSO), which was diluted at a final concentration of less than 0.2% to prevent its effect on platelets. All other chemicals were dissolved in deionized water.

Before the experiment, the cone and platen of the rotational viscometer (Ferranti-Shirley 781; Ferranti Electric Inc.) were treated with 1% Prosil 28® (PCR Research

Chemicals), the organic silicon coating inhibiting platelet-device surface interactions. 250 μl of PKH26 stained platelet suspensions ($1x10^8$ cells/ml) and 250 μl of protein-coated microsphere suspensions ($2x10^7$ particles/ml) were put into the viscometer and sheared at uniform shear rate of 100 $sec^{-1}$ for 5 minutes at 37 °C to mix and allow platelet-microsphere interactions. After shearing, 10 μl of the sample was added to each tube containing 40 μl of specific antibody solution, including either PAC-1 (12.5 μg/ml), anti-human CD61 (1.5 μg/ml), anti-human CD62P (6.25 μg/ml), IgG isotype control (6.25 μg/ml), or IgM isotype control (12.5 μg/ml). These concentrations used had been titrated so that the antibodies could saturate the receptor binding sites. After 15-minute incubation in the dark at room temperature, the sample-antibody mixture was fixed by adding 2 ml of 1% formaldehyde. The final samples could be examined immediately by flow cytometry, or kept in 4 °C and analyzed within 24 hours. The positive control sample for platelet activation was obtained by adding α-thrombin (final concentration 1 unit/ml) to the platelet suspensions, incubating stagnantly in 37 °C for 10 minutes, and labeling with FITC-conjugated specific antibodies as mentioned above. To check the inside-out signal pathway for GpIIb-IIIa activation after platelet adherence on collagen surfaces, individual inhibitors (cytochalasin D 10 μM, PP1 10 μM, staurosporine 500 nM, SKF-96365 100 μM, TMB-8 250 or 500 μM) were added to the platelet suspensions for 20-minute incubations before mixing with collagen-coated microspheres.

The microsphere population could be easily distinguished from the platelet region in the forward light scattering (FSC) and side light scattering (SSC) plot because of the

particle size and granularity. The criterion of 5,000 events within the microsphere population or 6 minutes, depending on which was reached first, was set for data acquisition. The measurements of FSC, SSC, FL-1 (FITC fluorescence), and FL-2 (PKH26 fluorescence) intensities were stored and could be analyzed later by using software CELLQuest (Becton Dickinson Immunocytometry Systems).

**Representative index calculation**

To show the platelet activation status quantitatively, two representative indexes were calculated from the flow cytometric data. An illustration of the flow cytometric methodology is given in Figure 3.2. Microsphere singlets are gated (R2) in the FSC vs. SSC diagram (Figure 3.2(a)), and then the fluorescent intensities of those events are plotted in the FL-1 vs. FL-2 diagram (Figure 3.2(b)). In the FSC vs. SSC dot plot, the microsphere population is easily recognized at right higher region (R1) and the platelet population is at the left lower region (R3). There are sub-populations of microspheres such as singlets and doublets because platelets may form the bridges for microsphere aggregation; yet the analysis will focus on the singlet sub-population at the left bottom corner (R2). Otherwise, the autofluorescence of the second or even the third microsphere may be misinterpreted as more platelet adhesion and receptor expression. In the FL-1 vs. FL-2 dot plot, the ordinate describes the fluorescent intensity of PKH26 dye linking into the membrane of the adherent platelets on the microsphere singlet; the abscissa represents the fluorescent intensity of FITC-conjugated antibodies binding to surface receptors of

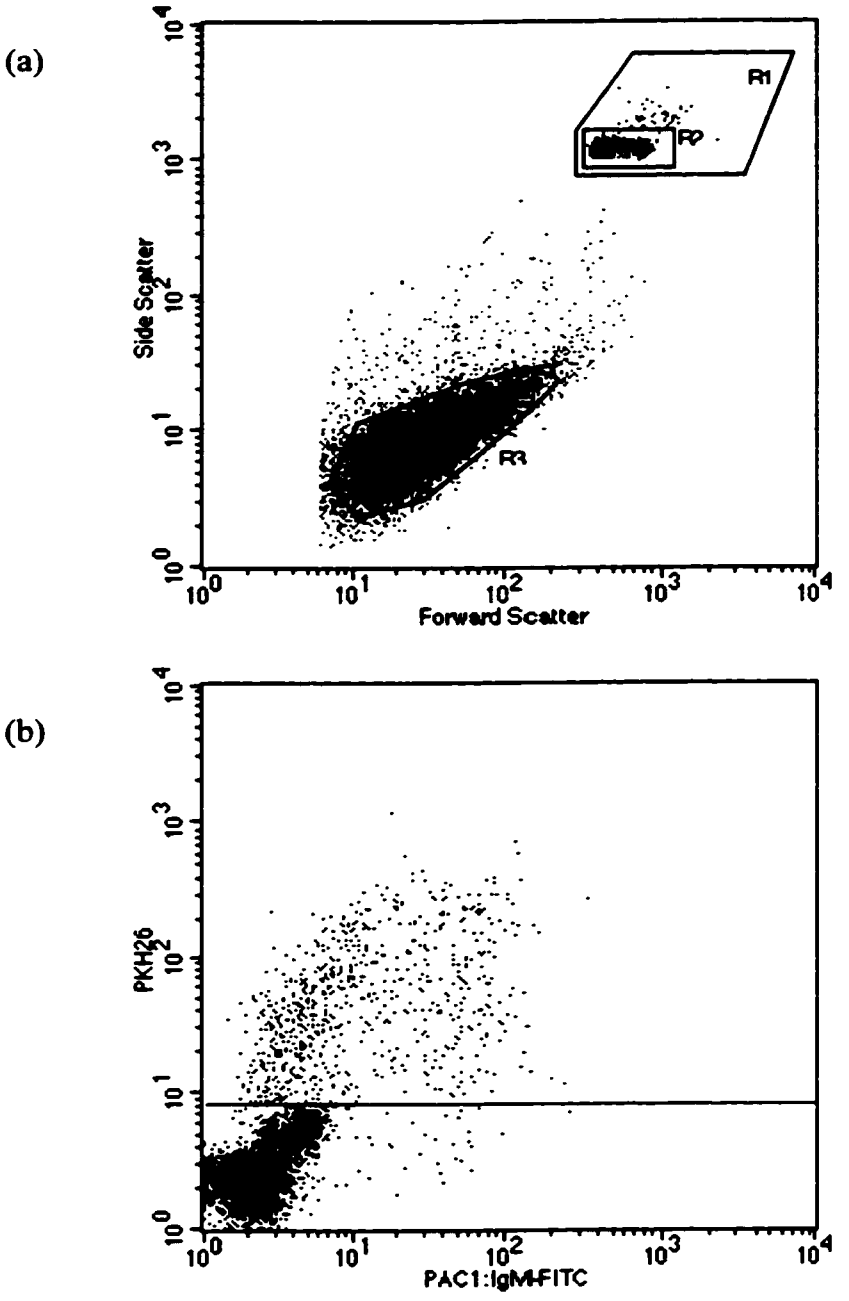


Figure 3.2 Flow cytometric analysis for platelet activation statuses. (a) is a forward scatter vs. side scatter dot plot. The microsphere population is within R1 and singlets are gated in R2. Platelets are located in R3. (b) is a fluorescent FL-1 (FITC) vs. FL-2 (PKH26) dot plot of the singlet microsphere population (R2). The dense population at the left bottom corner indicates the singlet microspheres without platelet association. The singlet microsphere on which platelets have adhered is shown as a dot above the horizontal line.

the adherent platelets on the microsphere singlet. A horizontal line is drawn based on the FL-2 autofluorescence of the microsphere singlet. Therefore, the dense population under the line in the left bottom corner shows the microspheres without platelet association; on the other hand, the scattered dots above the line indicate positively that platelets have adhered onto those microspheres. If the dot tends toward the right, it means that more receptors are expressed on the platelet surface and FITC-labeled antibodies have bound to them.

The geometric means of the FL-1 and FL-2 fluorescent intensity for the data above and below the horizontal line, in other words, microspheres with and without platelet association respectively, are used to quantify the amount and activation of the platelet receptors after adhering on the protein-coated surface. Because 5 different antibodies (PAC-1, anti-CD61, anti-CD62P, IgG isotype control, and IgM isotype control) are utilized to label the interested receptors on the adherent platelets, 5 similar diagrams can be generated for each run of the experiments. The fluorescent intensity for the average number of adherent platelets on the protein-coated microspheres ($Y$) is estimated by subtracting the autofluorescence of the microsphere, which is the mean of the ordinate values for the data below the line, from the mean of the ordinate values for those events above the line. The fluorescent intensity for the average number of those surface receptors detected by FITC-labeled antibodies, for example, activated GpIIb-IIIa receptors detected by antibody PAC-1 ($X_{\text{PAC-1}}$), is estimated by the difference between the mean of the abscissa values for those data above line in the FL-1 vs. FL-2 plot for PAC-1

and the mean measured in the plot for IgM isotype control, which indicates the non-specific binding of antibodies. The PAC-1 antibody only recognizes the GpIIb-IIIa with an activated conformation, but the mouse anti-human CD61 antibody can bind to all the GpIIb-IIIa integrins; as a result, the percentage of the activated GpIIb-IIIa shown on the adherent platelet surface is proportional to the *index1*,

$$index1 = \frac{X_{\text{activated GpIIb-IIIa}}}{X_{\text{total GpIIb-IIIa}}} = \frac{X_{\text{PAC-1}}}{X_{\text{anti-CD61}}},$$

There is a multiplying factor, the ratio of the fluorescent intensities of those FITC-labeled antibodies, between the index1 and the exact percentage; however, this factor will be a constant when the same batches of antibodies for all experiments are used. Therefore, the *index1* is a good analogue for the percentage of the activated GpIIb-IIIa shown on the adherent platelet surface. Because P-selectin is normally expressed on the surface of platelets only after platelets are activated and release granular contents, the P-selectin expression on the thrombin-treated platelet singlet is used as a reference. For each PKH26-stained platelet preparation, the geometric means of the fluorescent intensity for PKH26 ($Y_{\text{thr}}$) and FITC-labeled anti-CD62P ($X_{\text{thr}}$) on the thrombin-activated platelet singlets are recorded. Therefore, the P-selectin expression on the surface of the adherent platelets can be calculated as *index2*,

$$index2 = \frac{\text{P - selectin on an adherent platelet}}{\text{P - selectin on a thrombin - activated platelet}} = \frac{X_{anti-CD62P}/Y}{X_{thr}/Y_{thr}},$$

with the value for the thrombin-activated platelet equal to 1.

**Aggregometry experiments**

As a complementary functional study for the possible inside-out signal pathways of GpIIb-IIIa activation, effects of different inhibitors on collagen-stimulated platelets were investigated in the turbidometric platelet aggregometry. Platelet-rich plasma (PRP) was obtained as in the procedure mentioned earlier; the platelet concentration was then adjusted to $2x10^8$ cells/ml with HEPES buffer (10 mM HEPES, 145 mM NaCl, 5 mM KCl, 0.5 mM $Na_2HPO_4$, 1 mM $MgSO_4$, 5.5 mM glucose, 3.5 g/l BSA, and 1 mM $CaCl_2$, pH 7.4). About 1 ml of the platelet suspensions was further spun in an Eppendorf micro centrifuge to get platelet-poor plasma (PPP). The aggregometer (Dual Sample Aggregation Meter DP-247E; Sienco, Inc.) was prewarmed to 37 °C and adjusted for 100% aggregation using PPP and 0% aggregation using PRP. Before adding to a cuvette, PRP was incubated with different inhibitors, including cytochalasin D (10 or 20 μM), PP1 (10 or 20 μM), staurosporine (0.5 or 1 μM), SKF-96365 (100 or 200 μM) and TMB-8 (250 or 500 μM), for 20 minutes at room temperature. To measure platelet aggregation, 400 μl of PRP was added to a cuvette in the aggregometer and stirred at a rate of 1,000 rpm by means of a silicon-coated stir bar. After 1 minute stirring, collagen reagent (final concentration 10 mg/ml; from equine tendon; Helena Laboratories) was rapidly added and the resulting change in platelet aggregation over time was recorded for 4 more minutes.

**Statistical analysis**

Results are reported as the mean ± SEM. Two-factor (treatment, platelet preparation) analysis of variance (ANOVA) is carried out to determine the statistical significance of differences between means. The multiple comparison procedure Fisher's Protected Least Significant Difference (PLSD) test is used to determine which pair(s) of means are significantly different. All significance levels are set as 0.05.

## 3.3 Results

**Preparations of microspheres and platelets were suitable for the viscometric-flow cytometric experiments.**

The protein coating was checked by flow cytometry. The results (Figure 3.3) show that vWf, type I insoluble fibrillar collagen, and soluble VITROGEN 100® collagen were effectively adsorbed onto polystyrene microspheres. The distribution of the insoluble collagen immobilization is broader because the collagen fibrils are longer than the diameter of the microsphere, observing the immobilized fibrils on glass slide and microspheres by optical microscope, and a few long fibrils may make a difference in antibody detection.

In order to verify that we did not stimulate platelets much in the preparation so that we could further study platelet activation, we compared the expressions of activated GpIIb-IIIa and P-selectin on PKH26 stained washed platelets with those on platelets in platelet rich plasma (Figure 3.4(a) and (b)). After PKH26 staining and pelletizing twice,

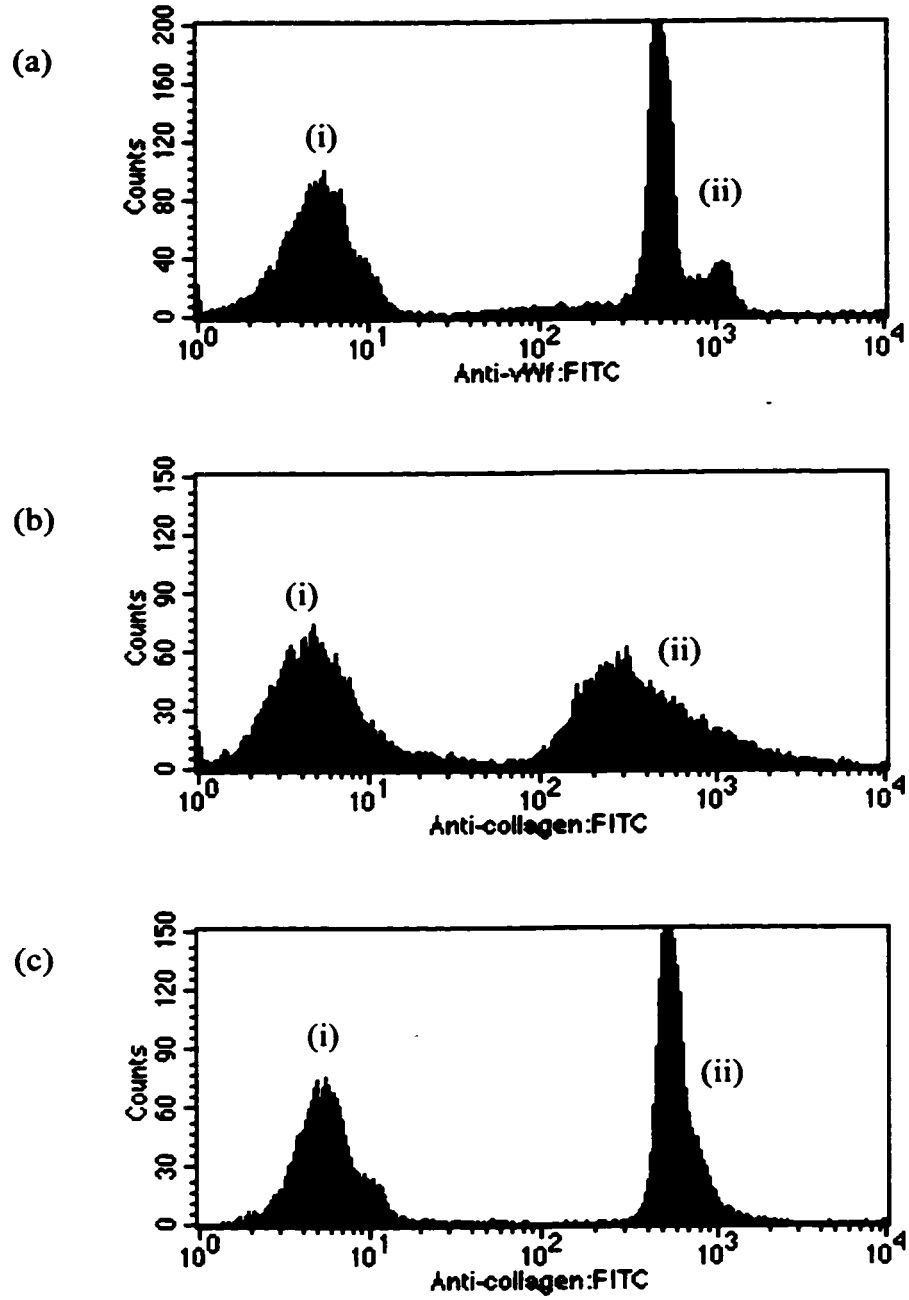


Figure 3.3 Histograms of protein coatings. The protein immobilization on microspheres is examined by using purified monoclonal antibodies specific for vWf or type I collagen and FITC-conjugated secondary antibodies. (a), (b), and (c) are the histograms of FITC fluorescent intensities of the microsphere singlets coated with vWf, insoluble type I fibrillar collagen, and soluble VITROGEN 100® collagen respectively. The peak (i) in each plot is the control, incubating with HEPES buffer instead of protein-specific antibodies. The peak (ii) shows that vWf or collagen is immobilized on microspheres positively.

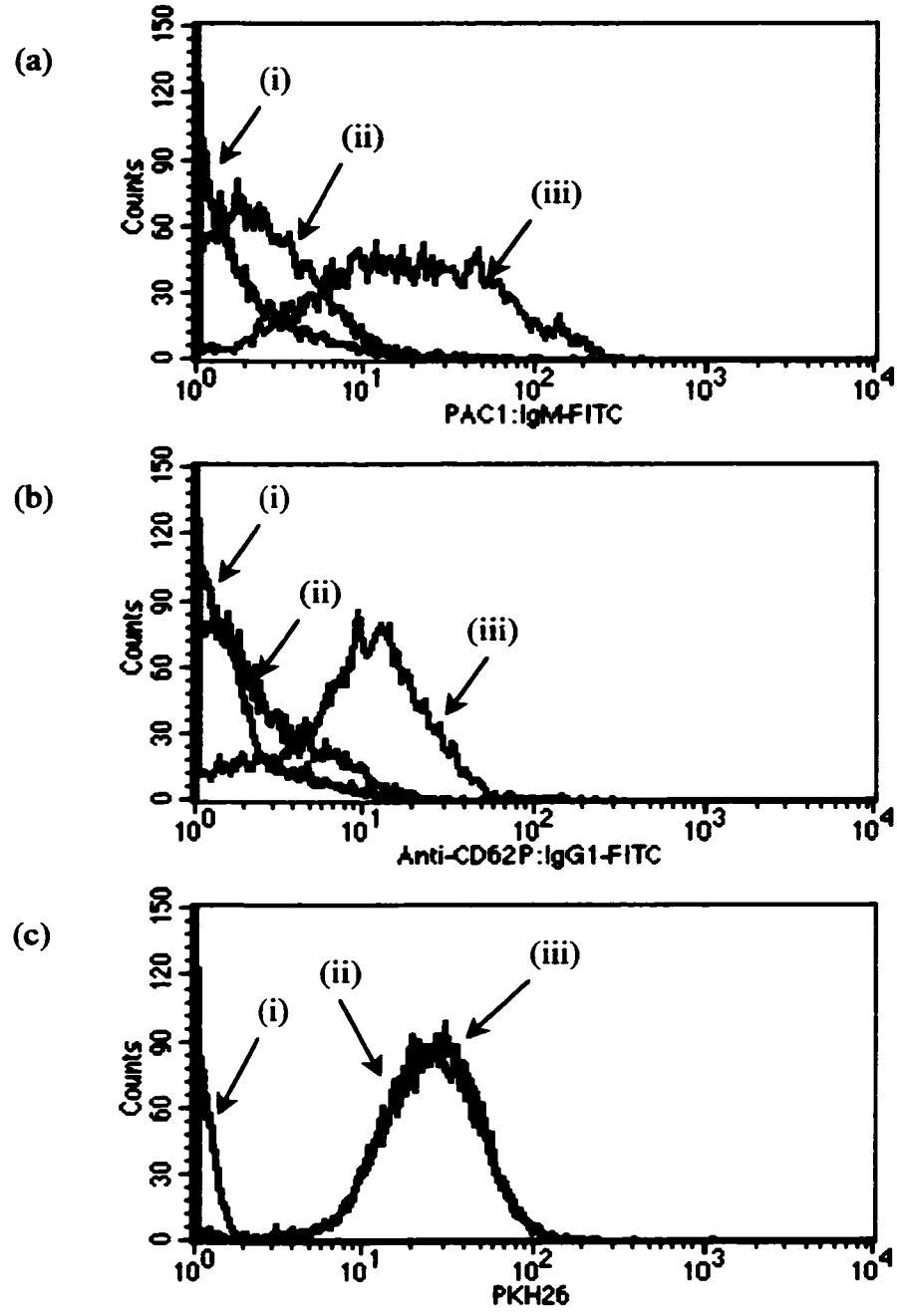


Figure 3.4 Platelet preparation. Platelets are stained with red membrane dye PKH26 and washed. The surface expressions of activated GpIIb-IIIa receptors, P-selectin, and the PKH26 staining are shown in plots (a), (b), and (c) respectively. These platelet surface receptors are detected by FITC-conjugated monoclonal antibodies specific to them. The histogram of stained washed platelets (curve (ii)) is compared with those of the rest platelets in PRP (curve (i)) and the stained washed platelets that are stimulated with 1 unit/ml α-thrombin (curve (iii)).

platelets did express some high affinity GpIIb-IIIa receptors and P-selectin molecules on their surface because the histogram shift to the right, even though we added prostaglandin $I_2$ to keep them quiescent and apyrase to prevent ADP-induced activation. However, those prepared platelets were not fully activated if we compared these with the activated GpIIb-IIIa and P-selectin expressions after stimulating them by 1 unit/ml α-thrombin, assumed to be the maximum activation state, there were still distinguishable differences. The optical setting in the FACScan® flow cytometer could detect the fluorescence of the PKH26 staining and there was a big distinction between fluorescent intensities of the unstained and stained platelets (Figure 3.4(c)). The membrane PKH26 fluorescence seemed not to be affected by platelet activation and this is good for quantifying the number of adherent platelets, unlike some conventional platelet detecting systems based on fluorescent labeled antibody binding to the platelet surface receptor whose expression is activation dependent and which may be also involved in the adhesion process. The fluorescence of the PKH26 stained platelet is also intense enough to set apart from the auto-fluorescence of microspheres, ranging from 1 to 10 with the geometric mean of about 2.5, so there will be a distinguishable fluorescent shift after platelets adhere onto the protein-coated microspheres.

**Platelets expressed more activated GpIIb-IIIa receptors and P-selectin molecules after adhering onto the immobilized type I insoluble fibrillar collagen.**

The interaction between platelets and protein-coated microsphere singlets and the status of platelet activation were analyzed in FL-1 (detecting FITC fluorescence) vs. FL-2 (detecting PKH26 fluorescence) flow cytometric plots. The typical results are shown in Figures 3.5 and 3.6. The dense population at the bottom left corner and those events above the horizontal criterion line indicate the microsphere singlets without and with platelet association respectively. Generally, there were more vWf-coated microspheres (about 40%) on which platelets adhered, so more events occurred above the line. In contrast, VITROGEN 100® collagen-coated microspheres were not very adhesive in this experimental setting and platelet association was usually less than 10%. Since FITC-conjugated monoclonal antibody PAC-1 binds to high affinity GpIIb-IIIa receptors (Figure 3.5) and the anti-human CD62P antibody recognizes P-selectin released from α granules to platelet surface (Figure 3.6), the dots will move toward right with higher FITC fluorescent intensity if there are more of those adhesion molecules expressed on adherent platelet surface. It is obvious that the adherent platelets on immobilized type I insoluble fibrillar collagen tend to express more activated GpIIb-IIIa receptors and P-selectin molecules from the FL-1 vs. FL-2 plots.

More quantitative indexes were calculated to compare the platelet activation status after interacting with immobilized vWf or collagen. Because the increase of FITC fluorescence in those events may result from more adherent platelets on a microsphere or more receptors shown on the individual platelet surface, those fluorescent intensity data need to be normalized or compared to a reference. *Index1* is a ratio of the population

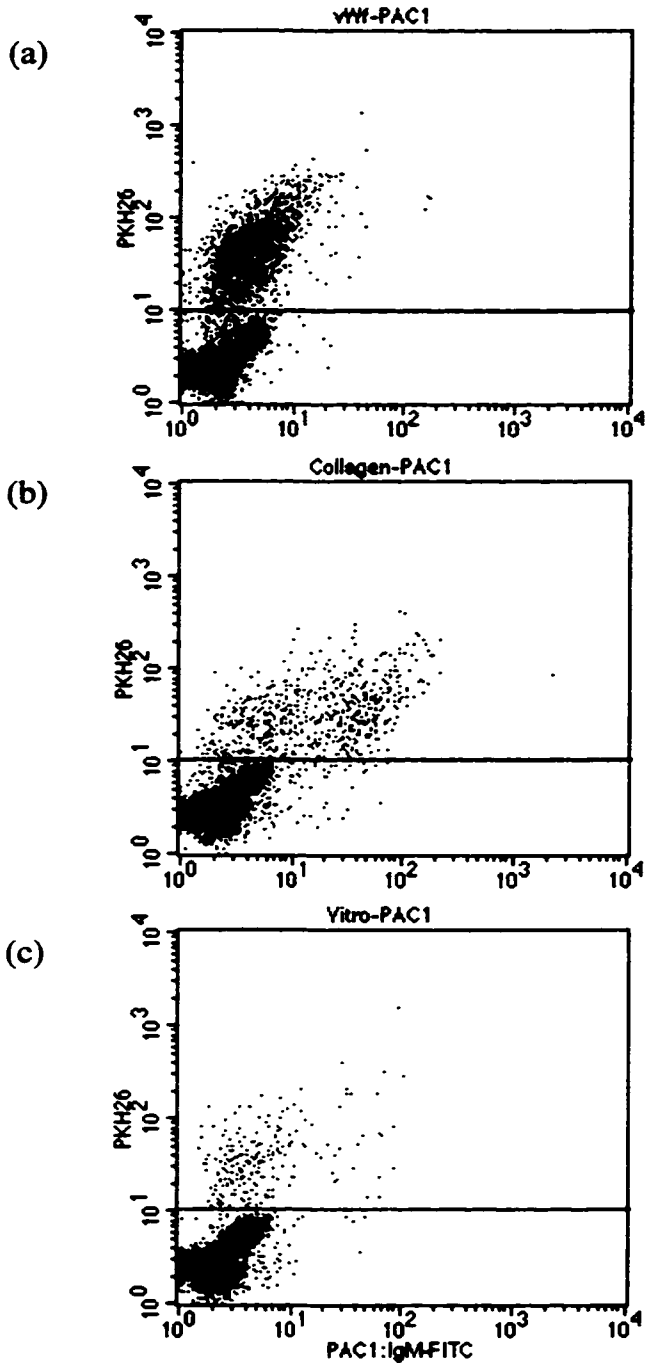


Figure 3.5 Flow cytometric dot plots of activated GpIIb-IIIa expression after platelets adhere on protein-coated microspheres. Activated platelet GpIIb-IIIa is detected by FITC-conjugated monoclonal antibody PAC-1, and the FL-1 vs. FL-2 dot plot of the microsphere singlets is shown. Typical results for activated GpIIb-IIIa expression after platelets adhere on microspheres coated with vWf, insoluble type I fibrillar collagen, and soluble VITROGEN 100® collagen are shown in (a), (b), and (c) respectively.

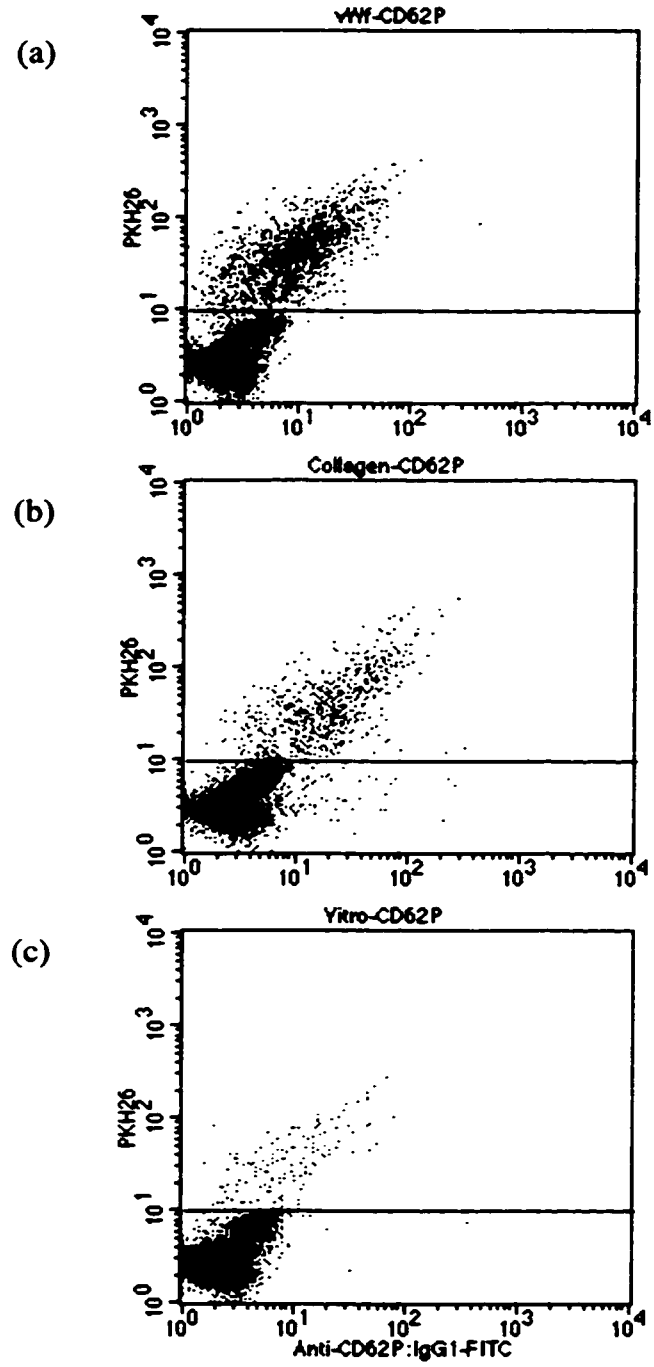


Figure 3.6 Flow cytometric dot plots of P-selectin expression after platelets adhere on protein-coated microspheres. P-selectin is detected by FITC-conjugated monoclonal mouse anti-human CD62P antibody, and the FL-1 vs. FL-2 dot plot of the microsphere singlets is shown. Typical results for P-selectin expression after platelets adhere on microspheres coated with vWf, insoluble type I fibrillar collagen, and soluble VITROGEN 100® collagen are shown in (a), (b), and (c) respectively.

mean of the fluorescence by activated GpIIb-IIIa specific antibody to that by GpIIIa specific antibody; therefore, it is a good analogue for the percentage of the activated forms in total GpIIb-IIIa receptors shown on the adherent platelet surface. *Index2* is a ratio of the average fluorescence by P-selectin specific antibody on each adherent platelet to that for a α-thrombin treated platelet. The comparisons of the platelet activation status after adhering on vWf-, insoluble collagen-, and soluble VITROGEN 100® collagen-coated microspheres are shown in Figures 3.7 and 3.8. Platelets indeed expressed significantly higher percentage of activated GpIIb-IIIa receptors and number of P-selectin molecules after interacting with immobilized fibrillar collagen surface than with other two surfaces ($p < 0.001$). Platelets adhered on soluble VITROGEN 100® collagen-coated microspheres also expressed slightly more adhesion molecules than those on immobilized vWf surface did ($p = 0.0891$ for *index1*; $p = 0.0060$ for *index2*).

**Intracellular $Ca^{2+}$ antagonist TMB-8 inhibited expressions of activated GpIIb-IIIa and P-selectin after platelets adhered onto the immobilized type I insoluble fibrillar collagen.**

The signaling pathways responsible for platelet activation after interacting with immobilized collagen have not been resolved. Some inhibitors that interrupt possible mechanisms were used to study the inside-out signal transduction pathways for the modulation of GpIIb-IIIa and the expression of P-selectin. Figures 3.9 and 3.10 present the effects of those inhibitors on platelet activation status represented as *index1* and

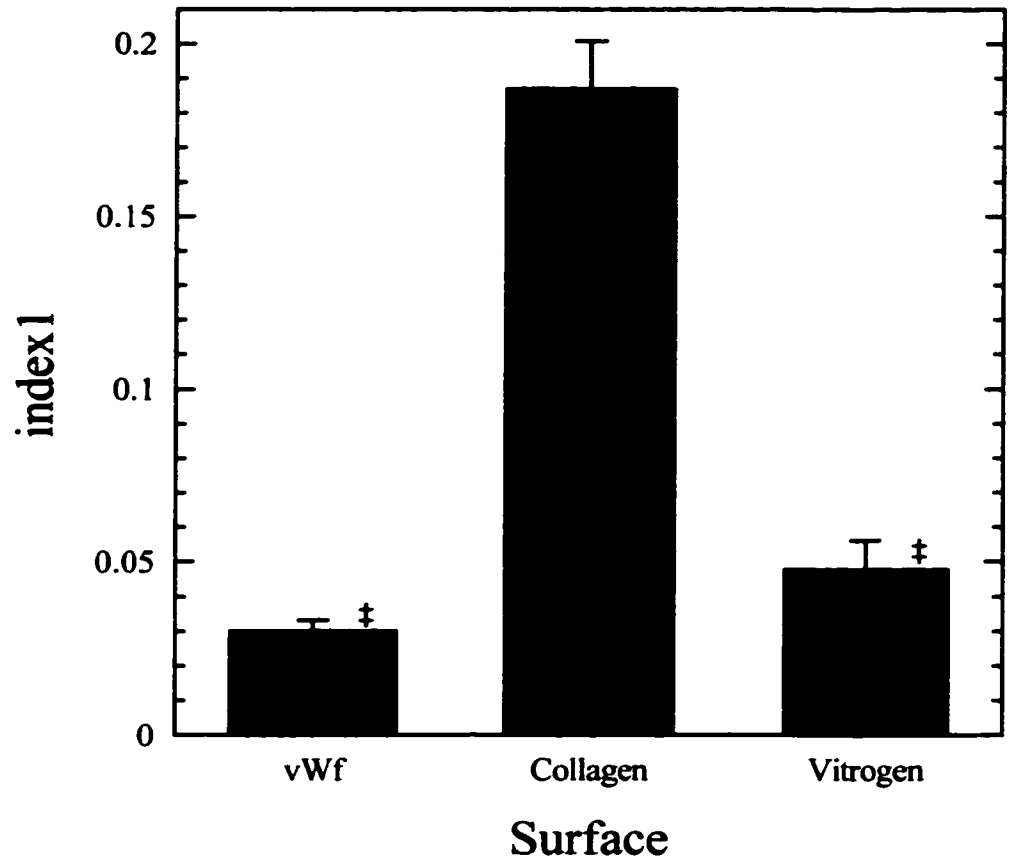


Figure 3.7 Comparison of the *index1* values after platelets adhere on protein-coated microspheres. *Index1*, an analogue for the percentage of the activated forms in total GpIIb-IIIa receptors shown on the adherent platelet surface, is calculated from flow cytometric data. Values are shown as means ± SEM, n = 9-10. The *index1* for the platelets adhering on the immobilized type I fibrillar collagen is significantly larger than that on vWf or VITROGEN 100® collagen. (‡ indicates that means are statistically different compared to the value of the fibrillar collagen surface, $p < 0.001$.)

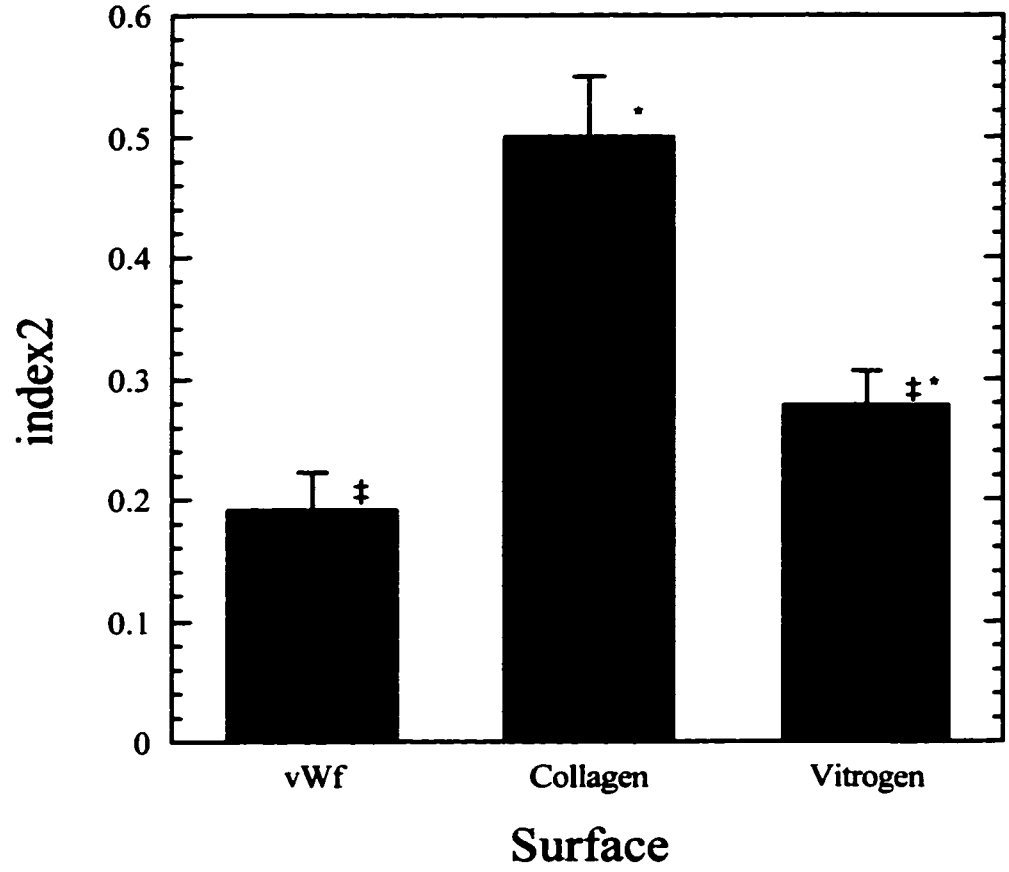


Figure 3.8 Comparison of the *index2* values after platelets adhere on protein-coated microspheres. *Index2*, a ratio of P-selectin expression on each adherent platelet to that on a α-thrombin treated platelet, is calculated from flow cytometric data. Values are shown as means ± SEM, n = 8-9. The *index2* values for the platelets adhering on the immobilized vWf, type I fibrillar collagen, and VITROGEN 100® collagen are significantly different to each other. (‡ compared to the value of the fibrillar collagen surface, $p < 0.001$; * compared to the value of the vWf surface, $p < 0.01$.)

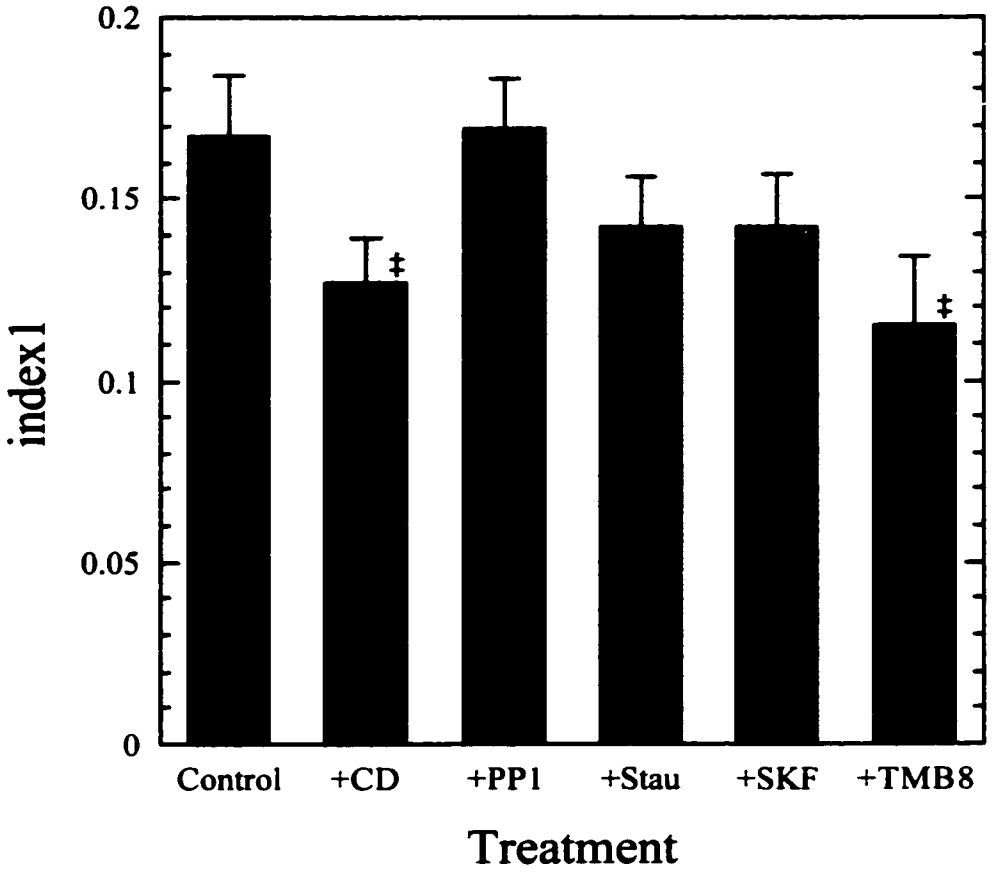


Figure 3.9 Effects of various signal transduction inhibitors on activated GpIIb-IIIa expression after platelets adhere on immobilized type I fibrillar collagen. *Index1* is calculated from flow cytometric data. Values are shown as means ± SEM, n = 6-8. Intracellular $Ca^{2+}$ inhibitor TMB-8 (250 μM) and cytoskeleton disrupter cytochalasin D (CD; 10 μM) have significantly effects on the collagen-induced expression of activated GpIIb-IIIa receptors on platelet surface that is represented by *index1*. (‡ indicates that means are statistically different compared to the value of the control sample without any inhibitor treatment, $p < 0.05$.) On the other hand, selective Src protein tyrosine kinase inhibitor PP1 (10 μM), receptor-mediated $Ca^{2+}$ entry blocker SKF-96365 (100 μM), and general protein kinase C antagonist staurosporine (500 nM) have no significant effect on *index1*.

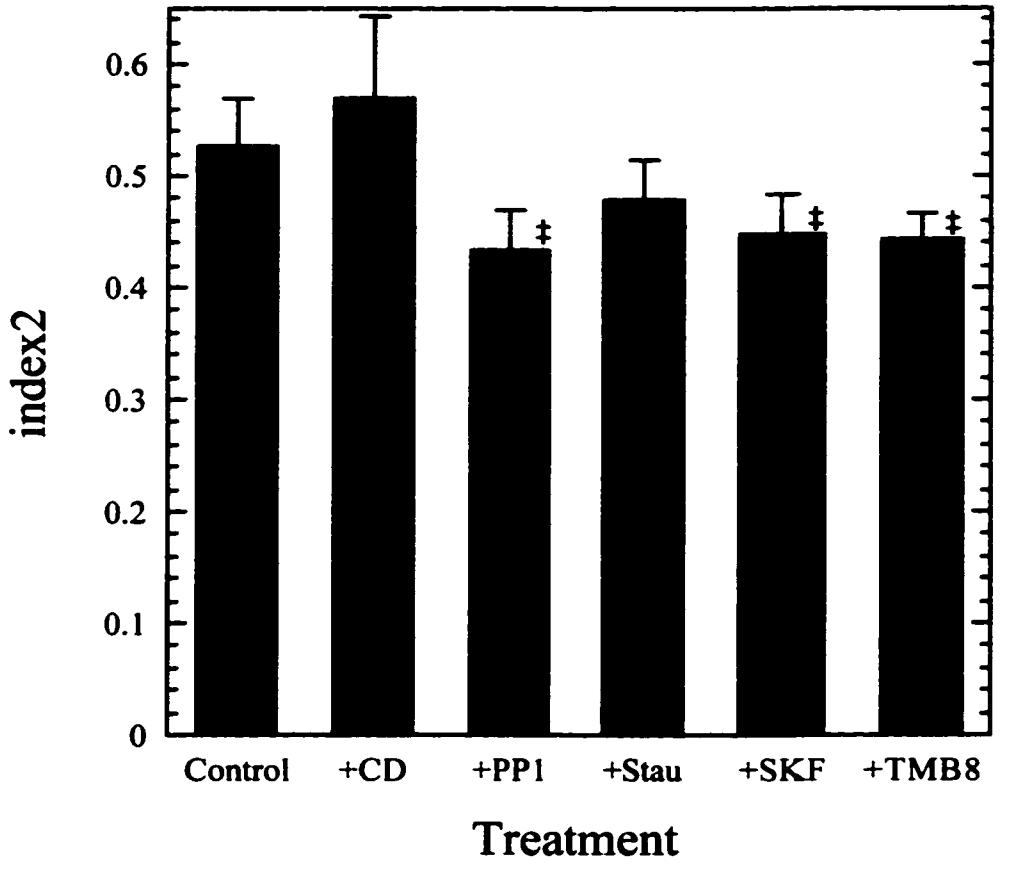


Figure 3.10 Effects of various signal transduction inhibitors on P-selectin expression after platelets adhere on immobilized type I fibrillar collagen. *Index2* is calculated from flow cytometric data. Values are shown as means ± SEM, n = 5-6. The inhibitors and their concentrations are used as describing in Figure 3.9. TMB-8, PP1, and SKF-96365 have significantly effects on the collagen-induced expression of P-selectins on platelet surface that is represented by *index2*. (‡ indicates that means are statistically different compared to the value of the control sample without any inhibitor treatment, $p < 0.05$.) However, cytochalasin D and staurosporine have no significant effect on *index2*.

*index2*. Platelets seem to have a robust signal transduction network to induce activation in response to adhesion onto the collagen surface because those inhibitors decreased the indexes either a little (15-30%) or none. However, the intracellular $Ca^{2+}$ antagonist TMB-8 that blocks the $Ca^{2+}$ release from intracellular stores inhibited both expressions of activated GpIIb-IIIa and P-selectin ($p = 0.0019$ for *index1*; $p < 0.001$ for *index2*). The cytoskeleton disrupter cytochalasin D had a negative effect on high affinity GpIIb-IIIa expression ($p = 0.0109$). On the other hand, the receptor-mediated $Ca^{2+}$ entry inhibitor SKF-96365 and the selective Src protein tyrosine kinase inhibitor PP1 blocked the P-selectin release from $\alpha$ granules to platelet surface ($p < 0.05$). Staurosporine, a general protein kinase C inhibitor, had no effect on the collagen-induced platelet activation as monitored by activated GpIIb-IIIa and P-selectin expressions.

**Intracellular $Ca^{2+}$ antagonist TMB-8 also inhibited platelet aggregation in turbidometric platelet aggregometry.**

Platelet-rich plasma (PRP) incubated with various signal transduction pathway inhibitors was tested in the in turbidometric platelet aggregometry as a complementary functional study for the possible collagen-induced inside-out signals of GpIIb-IIIa receptor activation. The effects of those antagonists with the same or twice amounts as that used in the flow cytometric experiment were tested. Typical aggregation curves are shown in Figure 3.11. Only the intracellular $Ca^{2+}$ antagonist TMB-8 partially inhibited platelet aggregation at 250 $\mu$M and almost totally blocked it at higher concentration (500

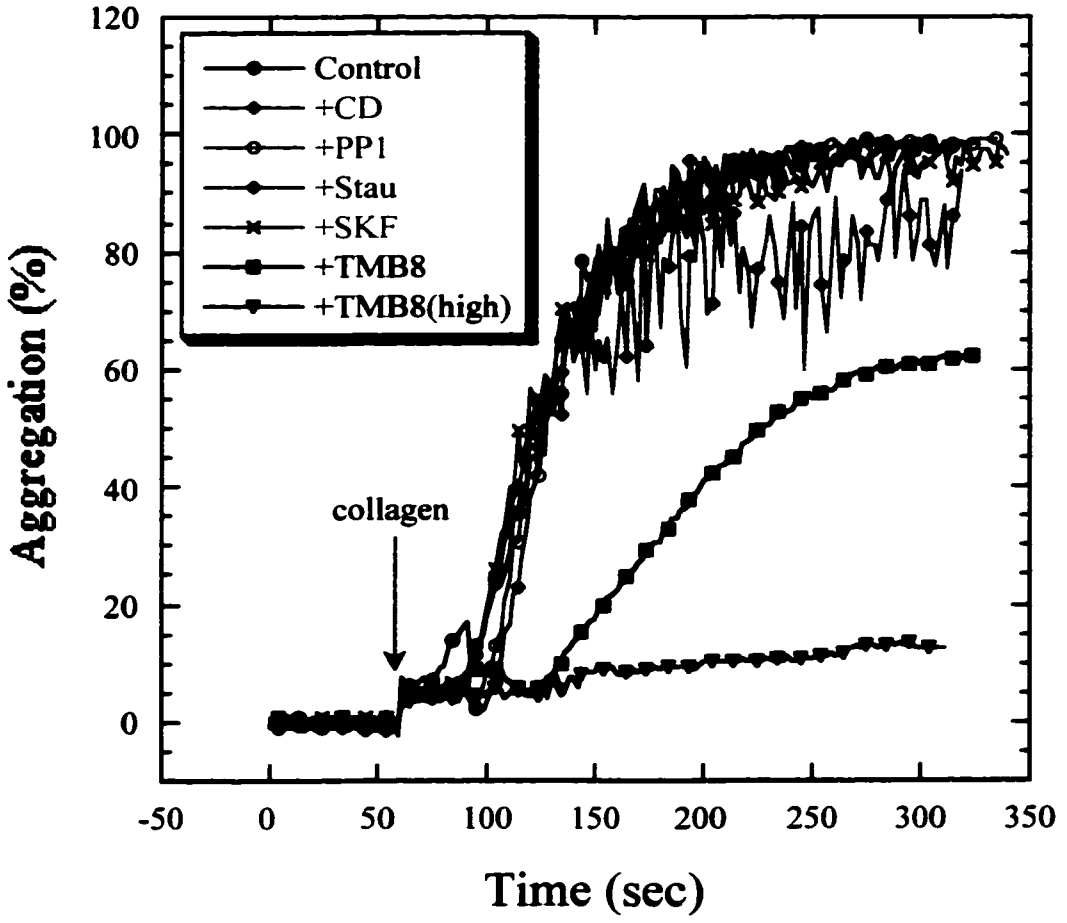


Figure 3.11 Effects of various signal transduction inhibitors on the collagen-induced platelet aggregation. The turbidometric platelet aggregometry is performed as a complementary functional study to the flow cytometric experiment. The signal pathway antagonists and their concentrations, as describing in Figure 3.9, were added into platelet-rich plasma (PRP) and incubated for 20 minutes. The collagen reagent was added into PRP after stirring at 1000 rpm for 1 minute in an aggregometer, and the response of platelet aggregation was recorded for 4 more minutes. Data were acquired every 2 seconds but for clarity only 20% of the points are marked. Typical aggregation curves are shown here (n = 3). Out of 5 different inhibitors, only 250 μM TMB-8 partially inhibit platelet aggregation. Twice amounts of those inhibitors were also tested but the curves showed the same trends. However, 500 μM TMB-8 could inhibit platelet aggregation almost completely.

μM). Cytochalasin D could not inhibit platelet aggregation; but the aggregates seemed not to be stable, as the light transmittance curve oscillated. These results are consistent with the findings in the previous viscometric-flow cytometric experiments.

**Higher concentration of TMB-8 further inhibited P-selectin expression.**

In order to examine the effect of higher dose (500 μM) of intracellular $Ca^{2+}$ inhibitor TMB-8 on platelet activation status after adhering onto the immobilized type I insoluble fibrillar collagen, more viscometric-flow cytometric experiments were performed. The results are presented in Figure 3.12. Compared to 250 μM TMB-8 treatment, higher concentration of TMB-8 further inhibited P-selectin expression ($p = 0.0015$ for *index2*) but not the percentage of activated GpIIb-IIIa.

## 3.4 Discussion

Many *in vitro* experiments have shown that platelets respond differently after interacting with immobilized extracellular matrix proteins, such as singlet adhesion on vWf and large aggregate formation on fibrillar collagen. In this study, we found a possible mechanism that could explain the phenomena. After platelets first adhere onto immobilized type I fibrillar collagen, more high affinity GpIIb-IIIa receptors and P-selectin molecules are expressed on the platelet surface. Activated GpIIb-IIIa can bind soluble vWf and fibrinogen molecules from the plasma and form another thrombogenic surface, thus recruiting other platelets to aggregate on top of the adherent platelets. The

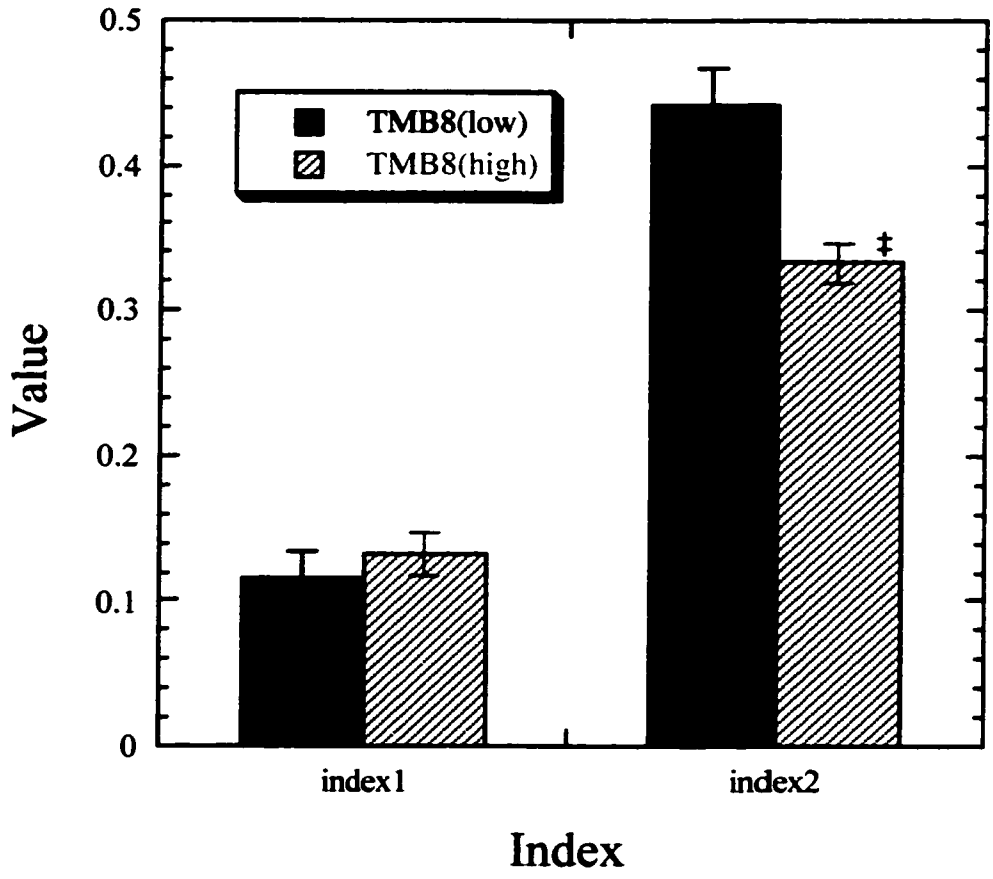


Figure 3.12 Comparison of the effects of low (250 μM) and high (500 μM) concentrations of TMB-8 on platelet activation statuses after platelets adhere on immobilized type I fibrillar collagen. *Index1* and *index2* are calculated from flow cytometric data. Values are shown as means ± SEM, n = 6. Higher dose of TMB-8 has the same effect on the collagen-induced expression of activated GpIIb-IIIa receptors on platelet surface that is represented by *index1*. However, this treatment further inhibits the expression of P-selectins that is represented by *index2*. (‡ indicates that the mean is statistically different compared to the value of lower TMB-8 treatment, $p < 0.01$.)

P-selectin, as well as vWf and fibrinogen released from α granules may also help in aggregation processes. The translocation of a subpopulation of GpIIb-IIIa associated with the actin cytoskeleton and from an intracellular source, probably α granules [134], may have a special function in platelet aggregation. In contrast, platelets express fewer activated GpIIb-IIIa receptors and P-selectin molecules after interacting with immobilized vWf, resulting in only singlet adhesion.

The current dogma that platelet GpIb-IX-V and vWf interaction leads to GpIIb-IIIa activation may not be always true. This belief is based on the observations of platelets, whose GpIIb-IIIa receptors are functionally blocked, transiently tethering and rolling on vWf-coated surface in flow chamber experiments [76], as well as those of soluble vWf binding onto platelet surface at abnormally high shear rates in viscometry experiments [77]. There is no doubt that GpIIb-IIIa can reinforce the interaction between GpIb-IX-V and immobilized vWf to form firm adhesion, especially under high shear conditions. However, to what extent the activated GpIIb-IIIa is enough to support the function is unknown and further investigation is needed. At extremely high shear conditions, the binding of soluble vWf to GpIb-IX-V induces some signal transduction in the platelets, such as $Ca^{2+}$ elevation [19,20], yet there is no direct evidence that those signals cause the conformation change of GpIIb-IIIa. In addition, platelets may have been activated by shear stress somehow in those experimental conditions, probably via the modulation of GTPase activities of G proteins [135]. There were data shown that more high affinity GpIIb-IIIa receptors expressed on platelet surfaces after adhering on vWf-

coated surface in static conditions than those in the presence of platelet activation antagonists $PGE_1$ and forskolin [136]. Nevertheless, those authors did not normalize the activated forms to the total GpIIb-IIIa receptors and the increase of PAC-1 binding to activated GpIIb-IIIa may have been an artifact of more platelet adhesion or total GpIIb-IIIa expression in the absence of activation inhibitors. In this work, *index1* is the analogue for the percentage of the activated GpIIb-IIIa forms in total receptors shown on the adherent platelet surface and the value for platelets bound on vWf-coated microspheres at low shear rate (100 $sec^{-1}$) is less than that on immobilized fibrillar collagen. A smaller number of activated GpIIb-IIIa receptors may be enough to help platelets adhere firmly on immobilized vWf but not to support platelet aggregate formation.

This study shows that platelets were less activated on VITROGEN 100® collagen coated microspheres than those on insoluble type I fibrillar collagen coated surface. Even though we had comparable thrombus formation at 2-minute end point on the fibrillar collagen and VITROGEN 100® collagen coated at high density on glass slides (Figure 3.1), there were more transient attachments on immobilized VITROGEN 100® collagen during the initial phase of flow. Those findings are consistent with other experimental results in the literature [137,138]. The native type I collagen fibrils are more thrombogenic than their monomers generated by pepsin treatment, and their preserved quaternary structure with telopeptides may activate or interact with additional platelet receptors capable of substituting GpIa-IIa and GpIV. In contrast, the pepsin-solubilized collagen

monomer such as VITROGEN 100® collagen, support less adhesion and aggregation and is dependent mainly on GpIa-IIa receptors and $Mg^{2+}$.

The inside-out signal pathways for inducing the conformation change of the GpIIb-IIIa have not been mapped completely. However, this study demonstrates that the $Ca^{2+}$ released from intercellular stores or cytoskeleton plays a role in this signal transduction. The integrin modulator, not yet identified, may trigger and regulate GpIIb-IIIa affinity through an interaction with the integrin cytoplasmic tail in a $Ca^{2+}$-dependent manner. The cytoskeleton is known to be involved in the process of irreversible fibrinogen binding at the late platelet aggregation phase [114]. However, cytoskeletal reorganization in thrombin-stimulated platelets also occurs earlier within seconds to minutes and is associated with an immediate change in platelet shape from discoid to spherical, accompanied by the formation of actin filament networks in developing filopodia and at the cell periphery [139-141]. The increase of actin filaments is due primary to additional actin polymerization at their increasing free barbed ends, occurring through a combination of filament severing and release of barbed-end-capping proteins; and the filament severing is mediated in a $Ca^{2+}$-dependent manner by gelsolin and other severing proteins [142]. In addition, the early phase of cytoskeletal rearrangement is coincident with centralization and secretion of platelet granules [139]. In this study, the GpIIb-IIIa activation and P-selectin release from α granules were inhibited by different sets of antagonists, except for the intracellular $Ca^{2+}$ inhibitor TMB-8. This indicates that both events are regulated by different signal transduction pathways and $Ca^{2+}$ release from

intracellular stores may be their common mechanism among many signal transduction networks of platelets. In a recent paper, the unexpected variation in concentration dependence for expression of different activation makers with a specific collagen type also suggested that α-granule secretion and GpIIb-IIIa redistribution were separate events from GpIIb-IIIa activation [143].

There is evidence for the involvement of Src-family tyrosine kinases $p59^{fyn}$ and $p53/56^{lyn}$ in collagen receptor signaling in human platelets [125]. In contrast, we found that platelets incubated with the selective inhibitor PP1 decreased the P-selectin expression after adhering onto insoluble fibrillar collagen coated microspheres, but were not affected in aggregation at agonist concentrations (10 μM) inhibiting both shape change and aggregation in that study. The discrepancy in the observations of platelet aggregation may be due to different experimental settings; that is, we used platelet-rich plasma but the other data was obtained with washed platelet suspensions. Plasma proteins might somehow reduce the effect of PP1 in our aggregometry experiments; on the other hand, PP1 did inhibit P-selectin expression on PKH26 stained washed platelets that adhered on collagen-coated microspheres.

Besides activated GpIIb-IIIa receptors, P-selectin may be also involved in platelet aggregation processes [144,145]. Our results showed that intercellular $Ca^{2+}$ antagonist TMB-8 at 250 μM could inhibit activated GpIIb-IIIa and P-selectin expressions, and that at 500 μM could further block P-selectin release from α granules but not the GpIIb-IIIa conformation change. On the other hand, platelet aggregation was partially inhibited at

lower concentration but blocked almost completely at higher concentration of TMB-8. Those observations suggest that P-selectin does play a role in platelet aggregation, especially for large aggregate formation because the turbidometric aggregometry is not very sensitive to the small aggregates.

# Chapter 4

## Platelets Interaction via GpIb-IX-V with von Willebrand Factor-Coated Microspheres under Shear Conditions

von Willebrand factor (vWf) plays important roles in hemostasis. This large multimeric glycoprotein is necessary for platelet adhesion and thrombus formation at sites of vascular injury, and also serves as a carrier and stabilizes the procoagulant factor VIII in the blood stream. Both roles are essential for the normal function of hemostasis. In pathological conditions, vWf is involved in the process leading to thrombotic arterial occlusion or systemic platelet aggregation such as thrombotic thrombocytopenic purpura (TTP). Congenital abnormalities of vWf or its platelet receptor GpIb result in the most common inherited human disorder of hemostasis, von Willebrand disease (vWD).

vWf links platelets to the subendothelium (adhesion) and to one another (aggregation) by means of specific interactions with two platelet receptors, GpIb-IX-V and GpIIb-IIIa. Endothelial cells produce and secret vWf into the plasma and the subendothelial matrix; in addition, different types of collagen in the injured vessel wall can bind plasma vWf. The interaction between GpIb-IX-V and vWf is thought to establish the initial contact or tethering of platelets to the thrombogenic surface and to generate an activation signal in the platelet, especially under high shear conditions. Activated GpIIb-IIIa with high ligand-binding affinity then binds vWf to form a more stable association and uses vWf or fibrinogen as a bridge, recruiting other platelets to

form aggregates. The binding between GpIb-IX-V and vWf seems to be essential because no shear-induced intracellular calcium elevation and platelet aggregation will occur if this receptor-ligand interaction is blocked [19].

Significant insight into the molecular mechanisms supporting mural thrombosis, including the roles of vWf and platelet receptors, has been gained through *in vitro* experimental systems such as a flow chamber. As shown in Chapter 3, The novel methodology of protein-coated microspheres and viscometric flow-cytometric experiments is useful to investigate platelet-surface interaction. In the work presented here, this protocol is modified to characterize the initial interaction between GpIb-IX-V and immobilized vWf under shear conditions.

## 4.1 Background

vWf is a multimeric protein consisting of a variable number of subunits that are produced by megakaryocytes (precursors of platelets) and endothelial cells. It is stored in the α granules of platelets and the Weibel-Palade bodies of endothelial cells, and is secreted by granule release after cell activation or by the endothelial cells into the plasma and the subendothelial matrix constitutively. Individual vWf multimers can range in the molecular weight from 500,000 to at least 20,000,000 Daltons, making vWf the largest known soluble plasma protein. These largest forms of vWf, found in the storage granules of platelets and endothelial cells, have been shown to be the most effective in promoting platelet adhesion and aggregation [146,147]. The repeating subunit structure of vWf

allows the molecule to bind in a multivalent manner to the platelet, thereby increasing the apparent affinity or strength of the interaction. This may be the reason why vWf is absolutely required to oppose the force of blood under high shear and allow platelet adherence.

GpIb-IX-V mediates platelet interaction with vWf of different forms. Plasma form of human vWf will not bind to GpIb-IX-V under static or low shear rate conditions unless the antibiotic ristocetin or the snake venom botrocetin is added. Unlike GpIIb-IIIa, which requires intact and activated platelets to bind to vWf, GpIb-mediated binding does not need platelet activation or even platelet metabolic integrity, since fixed platelets are readily agglutinated in the presence of vWf and either ristocetin or botrocetin. In contrast to plasma vWf, platelets are able to adhere to immobilized vWf even in the absence of ristocetin or botrocetin. When botrocetin binds to vWf, vWf exposes the site that binds GpIb-IX-V; in the same manner, when vWf is immobilized on a surface, it may undergo a conformational change that allows for direct interaction with GpIb-IX-V.

Shear stress is an important factor in GpIb-IX-V mediated adhesion of platelets to immobilized vWf. For example, platelet deposition to subendothelial matrix surfaces at high shear rates was strongly impaired in blood from patients with vWD [148]. In a related phenomenon, subjecting platelets to high shear stresses could induce platelet aggregation, which is mediated by soluble vWf binding initially to GpIb-IX-V, followed by platelet activation and GpIIb-IIIa dependent platelet aggregation [17,18]. It is uncertain whether the physical effect of shear is acting on GpIb-IX-V, on vWf, or on both.

Several vWf functional domains related to its adhesive functions have been identified. The GpIb-IX-V binding site is located within residues 509-695 in the disulfide loop of the A1-domain [149]. Also within the A1-domain are putative binding sites for collagen and heparin [150]. Recent studies have shown that vWf binds to purified type VI collagen via A1-domain [151,152]. Type VI collagen cannot support vWf binding at high shear [153], and this may explain why type VI collagen is not thrombogenic at high shear conditions because there is no immobilized vWf to initiate the platelet-surface interaction. Amino acids 948-998 in the A3-domain form another putative collagen binding site [154]. The RGDS tetra-peptide in residues 1,744-1,747 is a binding site on vWf for GpIIb-IIIa. The binding of vWf to GpIIb-IIIa is specifically inhibited by peptides containing the RGDS sequence or the dodecapeptide of the fibrinogen γ-chain [155,156]. Those sequences that may be required for ristocetin- or botrocetin-induced vWf binding have also been identified [157].

GpIb-IX-V, a platelet membrane glycoprotein essential for normal adhesion and aggregation in primary hemostasis, acts as a receptor for the adhesive protein vWf and for the platelet agonist thrombin. This receptor complex consists of four chains: GpIbα and GpIbβ are linked by a disulfide bond to which GpIX is strongly non-covalently bound in a 1:1 ratio (about 25,000 copies/platelet), and GpV is weakly non-covalently associated with the complex in a 1:2 ratio (GpV:GpIb-IX) [158,159]. All the subunits of GpIb-IX-V contain leucine-rich repeats, a motif found in a wide range of proteins but whose function is not well understood. Platelet adhesion to immobilized vWf is mediated

by the amino-terminal domain of the GpIbα chain containing the binding sites for the vWf A1 domain [160,161]; this interaction supports platelet tethering to a surface even at very high shear rates [76]. Congenital deficiency of GpIb-IX-V will result in the hemorrhagic disorder known as the Bernard-Soulier syndrome. GpIbα has a large number of O-linked carbohydrate chains terminating in sialic acid residues [162], and the latter contribute significantly to the negative charge of the platelet membrane [163]. Electron micrographic analysis indicated that GpIb exists as a long flexible rod (about 60 nm) with two globule domains of about 9 and 16 nm [164]; therefore, GpIb probably extends much further out from the platelet surface than GpIIb-IIIa does. The long extension may also make it susceptible to conformational changes induced by shear forces. A genetic polymorphism in GpIbα affects the number of repeating 13-amino acid units (1, 2, 3, or 4 copies) and was predicted to project the ligand-binding domain farther into the bloodstream and alter the susceptibility of platelet to shear-induced activation [165].

The mechanism of signal transduction by the GpIb-IX-V is a matter of great interest at present because at abnormally high shear stresses, this receptor plays a critical role in the initial stage of the interaction of platelets with exposed subendothelium and with soluble vWf molecules. In the resting platelet, the cytoplasmic domain of GpIb-IX-V is linked to the membrane-associated skeleton via the actin binding protein filamin [166]. Under some conditions, vWf binding to GpIb-IX-V on a platelet leads to activation of the calcium-dependent protease calpain, which cleaves and dissociates a number of

cytoskeletal-associated proteins such as actin binding protein and talin. This binding also regulates the recruitment of signaling proteins such as $pp60^{src}$ and $pp125^{fak}$, coincident with the platelet undergoing shape change, secretion and cytoskeletal rearrangement [167-169]. The GpIb-IX-V also plays a role in regulating the cytoskeletal rearrangement through cAMP-dependent phosphorylation at Ser166 of the cytoplasmic tail of GpIbβ, which is known to inhibit actin polymerization [170,171]. In addition to the actin binding protein, another protein directly associated with the cytoplasmic domain of the GpIb-IX-V is the ζ isoform of the ubiquitous 14-3-3 signaling protein, providing a major candidate for an early messenger in GpIb-IX-V dependent signal transduction [172]. There is evidence that GpIb-IX-V is associated with FcγRIIA, the receptor for binding the Fc portion of IgG and being responsible for the aggregation and activation of platelets induced by immune complexes, although any functional significance for this interaction remains to be established [173].

Characterization of the physical strength of the bonds linking biological cells to each other and to a surface is an important prerequisite for the understanding of adhesion processes such as platelet thrombosis, leukocyte margination, and cancer metastasis. For example, the adhesion molecule P-selectin, which had appeared to be unimportant based on static assays of binding, turned out to be essential for attachment in flow at physiological wall shear rates [174,175]. Adhesion of blood neutrophils to endothelial cells, the initial step in the inflammatory response, is mediated by selectins that facilitate leukocyte tethering to and rolling along endothelium in postcapillary venules until firm

adhesion is achieved at the site of inflammation. Selectins are distinguished by very fast forward and reverse reaction rates (on or off rates) compared to the more tenacious integrin-mediated bonds, which are now thought to be responsible for the eventual arrest of cells. The platelet receptors GpIb-IX-V and GpIIb-IIIa seem to work together with a 2-step process in mural thrombosis as the selectin and integrin do in inflammation. Platelet adhesion to immobilized vWf is initiated by the GpIb-IX-V complex, supporting platelet tethering to the surface at high shear rates but without irreversible attachment; consequently this interaction slows the cell down and allows the establishment of additional bonds typically mediated by GpIIb-IIIa [76]. These phenomena demonstrate the importance of the kinetics of bond formation and dissociation.

Several experimental systems have been developed to study the force dependence of bond kinetics. In a flow chamber system, researchers have visualized the transient tethering and detaching of neutrophils in hydrodynamic flow on lipid bilayers containing low surface density of P-selectin, which is critical to support rolling. That transient tether, suggesting a unimolecular interaction between P-selectin and its glycoprotein ligand, has first-order kinetics, and therefore the dissociation constant of the bond can be estimated [176]. In another experimental setup, the counter-rotating cone-and-plate rheoscope has been used to measure the time and force dependence of breaking up doublets of spherical, swollen, and fixed red cells agglutinated by monoclonal antibodies, or of latex spheres covalently linked with receptor and ligand [177,178]. Generally the fraction of breakup increases with increasing duration and magnitude of the applied force

and decreases with increasing ligand concentration in those studies. In a third system, the modified flow cytometer that has a customized converging funnel chamber and a built-in fluidic control has been developed to assess the strength of cell-cell adhesion [179,180]. These modifications are able to generate strong elongational stresses extending 3 orders of magnitude in the flow cytometry hydrodynamic focusing, and thus the forces can break adhesive cell pairs apart. The dissociation curve, defined as the relative amount of "sticking" cell pairs at different flow rates, is analyzed to determine if a receptor-ligand interaction effectively mediates adhesion.

In order to examine the force dependence of platelet GpIb-IX-V receptor and immobilized vWf, I have developed a protocol based on vWf-coated microspheres that provide thrombogenic surfaces as well as a cone-and-plate viscometer that generates a wide range of uniform shear stresses. This method employs the cone-and-plate viscometer to apply controlled levels of shear forces to the platelet and vWf-coated microsphere mixture, and platelet adhesion to microspheres is measured by fluorescent-labeled monoclonal antibodies in flow cytometry. This experimental setup was originally designed with the hope of characterizing the single bond strength between GpIb-IX-V and immobilized vWf. However, an unexpected platelet adhesion phenomenon has been observed and I switched the focus on this interesting finding.

## 4.2 Materials and Methods

**Microsphere preparation**

The preparation of vWf solution and microsphere coating followed the procedures described in Chapter 3. Briefly, human vWf was purified from normal human cryoprecipitate by glycine and sodium chloride fractionation, followed by agarose 4B column chromatography; the concentration or antigen level of the vWf solution was measured by an enzyme-linked immunoassay SPECTRO vWf (Ramco Laboratories, Inc.). For coating vWf, 12 drops of microsphere suspensions were mixed in an Eppendorf tube with 1 ml of the vWf solution of different antigen levels, which was diluted from stock solution with citrate-phosphate buffer (0.0394 M citric acid and 0.1212 M dibasic sodium phosphate, pH 5.8). After incubating for 1 hour at room temperature with gentle mixing by a nutator mixer, the suspension was spun for 2 minutes in an Eppendorf micro centrifuge (15,000 rpm). The pellet was washed once with 1 ml of storage buffer (Dulbecco's phosphate buffered salt solution, containing 10 mg/ml bovine serum albumin, 1 mg/ml sodium azide, and 5% glycerol, pH 7.4), and the final pellet was resuspended in the storage buffer and adjusted to $2x10^7$ microspheres/ml. The vWf coating densities from initial solutions with different concentrations were checked in flow cytometry by fluorescein isothiocyanate (FITC)-labeled monoclonal antibodies (purified mouse anti-human vWf and FITC-conjugated rat anti-mouse IgG monoclonal antibodies; PharMingen). The microspheres coated with vWf from 40% and 200% antigen level solutions were chosen as low and high coating densities respectively in this study. Bovine serum albumin (BSA)-coated microspheres, which were made by

incubating in the storage buffer (10 mg/ml BSA) instead of the vWf solution, were used as the control for non-specific adhesion.

**Platelet preparation**

Blood was obtained by venipuncture from healthy non-smoking volunteers who had not ingested any medications for at least 10 days before donation. The blood was anticoagulated with 1/10 volume of 3.8% sodium citrate solution. By spinning whole blood at 150g for 15 minutes at 25 °C, platelet-rich plasma (PRP) was obtained and the platelet concentration was adjusted to $2x10^8$ cells/ml with HEPES buffer (10 mM N-2-hydroxyethylpiperazine-N'-2-ethanesulfonic acid (HEPES), 145 mM NaCl, 5 mM KCl, 0.5 mM $Na_2HPO_4$, 1 mM $MgSO_4$, 5.5 mM glucose, 3.5 g/l BSA, and 1 mM $CaCl_2$, pH 7.4). In order to study only the interaction between GpIb-IX-V and immobilized vWf, which is calcium independent, PRP was incubated with 5 mM $Ca^{2+}$ chelator, ethylene glycol-bis(β-aminoethyl ether)-N,N,N',N'-tetraacetic acid (EGTA), for 1 hour at 37 °C. This treatment was shown to disrupt the GpIIb-IIIa irreversibly [181]; and the effect was verified by turbidometric platelet aggregometry (Dual Sample Aggregation Meter DP-247E; Sienco, Inc.).

**Viscometric-flow cytometric experiments**

250 μl of PRP and 250 μl of vWf-coated microsphere suspensions were put into the cone-and-plate viscometer (Ferranti-Shirley 781; Ferranti Electric Inc.), which was

pretreated with 1% Prosil 28® (PCR Research Chemicals), and sheared at a uniform shear rate to allow platelet-microsphere interactions. When platelets and microspheres undergo collisions by shear forces, the collision frequency is proportional to $G(a_1 + a_2)^3$ for two spheres of radii $a_1$ and $a_2$, where $G$ is the shear rate [182]. Since theoretically the collision frequency is proportional to the shear rate, the shearing duration is set inversely proportional to the shear rate to make the number of platelet-microsphere collisions essentially the same. For instance, platelet-microsphere mixtures were sheared at a shear rate of 10,000 $sec^{-1}$ for 30 seconds but at 500 $sec^{-1}$ for 10 minutes. After shearing at 37 °C for different time intervals and shear rates, 100 µl of 6% formaldehyde fixative was immediately added to the platelet-microsphere suspensions and gently mixed by moving the platen of the viscometer up and down several time. 10 µl of the fixed sample was then added to each tube containing 40 µl of either r-phycoerythrin (PE) conjugated mouse anti-human CD42b or IgG isotype control antibody (final concentration 5 µg/ml; PharMingen). After 30-minute incubation in the dark at room temperature, the sample-antibody mixture was diluted by adding 2 ml of 1% formaldehyde and kept at 4 °C until analyzed in flow cytometry.

The voltage and gain of the detecting system in the FACScan® flow cytometer (Becton Dickinson Immunocytometry Systems) were tuned to capture only microsphere populations in the linear forward light scattering (FSC) and linear side light scattering (SSC) plot. The criterion of 5,000 events within the microsphere singlet population was set for data acquisition. The intensities of FSC, SSC, and FL-2 (PE fluorescence) were

stored and were analyzed later by using software CELLQuest (Becton Dickinson Immunocytometry Systems).

The studies of platelet adhesion onto immobilized vWf via receptor GpIb-IX-V under shear conditions were performed first. However, an unexpected finding was observed, so some other experiments were designed to investigate the possible mechanisms behind this phenomenon. First, to verify whether the platelet-microsphere association resulted from the interaction between platelet GpIb-IX-V and immobilized vWf, aurintricarboxylic acid (ATA; 120 μg/ml) was used. This compound inhibits vWf-mediated platelet aggregation by binding to the A1 disulfide loop of vWf and competing with GpIb-IX-V, to selectively block the interactions [183]. Next, comparing the adhesion results with and without an additional 5-minute stagnant rest after shearing at 10,000 $sec^{-1}$ for 30 seconds showed the reversibility of the binding between GpIb-IX-V and immobilized vWf. In order to examine the role of platelet activation, such as α granule release in this experimental system, FITC-labeled mouse anti-human CD62P (P-selectin) antibody was utilized to measure the shear-induced activation of suspended platelets. The percentage of platelets with FITC fluorescent intensities higher than the threshold value, set by including 99.5% of the platelet singlet population in an isotype control sample, was quantified to show the positive P-selectin expression. In some experiments, PRP was incubated for 20 minutes with chemicals such as cytochalasin D and calpeptin that were suspected to affect the function of GpIb-IX-V by altering interactions with the cytoplasmic domain. Because the cytoplasmic domain of GpIb-IX-V is linked to the

membrane-associated skeleton in the resting platelet, cytochalasin D (10 μM) was used to depolymerize the existing actin filaments and inhibit agonist-induced actin filament polymerization. Calpeptin (50 μM) was used as a cell-permeable inhibitor of the calcium-dependent protease, calpain, which cleaves and dissociates a number of cytoskeletal-associated proteins as well as regulates the recruitment of signaling proteins. In some experiments, TMB-8 (250 μM) was also applied to block the $Ca^{2+}$ release from intracellular stores. Cytochalasin D and calpeptin were first dissolved in dimethyl sulfoxide (DMSO), which was diluted to a final concentration of less than 0.2% to prevent its effect on platelets.

Secondary flow in the cone-and-plate viscometer may cause significant deviations from the ideal primary flow field, especially at high shear rates. The use of the cone-and-plate viscometer is based on the primary flow analysis solution of the equations of motion; however, secondary flow is present at all shear rates even though it is assumed negligible in the primary flow analysis [184]. Nevertheless, decreasing the cone angle or the sample volume can reduce the secondary flow effects. In order to check whether secondary flow affects interactions between platelets and vWf-coated microspheres in this experimental setup, a smaller size (100 μl) of the platelet-microsphere sample was sheared, and the results were compared with those of the 500 μl sample.

**Data analysis**

An illustration for flow cytometric data analysis is given in Figure 4.1. Microsphere singlets are gated (R1) in the FSC vs. SSC diagram (Figure 4.1(a)), and then the histograms for PE fluorescent intensities of those events are plotted (Figure 4.1(b) and (c)). The result of the isotype control antibody binding is used to set the region (M1 in Figure 4.1(b)) including 99.5% of the microsphere singlets "without platelet adhesion." In fact, the platelets may adhere on the microspheres, but the isotype control antibodies cannot detect them so the result shows only the autofluorescence of microspheres and antibody non-specific binding. The histogram of the PE-conjugated anti-human CD42b antibody binding usually has two peaks (Figure 4.1(c)), and the population with higher fluorescent intensities (M2) indicates positively that platelets are associated with the microspheres, because this fluorescent labeled antibody recognizes and binds specifically to the GpIbα on the platelet surface. The percentages of the microspheres associated with platelets are recorded and compared. Because the collision numbers between platelets and microspheres have been controlled the same for all applied shear rates, the percentage of the platelet-microsphere association represents the adhesion efficiency, which depends on the interplay of shear flow hydrodynamic and platelet receptor biology.

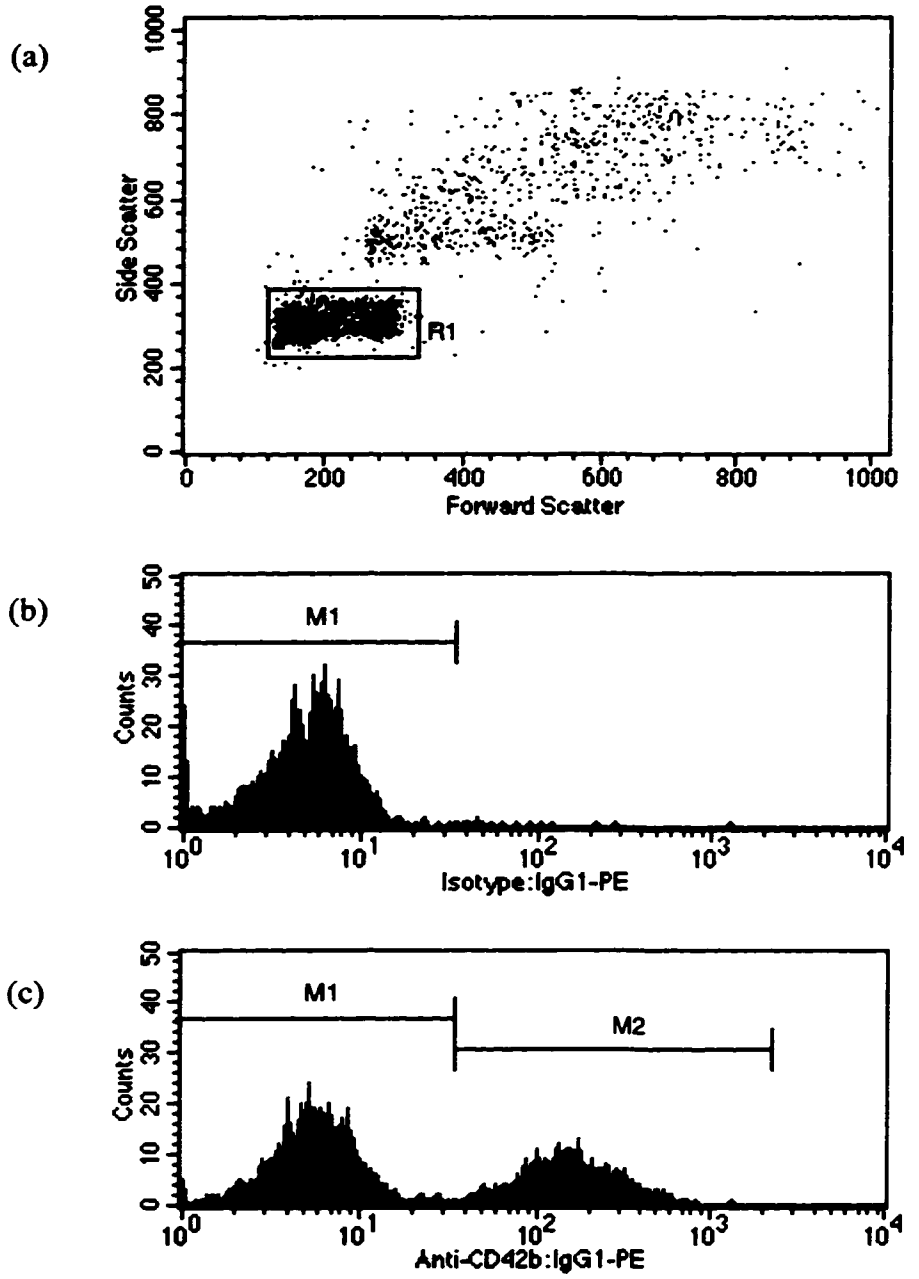


Figure 4.1 Flow cytometric analysis for platelet-microsphere association. (a) is a linear forward scatter vs. linear side scatter dot plot. The microsphere singlets are gated in R1. The histograms for FL-2 (PE) fluorescent intensities of the events in R1 are plotted. (b) is the histogram for the sample with isotype control antibody binding. The region M1 is set so that it includes 99.5% of the events, indicating microspheres "without platelet association." (c) is the histogram for the sample with anti-human CD42b antibody binding. The microspheres with platelet association are detected by the antibodies, increasing their fluorescent intensities, and gated in M2. The percentage of the M2 events in total microsphere singlets is recorded.

**Statistical analysis**

Results are reported as the mean ± SEM. The statistical significance of differences between means is determined by analysis of variance (ANOVA). The multiple comparison procedure Fisher's Protected Least Significant Difference (PLSD) test is used to determine which pair(s) of means are significantly different. All significance levels are set as 0.05.

## 4.3 Results

**Preparations of microspheres and platelets were suitable for the viscometric-flow cytometric experiments.**

The coating densities of immobilized vWf from stock solutions with different concentrations were checked in flow cytometry. The FITC fluorescent intensities of the detecting antibodies, proportional to the vWf antigen levels, are shown in Figure 4.2. The coating densities increased monotonically as the incubating vWf concentration increased. The microspheres incubated with the storage buffer (10 mg/ml BSA; 0% vWf) were used as the negative control. The microspheres incubated with 40% and 200% initial solutions were chosen as the surfaces of low and high vWf coating density respectively for the later experiments. The low vWf coating was statistically different from that of the negative control microspheres, $p = 0.0232$. The ratio of antigen levels between high and low density vWf-coated microspheres is about 9.4 fold.

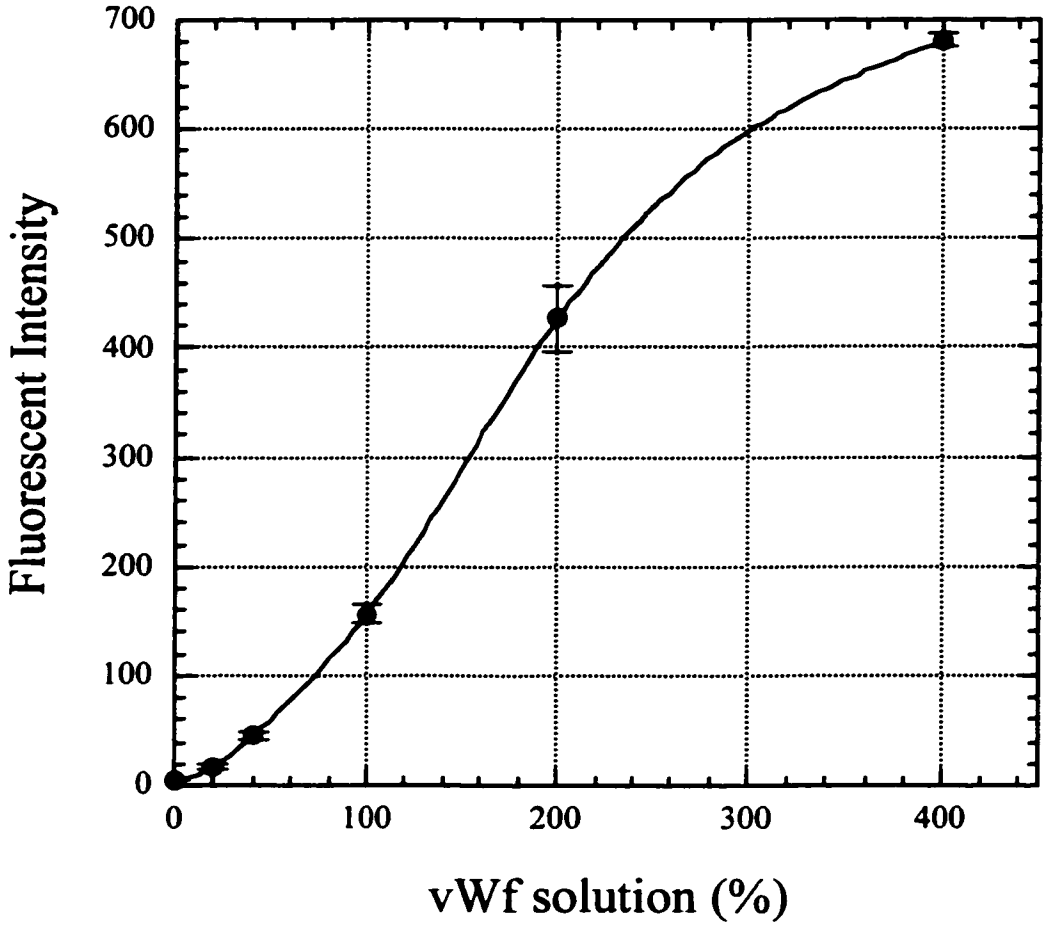


Figure 4.2 vWf coating density measured by fluorescent labeling. The vWf immobilized on microspheres is measured by purified anti-human vWf monoclonal antibody and FITC-conjugated secondary antibody. The abscissa indicates the concentration (antigen level) of the incubating vWf solution and the ordinate shows the fluorescent intensity (arbitrary units) of the vWf-coated microspheres by antibody binding. Values are showed as means ± SEM, n = 8-9.

After PRP was incubated with 5 mM $Ca^{2+}$ chelator EGTA for 1 hour at 37 °C, it was tested in turbidometric platelet aggregometry to verify that the function of GpIIb-IIIa receptors was blocked, as evidenced by the inhibition of platelet aggregation. The results are illustrated in Figure 4.3. Without EGTA treatment, platelets responded and aggregated normally to ADP (10 μM) and collagen (10 μg/ml) stimulation. Soon after adding ADP reagent, a brief decrease in light transmission (converted linearly to the percentage of platelet aggregation) due to platelet shape change was followed by a partial or "first wave" aggregation, and then an irreversible "second wave" of aggregation was seen. When platelets were stimulated with collagen, there was an initial lag phase followed by a gradual shape change and then a single wave aggregation. In contrast, with EGTA treatment the platelet aggregation was inhibited almost completely but not the shape change. These results indicate that the function of GpIIb-IIIa was disrupted and thus the GpIb-IX-V dependent interaction with immobilized vWf could be examined separately.

**Platelet adhesion on low density vWf-coated microspheres decreased but that on high density vWf-coated microspheres increased as the shear rate increased.**

The EGTA-treated platelets and the microspheres coated either with BSA, low density, or high density of vWf were put into the cone-and-plate viscometer and then sheared at a uniform shear rate for the corresponding duration, which was set inversely proportional to the shear rate to make the number of platelet-microsphere collisions

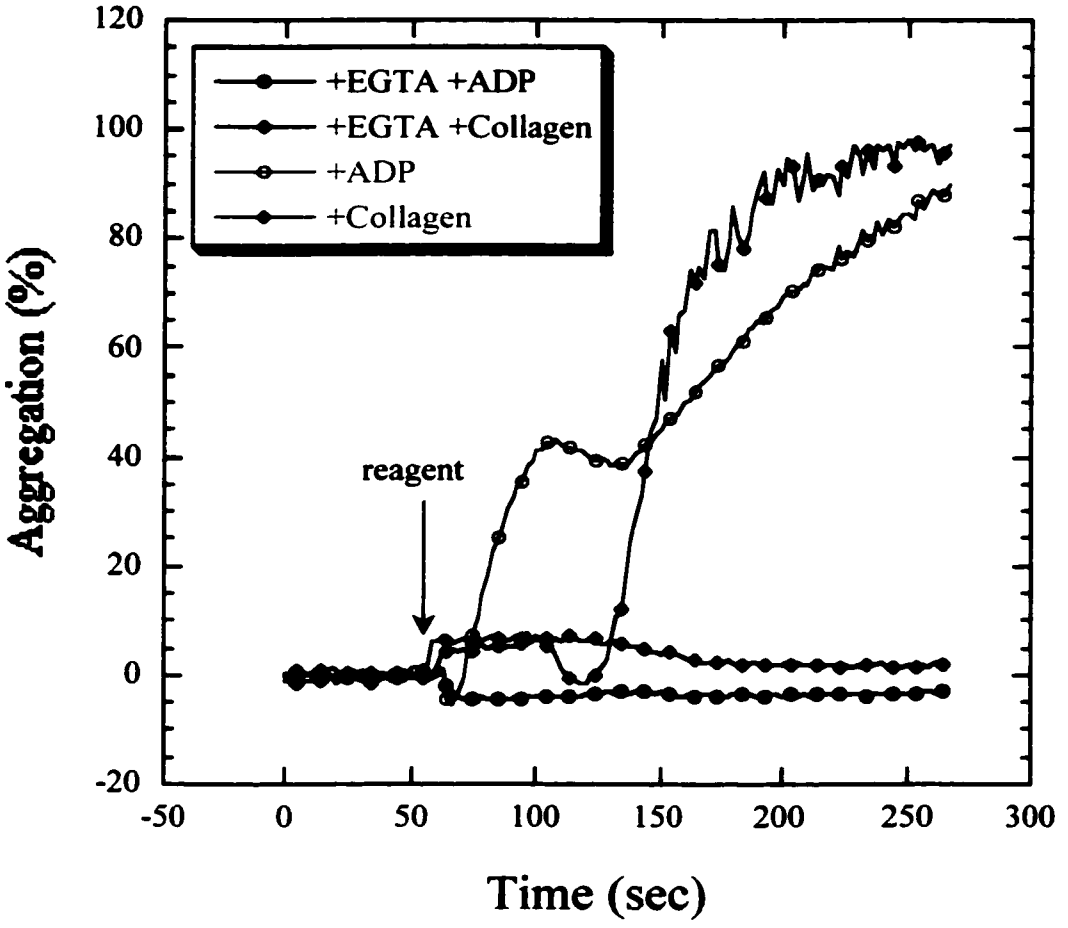


Figure 4.3 Aggregation curves of PRP with or without EGTA treatment. To block the function of platelet GpIIb-IIIa receptors, PRP is incubated with 5 mM EGTA at 37 °C for 1 hour. ADP (10 μM) or collagen (10 μg/ml) was added into the PRP with or without EGTA treatment after stirring at 1,000 rpm for 1 minute in an aggregometer and the response of platelet aggregation was recorded for about 3 more minutes. Data were acquired every 2 seconds but for clarity only 20% of the points are marked. EGTA treatment inhibits the platelet aggregation, indicating that GpIIb-IIIa receptors are disrupted.

essentially the same. After shearing, the sample was immediately fixed as well as incubated with PE-conjugated platelet specific antibody, and the percentage of microspheres associated with platelets was quantified in flow cytometry. The results of platelet adhesion onto vWf-coated microspheres at different shear rates are shown in Figure 4.4. On BSA- (0% vWf) or low density vWf-coated microspheres, platelet adhesion decreased as the shear rate increased. There was more platelet association to the microspheres with low vWf coating density than that to the negative control beads; however, this was not significantly different. (Note: if unpaired t-test was used to compare the means, the platelet associations on BSA- and low density vWf-coated microspheres were significantly different at shear rates of 5,000 and 10,000 $sec^{-1}$, $p<0.05$.) Unexpectedly, more high density vWf-coated microspheres had platelets bound on them when the shear rate increased. Because the contact time between platelets and microspheres is shorter and the shear stresses between them are stronger at higher shear rates, I expected that the adhesion efficiencies would go down and there would perhaps be less platelet association with vWf-coated microspheres as the shear rate increases. However, the platelet-microsphere association for high density vWf-coated microspheres had a trend in the opposite direction. Therefore, this shear-induced platelet adhesion on immobilized vWf was studied further.

**Platelets were associated with vWf-coated microspheres by GpIb-IX-V and vWf interaction.**

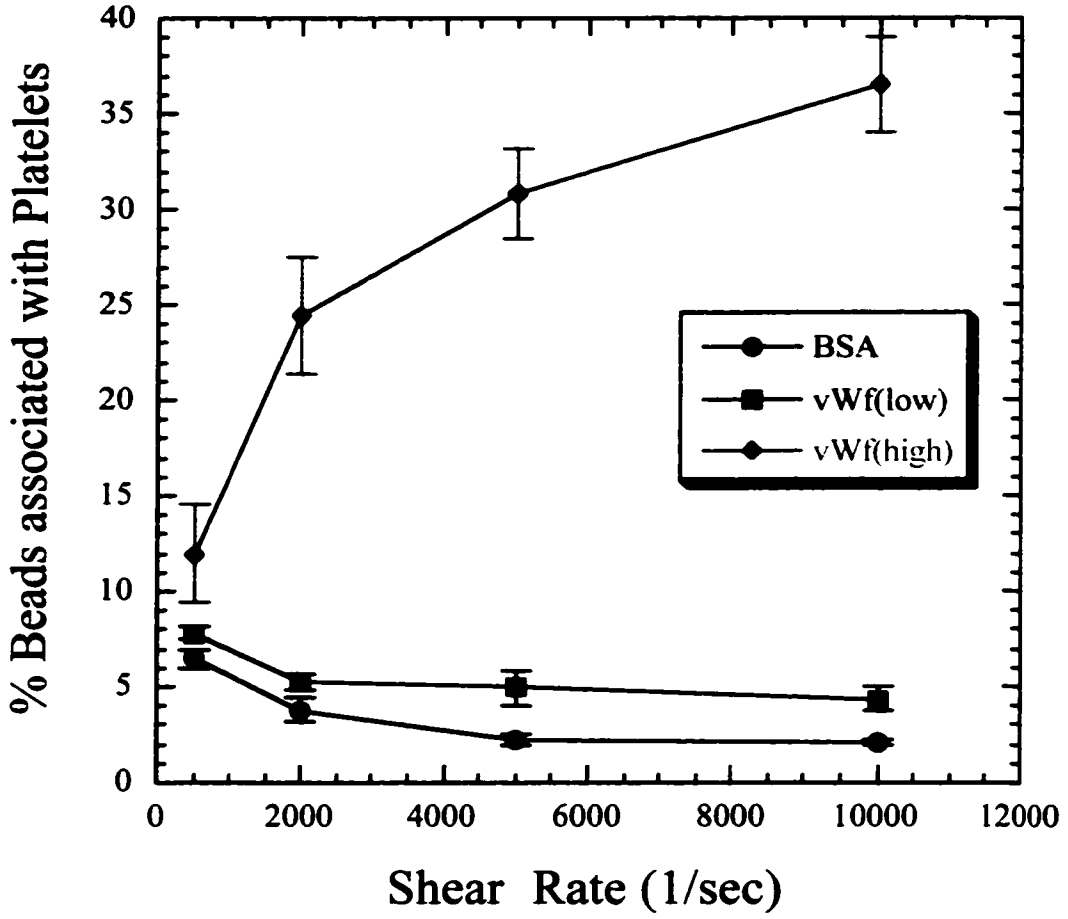


Figure 4.4 Platelet association with vWf-coated microspheres under shear conditions. The EGTA-treated PRP was sheared with the microspheres either coated with BSA, low density, or high density of vWf in the cone-and-plate viscometer. The sample was sheared at shear rates of 500, 2,000, 5,000, and 10,000 $sec^{-1}$ for 600, 150, 60, and 30 seconds respectively. The percentage of microspheres with platelet association is measured in flow cytometry. Values are showed as means ± SEM, n = 4-6. Platelet adhesion on BSA- or low density vWf-coated microspheres decreases, but that on high density vWf-coated microspheres increases as the shear rate increases.

In order to check whether the platelet-microsphere association was due to the interaction between platelet GpIb-IX-V and immobilized vWf, ATA (120 μg/ml) was added into the high density vWf-coated microsphere suspensions before mixing them with EGTA-treated PRP. ATA binds to the A1-domain of vWf, the GpIb-IX-V binding site, and therefore interferes with vWf-platelet interaction. The percentages of microspheres associated with platelets at different shear rates were plotted in Figure 4.5. ATA did inhibit the binding between platelet and immobilized vWf and the platelet association was reduced to the negative control level (2-6% association). However, in contrast to the results of BSA- or low density vWf-coated microspheres (Figure 4.4), platelet association to ATA-treated vWf surface was slightly increased as the shear rate increased. The result at highest shear rate of 10,000 $sec^{-1}$ was significantly larger than those of 5,000, 2,000, and 500 $sec^{-1}$ ($p < 0.05$).

**The platelet adhesion on vWf-coated microspheres was irreversible.**

In order to check the reversibility of platelet-microsphere associations, the results with and without an additional 5-minute incubation under static conditions after shearing the sample at 10,000 $sec^{-1}$ for 30 seconds were compared, as well as that by incubating EGTA-treated PRP with the microspheres of high vWf coating density under stagnant conditions for 30 minutes. If platelet adhesion to vWf-coated microspheres is reversible, the enhancement of platelet-microsphere association due to the high shear would be offset by the additional static incubation. The comparison is shown in Figure 4.6. The

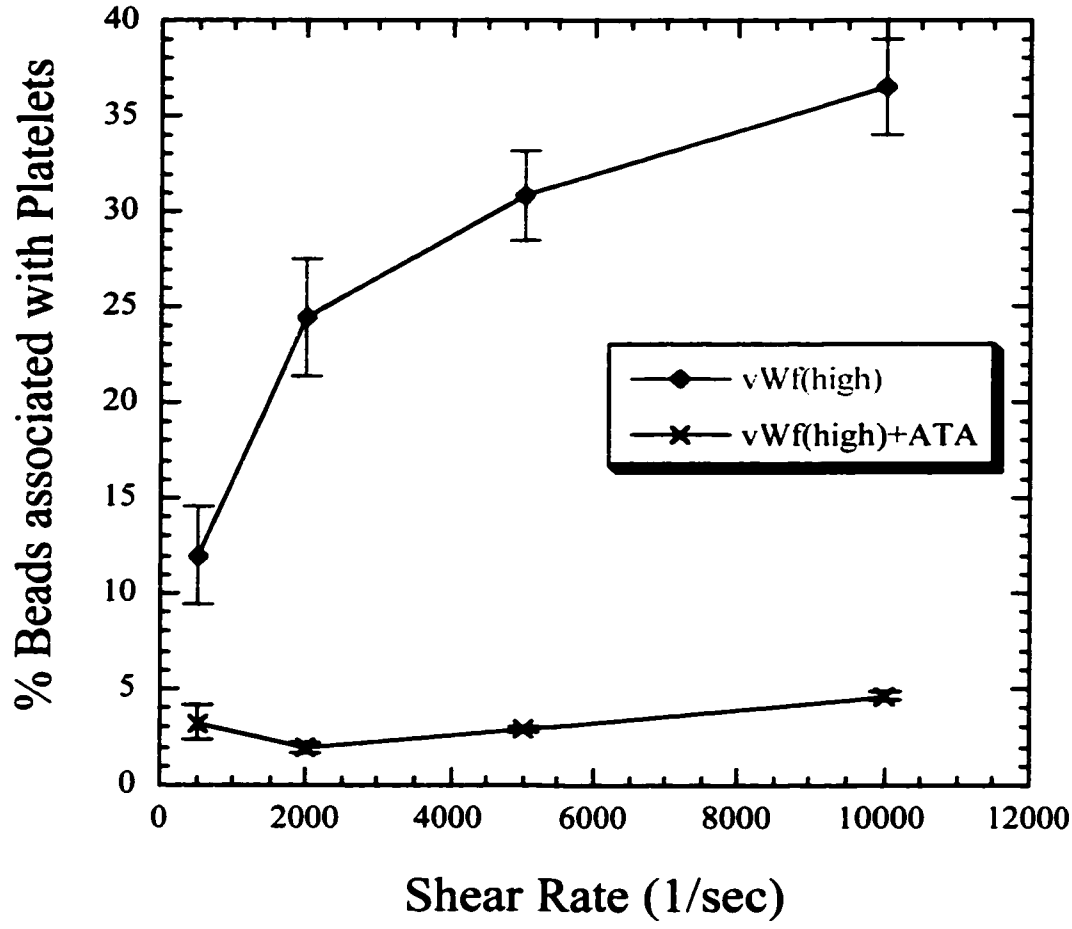


Figure 4.5 Platelet adhesion onto vWf-coated microspheres via GpIb-IX-V. ATA (120 μg/ml), which binds A1-domain of vWf and thus interferes with GpIb-IX-V binding, was added to check whether the platelet-microsphere association resulted from the interaction between platelet GpIb-IX-V and immobilized vWf. High density vWf-coated microspheres in the presence or absence of ATA were mixed with EGTA-treated PRP and sheared at shear rates of 500, 2,000, 5,000, and 10,000 $sec^{-1}$ for 600, 150, 60, and 30 seconds respectively. Values are showed as means ± SEM, n = 4-6. The ATA treatment inhibits the platelet adhesion, and the percentage of microspheres with platelet association is reduced to the negative control level (2-6% association).

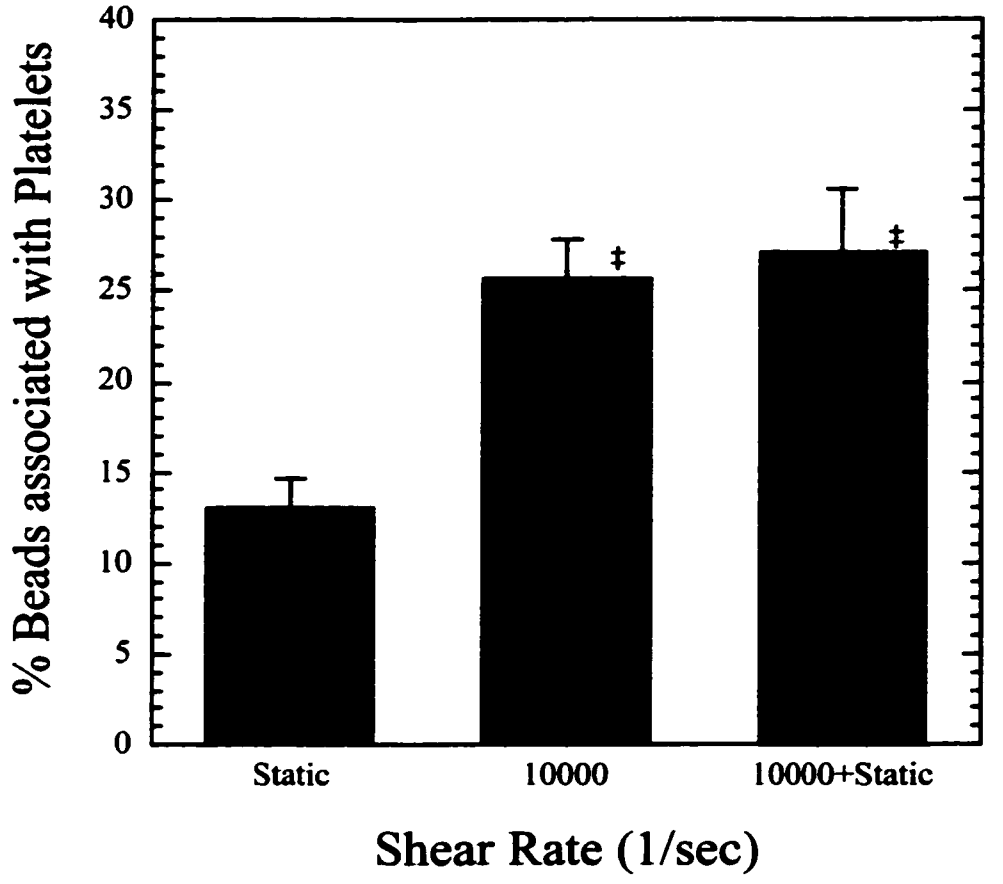


Figure 4.6 Reversibility of the association between platelets and microspheres of high vWf coating density. As soon as shearing at 10,000 $sec^{-1}$ for 30 seconds was completed, the sample was fixed immediately or after an additional 5-minute static incubation. The platelet adhesion onto high density vWf-coated microspheres at static condition for 30 minutes was also measured. Values are showed as means ± SEM, n = 7-8. The results of platelet-microsphere association with and without the additional static condition are not statistically different. This indicates that adherent platelets do not detach from the vWf-coated surface. However, the percentages of microspheres with platelet association in both shear settings are significantly larger than that in static incubation. (‡ indicates that the means are statistically different compared to the value of the static control, $p < 0.01$.)

platelet-microsphere association was maintained at the same level with or without an additional static incubation after shearing. However, in both shear cases the percentages of microspheres associated with platelets were significantly larger than that in static incubation alone ($p < 0.01$). These results indicate that adherent platelets did not detach from the vWf-coated surface.

**The increase of platelet-microsphere association at high shear rates was not due to shear-induced platelet activation, as monitored by P-selectin expression.**

It is possible that shear-induced platelet activation might play a role in the enhancement of platelet association to vWf-coated microspheres as the shear rate increased. For example, P-selectin and other adhesion molecules expressed on platelet surface, resulting from $\alpha$ granule release after platelet activation, might help to initiate or strengthen platelet adhesion to the immobilized vWf surface. Nevertheless, EGTA-treated platelets sheared with microspheres of high or low vWf coating density at 10,000 $sec^{-1}$ for 30 seconds or 500 $sec^{-1}$ for 10 minutes did not have significant differences in P-selectin expression (Figure 4.7). The sheared platelets showed slightly more P-selectin expression than the pre-sheared EGTA treated platelets, but this was not statistically different. The low P-selectin expression on sheared platelet surface did not result from the inability of the anti-human CD62P detecting antibody to bind without extracellular $Ca^{2+}$ because 72% of thrombin-stimulated (1 unit/ml) platelets expressed P-selectin positively when measured in the same environment.

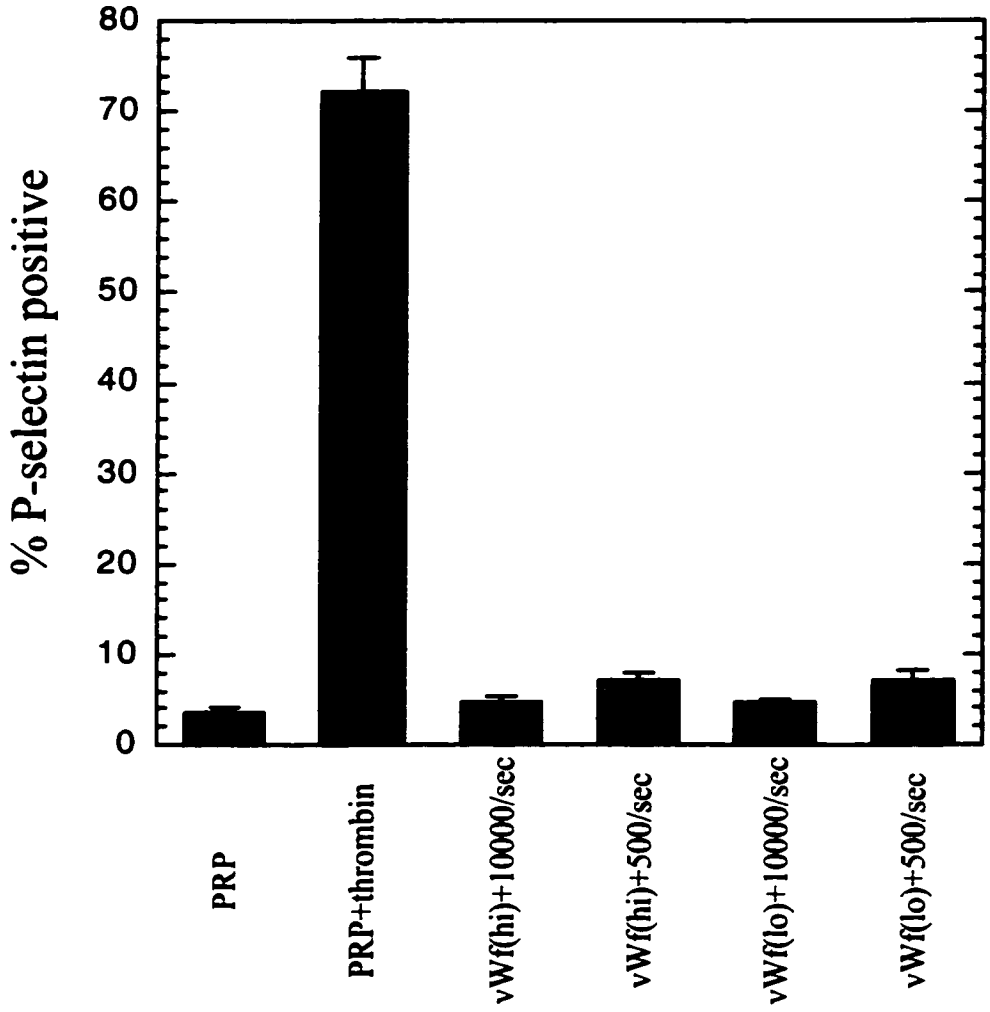


Figure 4.7 P-selectin expression on platelet singlets under shear conditions. In order to check whether shear-induced platelet activation is involved in the increase of platelet association to vWf-coated microspheres as the shear rate increases, we sheared EGTA-treated PRP with microspheres of high or low vWf coating density at 10,000 $sec^{-1}$ for 30 seconds or 500 $sec^{-1}$ for 10 minutes. The percentage of platelets with FITC fluorescent intensities higher than the threshold value, set by including 99.5% of the platelet singlet population in an isotype control sample, was quantified to show the positive P-selectin expression. Values are showed as means ± SEM, n = 6-7. The P-selectin expression on suspended platelet singlets in each shear experiment is not statistically different from others and that on pre-shear PRP sample. However, thrombin-treated platelets in an EGTA environment show 72% positive P-selectin expression.

**Cytoskeleton may be involved in the increase of platelet-microsphere association at high shear rates.**

The cytoplasmic domain of GpIb-IX-V is linked to the membrane-associated skeleton via actin binding protein (filamin) in the resting platelet, and after platelet activation the level of cytoplasmic $Ca^{2+}$ may control the activity of platelet calpains, the neutral proteases that preferentially cleave cytoskeletal elements. In order to check whether the association of GpIb-IX-V with cytoskeleton is involved in the increase of this receptor binding to immobilized vWf at high shear rates, either cytochalasin D, calpeptin, or TMB-8 was added into EGTA-treated PRP and shear with high density vWf-coated microspheres at 10,000 $sec^{-1}$ for 30 seconds. The calpain inhibitor calpeptin and intracellular $Ca^{2+}$ antagonist TMB-8 did not have an effect on the platelet-microsphere association, compared to the control that was without any inhibitor treatment (Figure 4.8). However, cytochalasin D at the concentration of 10 μM further enhanced the shear-induced increase of platelet adhesion ($p < 0.0001$). These results suggest that platelet cytoskeleton might be important in modulating the enhancement of platelet association with vWf-coated microspheres at high shear rates, but not via the cytoskeleton reorganization by calpains after platelet activation.

**The shear-induced enhancement of platelet-microsphere association did not result from artifacts of the secondary flow in the cone-and-plate viscometer at high shear rates.**

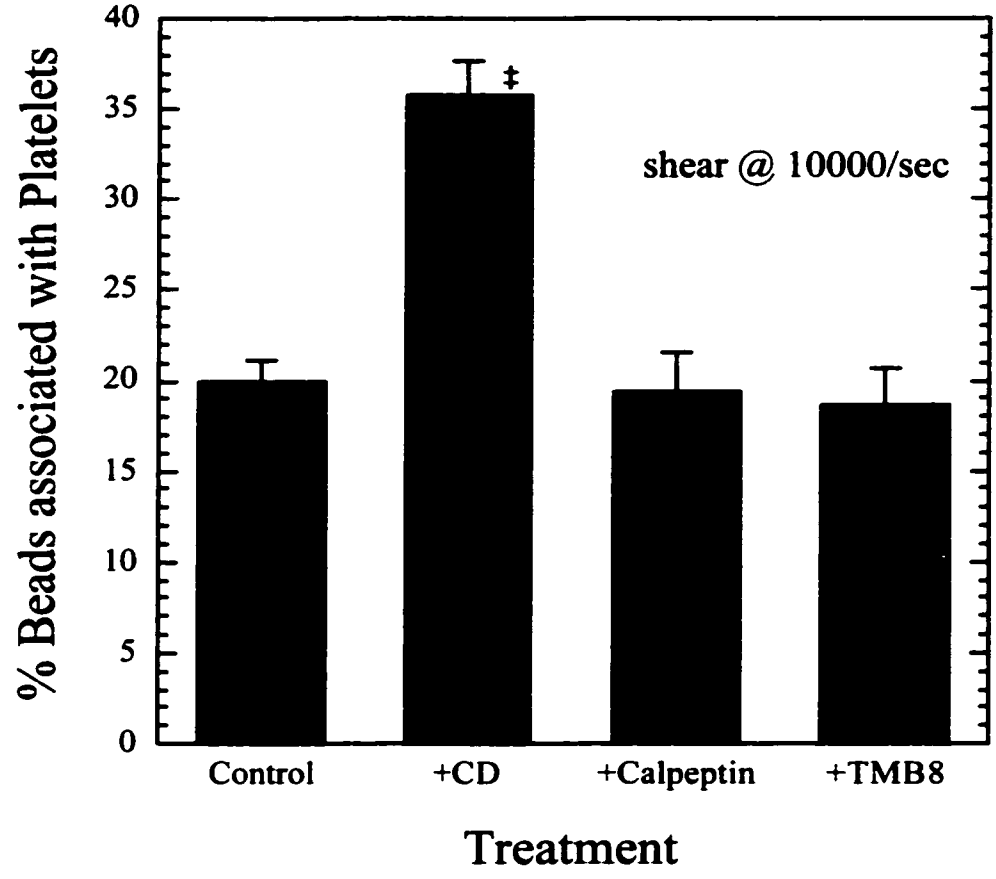


Figure 4.8 Involvement of platelet cytoskeleton in the increase of platelet-microsphere association at high shear rates. EGTA-treated PRP was incubated with cytochalasin D (10 μM), calpeptin (50 μM), or TMB-8 (250 μM) and then sheared with high density vWf-coated microspheres at 10,000 $sec^{-1}$ for 30 seconds. The percentage of microspheres with platelet association is measured in flow cytometry. Values are showed as means ± SEM, n = 6. The results of the runs with calpain inhibitor calpeptin or intracellular Ca2+ antagonist TMB-8 treatment are not statistically different from that of the control that is without any inhibitor treatment. However, cytochalasin D treatment enhances the shear-induced increase of platelet adhesion significantly. (‡ indicates that the mean is statistically different compared to the value of the control, $p < 0.0001$.)

Secondary flows in the cone-and-plate viscometer at high shear rates were suspected to increase the chance of platelet-microsphere collisions and thus cause more adhesion. The use of a smaller angle rotating cone or a smaller volume of sample can reduce the secondary flow effects. Because in all experiments I had applied the 1/3° cone, the smallest cone angle available, the sample volumes were changed to investigate the effects of the secondary flow. Either 100 or 500 μl of platelet and high density vWf-coated microsphere mixture was sheared at 10,000 $sec^{-1}$ for 30 seconds or 500 $sec^{-1}$ for 10 minutes. The results are shown in Figure 4.9. There was no statistical difference between the results for small and large sample volumes at each shear rate. Using a smaller volume of sample did not reduce the shear-induced enhancement of platelet-microsphere association; the outcomes for the 100-μl sample increased significantly when the shear rate increased from 500 to 10,000 $sec^{-1}$ ($p = 0.0036$), the same as did those for the 500-μl sample ($p = 0.0002$). Therefore, it is not secondary flows that caused more platelet-microsphere association at high shear rates.

## 4.4 Discussion

The viscometric-flow cytometric experimental setup was originally designed to study the binding strength between the platelet GpIb-IX-V receptor and immobilized vWf, but an unexpected phenomenon described above was observed. The cone-and-plate viscometer generates a uniform shear field, and the shear stresses and interactions between platelets and vWf-coated microsphere can be clearly defined. Because of the

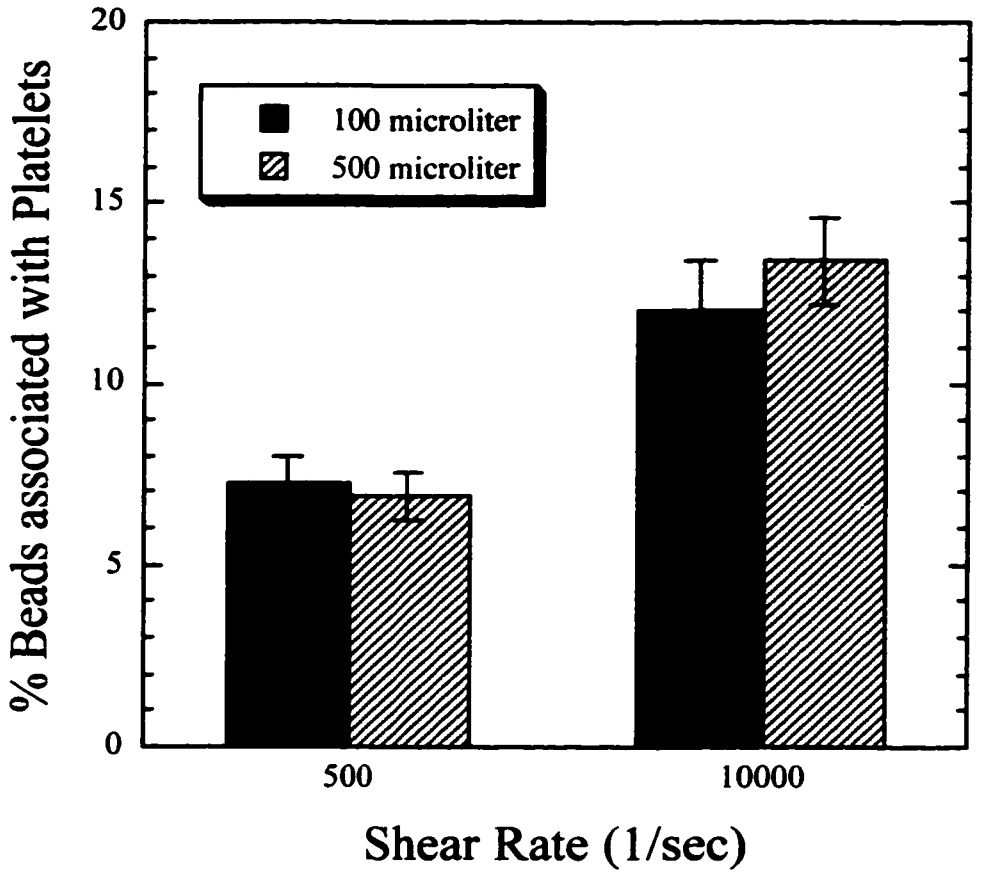


Figure 4.9 Involvement of secondary flow effects in the increase of platelet-microsphere association at high shear rates. In order to examine whether the secondary flows in cone-and-plate viscometer at high shear rates increase the chance of platelet-microsphere collisions and thus cause more adhesion, a reduced sample volume of 100 μl was used instead of 500 μl. Values are showed as means ± SEM, n = 8-9. The percentages of platelet-microsphere association for the 100-μl sample increase significantly as the shear rate increasing from 500 to 10,000 $sec^{-1}$ ($p < 0.01$), as well as those for the 500-μl sample ($p < 0.001$). However, there is no statistical difference between the results for small and large sample volumes at each shear rate.

shorter contact duration and stronger separation forces at higher shear rates, one would expect less effective GpIb-IX-V binding to the immobilized vWf surface. With the same number of collisions, by adjusting the shearing duration inversely with the shear rate, fewer microspheres associated with platelets as the shear rate increases will be predicted. In addition, because of fewer available ligands, the platelet adhesion onto the microspheres with lower vWf coating density would be less than that onto high density vWf-coated microspheres. Consequently at the lower vWf coating density limit, the information concerning the bond strength between GpIb-IX-V and immobilized vWf may be obtained by analyzing the association curve (Figure 4.10). Nevertheless under experimental conditions, although the results of the low density vWf-coated microsphere were as predicted, the platelet association to the microspheres with high vWf coating density surprisingly increased as the shear rate increased. This interesting finding challenged the methodology; therefore, more attention was focused on this shear-induced enhancement of platelet and high density vWf-coated microsphere association.

The increase of platelet adhesion onto microspheres with high vWf coating density as the shear rate increases may result from either mechanical or biological effects, or both. Secondary flows in the cone-and-plate viscometer at high shear rate could increase the number of platelet-microsphere collisions and thus lead to more association. However, using a smaller volume of sample indicated that secondary flows did not play a role in causing the enhancement. It was also possible that well known shear-induced platelet activation would release some agonists and adhesive molecules from granules to

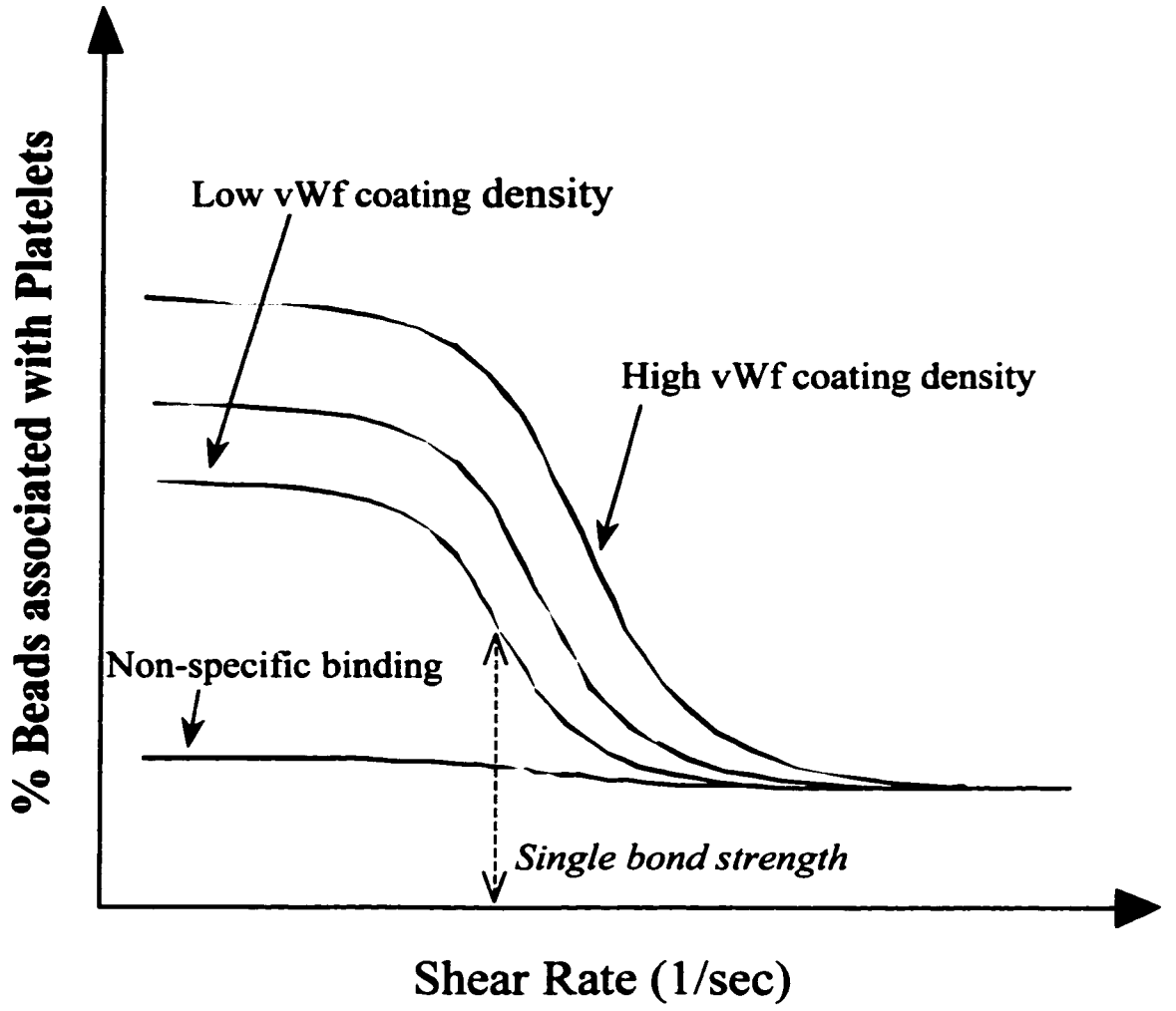


Figure 4.10 An illustration for the original idea to characterize the single bond strength by viscometric-flow cytometric analysis. The reasoning is described in the main text.

help or strengthen GpIb-IX-V binding to immobilized vWf. However, there was no significant shear-induced platelet activation, as evidenced by P-selectin expression in this experimental system. In addition, the role of the anchorage of GpIb-IX-V into the membrane-associated skeleton and of cytoskeleton reorganization in the increase of platelet adhesion to vWf-coated microspheres at high shear rates was examined. The actin filament disrupter cytochalasin D further enhanced platelet-microsphere association, whereas TMB-8 and calpeptin that inhibited the cytoskeleton rearrangement did not have effects on this phenomenon. It is also possible that molecular conformation change of platelet GpIb-IX-V or immobilized vWf at high shear rates might increase the binding affinity, but this mechanism is very difficult to verify at the molecular level under shear conditions.

Although secondary flow effects on this shear-induced platelet-microsphere association are unlikely, there still are some possible mechanical explanations for these observations. Even though the mechanical stresses to separate platelets and microspheres are larger at higher shear rates, the colliding forces are larger, too. As a result, the flexible platelet membrane may form a larger contact area with the vWf-coated microsphere and thus more bonds may be formed when platelets and microspheres collide. If the binding strength due to this increase of receptor-ligand bonds is larger than the separation forces, we may expect more platelet-microsphere associations at higher shear rates. In order to examine this aspect in the future, relatively rigid microspheres coated with GpIbα molecules instead of platelets could be used.

Shear-induced platelet activation, evidenced by P-selectin expression in this study, was not observed even though this phenomenon has been shown in many *in vitro* studies [21]. This difference results from the extracellular $Ca^{2+}$ environment, because in this study the $Ca^{2+}$ chelator EGTA was added to block the undesired interaction between GpIIb-IIIa and vWf, but in other studies citrate or heparin was used. External $Ca^{2+}$ influx may be crucial in the signal transduction pathway for shear-induced platelet activation to cause granule secretion and P-selectin expression. Although granule release from the suspended platelets is unlikely to be involved in helping platelet association with vWf-coated microspheres at high shear rates, there may be a GpIb-IX-V dependent signal after receptor-ligand binding to induce platelet change that strengthens the adhesion. Future experiments inhibiting possible platelet activation, for example, adding forskolin or prostaglandin $I_2$ to increase cytoplasmic cyclic AMP that has inhibitory effects, could be performed to investigate this potential mechanism.

It is an interesting finding that the cytoskeleton disrupter cytochalasin D further increased the association between platelets and microspheres with high vWf coating density at high shear rates, suggesting that platelet cytoskeleton may be involved in this phenomenon. Some experiments using Chinese hamster ovary (CHO) cells transfected with mutant DNAs for GpIbα have shown that the cytoplasmic domain of this molecule affected its adhesive property [185,186]. Truncation of only the actin binding protein (ABP) binding region or various lengths of the GpIbα cytoplasmic tail increased the rolling velocities of those transfected CHO cells on immobilized vWf surface in flow

chamber experiments. The increase of the rolling velocity indicated a larger dissociation rate between GpIb-IX-V and immobilized vWf. However, those observations cannot explain and may even contradict why disrupting the anchorage of GpIb-IX-V into membrane-associated skeleton by cytochalasin D enhances platelet-microsphere association to a greater degree at high shear rates. Therefore, the effect of cytochalasin D may not directly change the binding properties of GpIb-IX-V. Another more likely explanation is a mechanical reason that GpIb-IX-V complexes freed of cytoskeletal restraint can be dragged or diffuse into the tethered region and cluster to form stronger binding. This behavior has been observed in cytochalasin-treated neutrophils that converted their rolling motion to stationary adhesion on P-selectin surface in flow conditions [187].

A less likely explanation for the enhancement of platelet adhesion to microspheres with high vWf coating density at high shear rates is that the interaction between GpIb-IX-V and immobilized vWf is a "catch bond." The "catch bond" was originally predicted by a mathematical model [188] but no direct evidence of this kind of bond has been reported. In the case of catch bonds, the rate of disruption of a highly stretched bond is slower than that of an unstressed bond, like the basic mechanism of the child's toy known as the "finger-prison." Findings that show a resemblance to what one expects for catch bonds have been reported in a study of red blood cell adhesion mediated by wheatgerm agglutinin [189]. If the GpIb-IX-V binding to immobilized vWf is similar to a catch bond, it will be hard to separate them by applying larger separation forces at

high shear rates and thus may cause more platelet-microsphere association. Nevertheless, the concept of the "catch bond" has difficulty explaining the GpIb-IX-V mediated platelet rolling on immobilized vWf surfaces because the rolling relies on the quick dissociation rate of the binding.

The interaction between GpIb-IX-V and immobilized vWf is believed to have intrinsically fast association and dissociation rates. These distinctive properties enable the initiation of platelet tethering to vWf surface at high shear conditions and support platelet rolling until irreversible adhesion through the help of integrin receptors such as GpIIb-IIIa [76]. However, the transient phenomena mediated by the binding between GpIb-IX-V and immobilized vWf such as platelet rolling do not mean that when multiple bonds are formed, the pairing is not strong enough to assist firm platelet adhesion. This study demonstrates that adherent platelets did not detach from high density vWf-coated microspheres in conditions without functional GpIIb-IIIa receptors. It is plausible that a large number of GpIb-IX-V and vWf bonds can support "irreversible" platelet adhesion without the help of integrins.

In addition to the study at high shear rates, I also studied the platelet association to vWf-coated microspheres at low shear rates and at stagnant conditions. The results are shown in Figure 4.11. At low shear rates, there was no statistical difference in the platelet-microsphere association for each kind of vWf-coated microspheres. However, the platelet adhesion onto the microspheres with high vWf coating density was significantly more than those onto BSA- and low density vWf-coated microspheres at

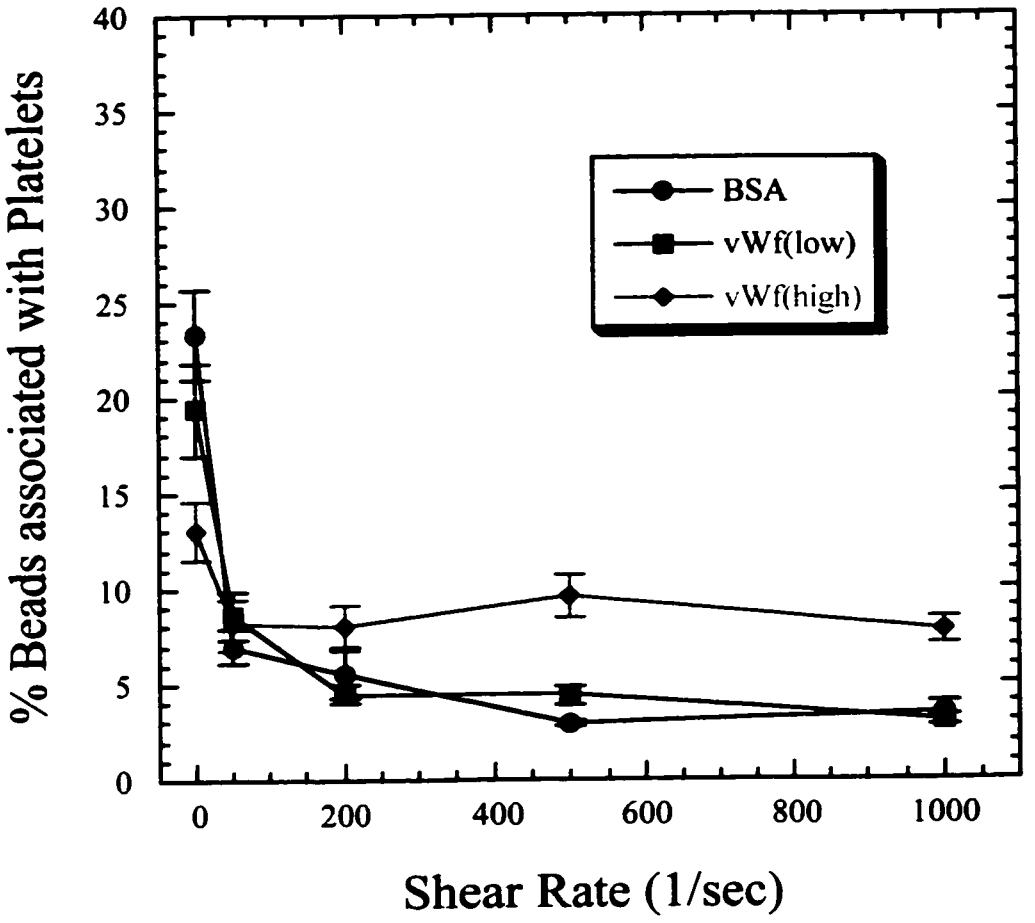


Figure 4.11 Platelet association with vWf-coated microspheres at low shear rates. The EGTA-treated PRP was sheared with the microspheres either coated with BSA, low density, or high density of vWf in the cone-and-plate viscometer. The sample was sheared at shear rates of 50, 200, 500, and 1,000 $sec^{-1}$ for 600, 150, 60, and 30 seconds respectively. The platelet association to the microspheres at static condition for 30 minutes was also measured. Values are showed as means ± SEM, n = 4-7. For the shear experiments, the results for each kind of vWf-coated microspheres are not statistically different among those shear rates applied. However, the percentages of high density vWf-coated microspheres with platelet association are significantly larger than those of low density vWf-coated and negative control microspheres at the shear rates of 500 and 1,000 $sec^{-1}$ ($p < 0.01$). In contrast, at static condition, platelet adhesion on high density vWf-coated microspheres is less than those on BSA- and low density vWf-coated microspheres ($p < 0.05$).

shear rates greater than 500 $sec^{-1}$ ($p < 0.01$). Interestingly, the outcomes for 30 minutes static incubation were in reverse order compared to those for shear experiments. The negative control and low density vWf-coated microspheres had more platelet association than the high density vWf-coated microspheres did ($p < 0.05$). These findings may be due to various surface properties, such as surface charge and hydrophobicity, of the microspheres with different amounts of protein coating. Although albumin appears to passivate nearly all materials and minimize platelet deposition, under static conditions it has been shown that BSA does not have passivation effect that reduces platelet spreading on some synthetic biomaterials [190], and the platelet activation increases as the degree of denaturation of adsorbed BSA increases [191].

In conclusion, characterizing the interaction between GpIb-IX-V and immobilized vWf is challenging and worth further investigation. The exact mechanism that causes the enhancement of platelet adhesion to high density vWf-coated microspheres as the shear rate increases has not been distinctly found, but several possible explanations have been ruled out. The viscometric-flow cytometric experiment may be useful to study the strength of a single receptor-ligand bond even though I have not pursued this issue in detail so far. However, from the data presented, the difference between those results for the microspheres with low vWf coating density and the negative control microspheres is not large enough; it is difficult to distinguish between the single bond and non-specific binding. Using transfected CHO cells with GpIb-IX-V expression instead of EGTA treated platelets in this experimental setup may be an alternative way to study the binding

of GpIb-IX-V to immobilized vWf. Because CHO cells are spherical and larger than platelets, the estimation of the separation forces between cells and microspheres is more accurate and one can generate the same level of the separation forces at lower shear rates; this may also increase the sensitivity of the methodology.

# Chapter 5

# Future Work

Pathological mural thrombosis is an important problem in cardiovascular and cerebrovascular diseases. This blood clotting process is dynamic and its determinants, including blood flow, blood components, and the vessel wall, are interconnected. Without considering all these factors, clinical and experimental results are often difficult to interpret. These essential mechanisms of mural thrombosis must be investigated to help in developing more potent therapeutics. Many insights have been obtained by extensive research in the area, and current therapies can provide moderate protection from these diseases. This thesis includes three projects that investigate the questions raised from discrepant experimental observations and characterize mural thrombosis not only from a biologist's but also from an engineer's viewpoints. Some questions raised from these studies are worthy of further investigation.

The mathematical model proposed in this thesis, based on the constitutive equation of concentrated suspensions, is able to describe steady-state red blood cell distributions and predict wall concentrations of platelets at different shear rates and average hematocrits in a parallel–plate flow chamber. However, this method has intrinsic limitations, including that the relative size of the red blood cell to the flow channel cannot be taken into account and the red blood cell-depletion layer near the wall cannot be predicted. Perhaps the computationally intensive dynamic simulations of many-body

systems may tackle these problems. It will be challenging to modify the traditional mass transport analysis with the governing equation that accounts for cell sizes and the boundary conditions that incorporate wall effects. In addition, the parameters $K(\equiv K_\eta / K_c)$, $(\frac{D^\phi}{D^{plt}})_0$, and $\alpha$ need to be estimated by fitting the predictions of steady-state cell distributions to experimental data. Epifluorescence video microscopy combined with the freeze-capture technique as well as the laser-Doppler technique could be utilized to directly measure the concentration profiles of red blood cells and platelets. The information of transient cell distributions could aid in estimating individual $K_\eta$ and $K_c$. The current setup of the epifluorescence video microscopy and the parallel-plate flow chamber system here at Rice university may only provide the information of platelet fluxes at the wall, which could be used in narrowing the value range of model parameters. After the parameters have been determined, this mathematical model could be implemented to simulate the flow system with more complicated geometry and to examine the importance of cell distributions in mural thrombosis [192].

For the activation by interaction with immobilized von Willebrand factor or collagen, platelets express fewer activated GpIIb-IIIa receptors and P-selectin molecules on the vWf- coated surface compared to that on the insoluble fibrillar collagen-coated surface. This finding explains why platelets adhere separately on vWf-coated surfaces but form aggregates on collagen-coated surfaces observed in the flow chamber experiments. However, activated GpIIb-IIIa receptors play a role in forming firm platelet adhesion on the immobilized vWf. Investigating to what extent activated GpIIb-IIIa can

help in the platelet adhesion might help in developing new therapeutic approaches and adjusting the dosage of medicines. The experimental results also demonstrate that the $Ca^{2+}$ released from intracellular pools is involved in signal transduction for the GpIIb-IIIa conformation change and the P-selectin expression after platelets interact with collagen. This suggests directions for finding the potential modulator for activating the GpIIb-IIIa, such as calmodulin-dependent protein kinases.

In the viscometric-flow cytometric experiments with EGTA-treated platelets and vWf-coated microspheres, an unexpected phenomenon occurs; that is, platelet association to microspheres with high vWf coating density increases as the shear rate increases. This enhancement does not result from the shear-induced platelet activation in suspensions, the platelet cytoskeletal rearrangement by calpains, or secondary flows in the cone-and-plate viscometer at high shear rates. These results indicate that the characteristic of the binding between GpIb-IX-V and immobilized vWf is an interesting subject for further studies. CHO cells transfected with human GpIb-IX-V molecules could be a good model system to characterize the GpIb-IX-V and immobilized vWf interaction. The viscometric-flow cytometric techniques developed in this work could be utilized to examine shear-induced association increases and perhaps to estimate the strength of the single bond between GpIb-IX-V and immobilized vWf at the low limit of vWf coating density. Some flow chamber techniques developed to study the interactions of selectins and their ligands [176,193] could also be used to investigate the GpIb-IX-V transfected CHO cells tethering/rolling on the vWf-coated surface, and thus characterize the binding.

Atomic force microscopy (AFM) techniques [194,195] could also be used to obtain more details about the characteristic of the single bond between GpIb-IX-V and immobilized vWf, such as the "catch bond" behavior.

# References

1. Virchow R. Phlogose und Thrombose in Gefaszsystem. In: Virchow R, ed. *Gesammelte Abhandlungen zur Wissenschaftlichen Medicin.* Frankfurt: von Meidinger Sohn; 1856:458-636.

2. Beck MR, Jr., Eckstein EC. Preliminary report on platelet concentration in capillary tube flows of whole blood. *Biorheology.* 1980;17:455-464.

3. Eckstein EC, Bilsker DL, Waters CM, Kippenhan JS, Tilles AW. Transport of platelets in flowing blood. *Ann N Y Acad Sci.* 1987;516:442-452.

4. Tilles AW, Eckstein EC. The near-wall excess of platelet-sized particles in blood flow: its dependence on hematocrit and wall shear rate. *Microvasc Res.* 1987;33:211-223.

5. Eckstein EC, Tilles AW, Millero FJd. Conditions for the occurrence of large near-wall excesses of small particles during blood flow. *Microvasc Res.* 1988;36:31-39.

6. Aarts PA, van den Broek SA, Prins GW, Kuiken GD, Sixma JJ, Heethaar RM. Blood platelets are concentrated near the wall and red blood cells, in the center in flowing blood. *Arteriosclerosis.* 1988;8:819-824.

7. Tangelder GJ, Teirlinck HC, Slaaf DW, Reneman RS. Distribution of blood platelets flowing in arterioles. *Am J Physiol.* 1985;248:H318-323.

8. Back LD, Radbill JR, Crawford DW. Analysis of pulsatile, viscous blood flow through diseased coronary arteries of man. *J Biomech.* 1977;10:339-353.

9. Strony J, Beaudoin A, Brands D, Adelman B. Analysis of shear stress and hemodynamic factors in a model of coronary artery stenosis and thrombosis. *Am J Physiol.* 1993;265:H1787-1796.

10. Brown CHd, Leverett LB, Lewis CW, Alfrey CP, Jr., Hellums JD. Morphological, biochemical, and functional changes in human platelets subjected to shear stress. *J Lab Clin Med.* 1975;86:462-471.

11. Anderson GH, Hellums JD, Moake J, Alfrey CP, Jr. Platelet response to shear stress: changes in serotonin uptake, serotonin release, and ADP induced aggregation. *Thromb Res.* 1978;13:1039-1047.

12. Anderson GH, Hellums JD, Moake JL, Alfrey CP, Jr. Platelet lysis and aggregation in shear fields. *Blood Cells.* 1978;4:499-511.

13. Weiss HJ, Baumgartner HR, Tschopp TB, Turitto VT, Cohen D. Correction by factor VIII of the impaired platelet adhesion to subendothelium in von Willebrand disease. *Blood.* 1978;51:267-279.

14. Weiss HJ, Turitto VT, Baumgartner HR. Effect of shear rate on platelet interaction with subendothelium in citrated and native blood. I. Shear rate--dependent decrease of adhesion in von Willebrand's disease and the Bernard-Soulier syndrome. *J Lab Clin Med.* 1978;92:750-764.

15. Sakariassen KS, Bolhuis PA, Sixma JJ. Human blood platelet adhesion to artery subendothelium is mediated by factor VIII-Von Willebrand factor bound to the subendothelium. *Nature.* 1979;279:636-638.

16. Baumgartner HR, Tschopp TB, Meyer D. Shear rate dependent inhibition of platelet adhesion and aggregation on collagenous surfaces by antibodies to human factor VIII/von Willebrand factor. *Br J Haematol.* 1980;44:127-139.

17. Moake JL, Turner NA, Stathopoulos NA, Nolasco LH, Hellums JD. Involvement of large plasma von Willebrand factor (vWF) multimers and unusually large vWF forms derived from endothelial cells in shear stress-induced platelet aggregation. *J Clin Invest.* 1986;78:1456-1461.

18. Ruggeri ZM. Mechanisms of shear-induced platelet adhesion and aggregation. *Thromb Haemost.* 1993;70:119-123.

19. Chow TW, Hellums JD, Moake JL, Kroll MH. Shear stress-induced von Willebrand factor binding to platelet glycoprotein Ib initiates calcium influx associated with aggregation. *Blood.* 1992;80:113-120.

20. Ikeda Y, Handa M, Kamata T, Kawano K, Kawai Y, Watanabe K, Kawakami K, Sakai K, Fukuyama M, Itagaki I, et al. Transmembrane calcium influx associated with von Willebrand factor binding to GP Ib in the initiation of shear-induced platelet aggregation. *Thromb Haemost.* 1993;69:496-502.

21. Konstantopoulos K, Wu KK, Udden MM, Banez EI, Shattil SJ, Hellums JD. Flow cytometric studies of platelet responses to shear stress in whole blood. *Biorheology.* 1995;32:73-93.

22. DeBakey ME, Lawrie GM, Glaeser DH. Patterns of atherosclerosis and their surgical significance. *Ann Surg.* 1985;201:115-131.

23. Frangos SG, Gahtan V, Sumpio B. Localization of atherosclerosis: role of hemodynamics. *Arch Surg.* 1999;134:1142-1149.

24. Goldsmith HL, Turitto VT. Rheological aspects of thrombosis and haemostasis: basic principles and applications. ICTH-Report--Subcommittee on Rheology of the International Committee on Thrombosis and Haemostasis. *Thromb Haemost.* 1986;55:415-435.

25. Mayadas T, Wagner DD, Simpson PJ. von Willebrand factor biosynthesis and partitioning between constitutive and regulated pathways of secretion after thrombin stimulation. *Blood.* 1989;73:706-711.

26. Sporn LA, Marder VJ, Wagner DD. von Willebrand factor released from Weibel-Palade bodies binds more avidly to extracellular matrix than that secreted constitutively. *Blood.* 1987;69:1531-1534.

27. Wencel-Drake JD, Plow EF, Zimmerman TS, Painter RG, Ginsberg MH. Immunofluorescent localization of adhesive glycoproteins in resting and thrombin-stimulated platelets. *Am J Pathol.* 1984;115:156-164.

28. Adelman B, Carlson P, Powers P. von Willebrand factor is present on the surface of platelets stimulated in plasma by ADP. *Blood.* 1987;70:1362-1366.

29. Coller BS. Platelets in cardiovascular thrombosis and thrombolysis. In: Fozzard HA, Haber E, Jennings RB, Katz AM, Morgan HE, eds. *The Heart and Cardiovascular System.* 2nd ed. New York: Raven; 1991:219-274.

30. Folie BJ, McIntire LV, Lasslo A. Effects of a novel antiplatelet agent in mural thrombogenesis on collagen-coated glass. *Blood.* 1988;72:1393-1400.

31. Alevriadou BR, Moake JL, Turner NA, Ruggeri ZM, Folie BJ, Phillips MD, Schreiber AB, Hrinda ME, McIntire LV. Real-time analysis of shear-dependent thrombus formation and its blockade by inhibitors of von Willebrand factor binding to platelets. *Blood.* 1993;81:1263-1276.

32. Ross JM, McIntire LV, Moake JL, Rand JH. Platelet adhesion and aggregation on human type VI collagen surfaces under physiological flow conditions. *Blood.* 1995;85:1826-1835.

33. Zaidi TN, McIntire LV, Farrell DH, Thiagarajan P. Adhesion of platelets to surface-bound fibrinogen under flow. *Blood.* 1996;88:2967-2972.

34. Houdijk WP, Sakariassen KS, Nievelstein PF, Sixma JJ. Role of factor VIII-von Willebrand factor and fibronectin in the interaction of platelets in flowing blood with monomeric and fibrillar human collagen types I and III. *J Clin Invest.* 1985;75:531-540.

35. Bastida E, Escolar G, Ordinas A, Sixma JJ. Fibronectin is required for platelet adhesion and for thrombus formation on subendothelium and collagen surfaces. *Blood.* 1987;70:1437-1442.

36. Endenburg SC, Hantgan RR, Lindeboom-Blokzijl L, Lankhof H, Jerome WG, Lewis JC, Sixma JJ, de Groot PG. On the role of von Willebrand factor in promoting platelet adhesion to fibrin in flowing blood. *Blood.* 1995;86:4158-4165.

37. Jen CJ, Lin JS. Direct observation of platelet adhesion to fibrinogen- and fibrin-coated surfaces. *Am J Physiol.* 1991;261:H1457-1463.

38. Sakariassen KS, Aarts PA, de Groot PG, Houdijk WP, Sixma JJ. A perfusion chamber developed to investigate platelet interaction in flowing blood with human vessel wall cells, their extracellular matrix, and purified components. *J Lab Clin Med.* 1983;102:522-535.

39. Sixma JJ, Pronk A, Nievelstein PN, Zwaginga JJ, Hindriks G, Tijburg P, Banga JD, De Groot PG. Platelet adhesion to extracellular matrices of cultured cells. *Ann N Y Acad Sci.* 1991;614:181-192.

40. Tran-Son-Tay R. Techniques for Studying the Effects of Physical Forces on Mammalian Cells and Measuring Cell Mechanical Properties. In: Frangos JA, ed. *Physical Forces and the Mammalian Cell.* San Diego: Academic Press; 1993:1-59.

41. Minamoto Y, Hato T, Nakatani S, Fujita S. Detection of platelet adhesion/aggregation to immobilized ligands on microbeads by an aggregometer. *Thromb Haemost.* 1996;76:1072-1079.

42. Stewart MW, Etches WS, Boshkov LK, Mant MJ, Gordon PA, Shaw AR. Platelet activation by a novel solid-phase agonist: effects of VWF immobilized on polystyrene beads. *Br J Haematol.* 1997;97:321-329.

43. Smith JW, Steinhubl SR, Lincoff AM, Coleman JC, Lee TT, Hillman RS, Coller BS. Rapid platelet-function assay: an automated and quantitative cartridge-based method. *Circulation.* 1999;99:620-625.

44. Jen CJ, McIntire LV. Characteristics of shear-induced aggregation in whole blood. *J Lab Clin Med.* 1984;103:115-124.

45. Alkhamis TM, Beissinger RL, Chediak JR. Red blood cell effect on platelet adhesion and aggregation in low- stress shear flow. Myth or fact? *ASAIO Trans.* 1988;34:868-873.

46. Giorgio TD, Hellums JD. A cone and plate viscometer for the continuous measurement of blood platelet activation. *Biorheology.* 1988;25:605-624.

47. Ikeda Y, Handa M, Kawano K, Kamata T, Murata M, Araki Y, Anbo H, Kawai Y, Watanabe K, Itagaki I, et al. The role of von Willebrand factor and fibrinogen in platelet aggregation under varying shear stress. *J Clin Invest.* 1991;87:1234-1240.

48. Goto S, Handa S, Takahashi E, Abe S, Handa M, Ikeda Y. Synergistic effect of epinephrine and shearing on platelet activation. *Thromb Res.* 1996;84:351-359.

49. Ohshima N, Onohara M, Sato M. Dynamics of platelet adhesion to artificial materials and cultured endothelial cells under shear flow. *ASAIO Trans.* 1989;35:379-381.

50. Tsuji S, Sugimoto M, Kuwahara M, Nishio K, Takahashi Y, Fujimura Y, Ikeda Y, Yoshioka A. Role and initiation mechanism of the interaction of glycoprotein Ib with surface-immobilized von Willebrand factor in a solid-phase platelet cohesion process. *Blood.* 1996;88:3854-3861.

51. Voisin P, Guimont C, Stoltz JF. Experimental investigation of the rheological activation of blood platelets. *Biorheology.* 1985;22:425-435.

52. Xia Z, Frojmovic MM. Aggregation efficiency of activated normal or fixed platelets in a simple shear field: effect of shear and fibrinogen occupancy. *Biophys J.* 1994;66:2190-2201.

53. Hubbell JA, McIntire LV. Visualization and analysis of mural thrombogenesis on collagen, polyurethane and nylon. *Biomaterials.* 1986;7:354-363.

54. Muggli R, Baumgartner HR, Tschopp TB, Keller H. Automated microdensitometry and protein assays as a measure for platelet adhesion and aggregation on collagen-coated slides under controlled flow conditions. *J Lab Clin Med.* 1980;95:195-207.

55. Fressinaud E, Baruch D, Girma JP, Sakariassen KS, Baumgartner HR, Meyer D. von Willebrand factor-mediated platelet adhesion to collagen involves platelet membrane glycoprotein IIb-IIIa as well as glycoprotein Ib. *J Lab Clin Med.* 1988;112:58-67.

56. Weiss HJ, Turitto VT, Baumgartner HR. Platelet adhesion and thrombus formation on subendothelium in platelets deficient in glycoproteins IIb-IIIa, Ib, and storage granules. *Blood.* 1986;67:322-330.

57. Sakariassen KS, Nievelstein PF, Coller BS, Sixma JJ. The role of platelet membrane glycoproteins Ib and IIb-IIIa in platelet adherence to human artery subendothelium. *Br J Haematol.* 1986;63:681-691.

58. Fredrickson BJ, Dong JF, McIntire LV, Lopez JA. Shear-dependent rolling on von Willebrand factor of mammalian cells expressing the platelet glycoprotein Ib-IX-V complex. *Blood.* 1998;92:3684-3693.

59. Romo GM, Dong JF, Schade AJ, Gardiner EE, Kansas GS, Li CQ, McIntire LV, Berndt MC, Lopez JA. The glycoprotein Ib-IX-V complex is a platelet counterreceptor for P- selectin. *J Exp Med.* 1999;190:803-814.

60. Shen Y, Romo GM, Dong JF, Schade A, McIntire LV, Kenny D, Whisstock JC, Berndt MC, Lopez JA, Andrews RK. Requirement of leucine-rich repeats of glycoprotein (GP) Ibalpha for shear-dependent and static binding of von Willebrand factor to the platelet membrane GP Ib-IX-V complex. *Blood.* 2000;95:903-910.

61. Badimon L, Badimon JJ. Mechanisms of arterial thrombosis in nonparallel streamlines: platelet thrombi grow on the apex of stenotic severely injured vessel wall. Experimental study in the pig model. *J Clin Invest.* 1989;84:1134-1144.

62. Barstad RM, Roald HE, Cui Y, Turitto VT, Sakariassen KS. A perfusion chamber developed to investigate thrombus formation and shear profiles in flowing native human blood at the apex of well-defined stenoses. *Arterioscler Thromb.* 1994;14:1984-1991.

63. Barstad RM, Kierulf P, Sakariassen KS. Collagen induced thrombus formation at the apex of eccentric stenoses--a time course study with non-anticoagulated human blood. *Thromb Haemost.* 1996;75:685-692.

64. Schoephoerster RT, Oynes F, Nunez G, Kapadvanjwala M, Dewanjee MK. Effects of local geometry and fluid dynamics on regional platelet deposition on artificial surfaces. *Arterioscler Thromb.* 1993;13:1806-1813.

65. Bluestein D, Niu L, Schoephoerster RT, Dewanjee MK. Fluid mechanics of arterial stenosis: relationship to the development of mural thrombus. *Ann Biomed Eng.* 1997;25:344-356.

66. Usami S, Chen HH, Zhao Y, Chien S, Skalak R. Design and construction of a linear shear stress flow chamber. *Ann Biomed Eng.* 1993;21:77-83.

67. Cao J, Usami S, Dong C. Development of a side-view chamber for studying cell-surface adhesion under flow conditions. *Ann Biomed Eng.* 1997;25:573-580.

68. Baumgartner HR, Haudenschild C. Adhesion of platelets to subendothelium. *Ann N Y Acad Sci.* 1972;201:22-36.

69. Badimon L, Turitto V, Rosemark JA, Badimon JJ, Fuster V. Characterization of a tubular flow chamber for studying platelet interaction with biologic and prosthetic materials: deposition of indium 111-labeled platelets on collagen, subendothelium, and

expanded polytetrafluoroethylene [published erratum appears in J Lab Clin Med 1988 Jan;111(1):5]. *J Lab Clin Med.* 1987;110:706-718.

70. Keller KH. Effect of fluid shear on mass transport in flowing blood. *Fed Proc.* 1971;30:1591-1599.

71. Wang NH, Keller KH. Solute transport induced by erythrocyte motions in shear flow. *Trans Am Soc Artif Intern Organs.* 1979;25:14-18.

72. Baumgartner HR. The role of blood flow in platelet adhesion, fibrin deposition, and formation of mural thrombi. *Microvasc Res.* 1973;5:167-179.

73. Turitto VT, Weiss HJ. Red blood cells: their dual role in thrombus formation. *Science.* 1980;207:541-543.

74. Eckstein EC. Rheophoresis--a broader concept of platelet dispersivity. *Biorheology.* 1982;19:717-724.

75. Reimers RC, Sutera SP, Joist JH. Potentiation by red blood cells of shear-induced platelet aggregation: relative importance of chemical and physical mechanisms. *Blood.* 1984;64:1200-1206.

76. Savage B, Saldivar E, Ruggeri ZM. Initiation of platelet adhesion by arrest onto fibrinogen or translocation on von Willebrand factor. *Cell.* 1996;84:289-297.

77. Goto S, Salomon DR, Ikeda Y, Ruggeri ZM. Characterization of the unique mechanism mediating the shear-dependent binding of soluble von Willebrand factor to platelets. *J Biol Chem.* 1995;270:23352-23361.

78. Konstantopoulos K, Chow TW, Turner NA, Hellums JD, Moake JL. Shear stress-induced binding of von Willebrand factor to platelets. *Biorheology.* 1997;34:57-71.

79. Kroll MH, Harris TS, Moake JL, Handin RI, Schafer AI. von Willebrand factor binding to platelet GpIb initiates signals for platelet activation. *J Clin Invest.* 1991;88:1568-1573.

80. Weiss HJ. von Willebrand factor and platelet function. *Ann N Y Acad Sci.* 1991;614:125-137.

81. Weiss HJ, Turitto VT, Baumgartner HR. Further evidence that glycoprotein IIb-IIIa mediates platelet spreading on subendothelium. *Thromb Haemost.* 1991;65:202-205.

82. Smith EB, Keen GA, Grant A, Stirk C. Fate of fibrinogen in human arterial intima. *Arteriosclerosis.* 1990;10:263-275.

83. Bini A, Fenoglio JJ, Jr., Mesa-Tejada R, Kudryk B, Kaplan KL. Identification and distribution of fibrinogen, fibrin, and fibrin(ogen) degradation products in atherosclerosis. Use of monoclonal antibodies. *Arteriosclerosis*. 1989;9:109-121.

84. Sheppeck RA, Bentz M, Dickson C, Hribar S, White J, Janosky J, Berceli SA, Borovetz HS, Johnson PC. Examination of the roles of glycoprotein Ib and glycoprotein IIb/IIIa in platelet deposition on an artificial surface using clinical antiplatelet agents and monoclonal antibody blockade. *Blood*. 1991;78:673-680.

85. Nagai H, Handa M, Kawai Y, Watanabe K, Ikeda Y. Evidence that plasma fibrinogen and platelet membrane GPIIb-IIIa are involved in the adhesion of platelets to an artificial surface exposed to plasma. *Thromb Res*. 1993;71:467-477.

86. Goldsmith HL, Marlow JC. Flow behavior of erythrocytes. II. Particle motions in concentrated suspensions of ghost cells. *J. Colloid Interface Sci.* 1979;71:383-407.

87. Turitto VT, Baumgartner HR. Platelet deposition on subendothelium exposed to flowing blood: mathematical analysis of physical parameters. *Trans Am Soc Artif Intern Organs*. 1975;21:593-601.

88. Goldsmith HL, Marlow J. Flow behaviour of erythrocytes. I. Rotation and deformation in dilute suspensions. *Proc. R. Soc. Lond. B.* 1972;182:351-384.

89. Eckstein EC, Belgacem F. Model of platelet transport in flowing blood with drift and diffusion terms. *Biophys J.* 1991;60:53-69.

90. Yeh C, Calvez AC, Eckstein EC. An estimated shape function for drift in a platelet-transport model. *Biophys J.* 1994;67:1252-1259.

91. Leighton D, Acrivos A. Measurement of shear-induced self-diffusion in concentrated suspensions of spheres. *J. Fluid Mech.* 1987;177:109-131.

92. Leighton D, Acrivos A. The shear-induced migration of particles in concentrated suspensions. *J. Fluid Mech.* 1987;181:415-439.

93. Phillips RJ, Armstrong RC, Brown RA, Graham AL, Abbott JR. A constitutive equation for concentrated suspensions that accounts for shear-induced particle migration. *Phys. Fluids A*. 1992;4:30-40.

94. Quemada D. Rheology of concentrated disperse systems and minimum energy dissipation principle. I. Viscosity-concentration relationship. *Rheol. Acta*. 1977;16:82-94.

95. Quemada D. Rheology of concentrated disperse systems. II. A model for non-Newtonian shear viscosity in steady flows. *Rheol. Acta*. 1978;17:632-642.

96. Quemada D. A rheological model for studying the hematocrit dependence of red cell-red cell and red cell-protein interactions in blood. *Biorheology*. 1981;18:501-516.

97. Cokelet GR. The Rheology and Tube Flow of Blood. In: Skalak R, Chien S, eds. *Handbook of Bioengineering*. New York: McGraw-Hill; 1987:14.11-14.17.

98. Easthope PL, Brooks DE. A comparison of rheological constitutive functions for whole human blood. *Biorheology*. 1980;17:235-247.

99. Das B, Johnson PC, Popel AS. Effect of nonaxisymmetric hematocrit distribution on non-Newtonian blood flow in small tubes. *Biorheology*. 1998;35:69-87.

100. Press WH, Teukolsky SA, Vetterling WT, Flannery BP. *Numerical Recipes in Fortran 77: The Art of Scientific Computing*. 2nd ed. New York: Cambridge University Press; 1996.

101. Cussler EL. *Diffusion: Mass Transfer in Fluid Systems*. 2nd ed. New York: Cambridge University Press; 1997.

102. Segre G, Silberberg A. Behaviour of macroscopic rigid spheres in Poiseuille flow. Part 1. Determination of local concentration by statistical analysis of particle passages through crossed light beams. *J. Fluid Mech.* 1962;14:115-135.

103. Segre G, Silberberg A. Behaviour of macroscopic rigid spheres in Poiseuille flow. Part 2. Experimental results and interpretation. *J. Fluid Mech.* 1962;14:136-157.

104. Fernandez-Ortiz A, Badimon JJ, Falk E, Fuster V, Meyer B, Mailhac A, Weng D, Shah PK, Badimon L. Characterization of the relative thrombogenicity of atherosclerotic plaque components: implications for consequences of plaque rupture. *J Am Coll Cardiol*. 1994;23:1562-1569.

105. Chen YP, Djaffar I, Pidard D, Steiner B, Cieutat AM, Caen JP, Rosa JP. Ser-752-->Pro mutation in the cytoplasmic domain of integrin beta 3 subunit and defective activation of platelet integrin alpha IIb beta 3 (glycoprotein IIb-IIIa) in a variant of Glanzmann thrombasthenia. *Proc Natl Acad Sci U S A*. 1992;89:10169-10173.

106. Shattil SJ, Hoxie JA, Cunningham M, Brass LF. Changes in the platelet membrane glycoprotein IIb.IIIa complex during platelet activation. *J Biol Chem*. 1985;260:11107-11114.

107. Kawaguchi H, Koiwai N, Ohtsuka Y, Miyamoto M, Sasakawa S. Phagocytosis of latex particles by leucocytes. I. Dependence of phagocytosis on the size and surface potential of particles. *Biomaterials*. 1986;7:61-66.

108. Miyamoto M, Sasakawa S, Ozawa T, Kawaguchi H, Ohtsuka Y. Platelet aggregation induced by latex particles. I. Effects of size, surface potential and hydrophobicity of particles. *Biomaterials*. 1989;10:251-257.

109. Miyamoto M, Sasakawa S, Ozawa T, Kawaguchi H, Ohtsuka Y. Mechanisms of blood coagulation induced by latex particles and the roles of blood cells. *Biomaterials*. 1990;11:385-388.

110. Gemmell CH. Platelet adhesion onto artificial surfaces: inhibition by benzamidine, pentamidine, and pyridoxal-5-phosphate as demonstrated by flow cytometric quantification of platelet adhesion to microspheres. *J Lab Clin Med*. 1998;131:84-92.

111. Liu Q, Rooney MM, Kasirer-Friede A, Brown E, Lord ST, Frojmovic MM. Role of the gamma chain Ala-Gly-Asp-Val and Aalpha chain Arg-Gly-Asp-Ser sites of fibrinogen in coaggregation of platelets and fibrinogen-coated beads. *Biochim Biophys Acta*. 1998;1385:33-42.

112. Peerschke EI. Events occurring after thrombin-induced fibrinogen binding to platelets. *Semin Thromb Hemost*. 1992;18:34-43.

113. Graber SE, Hawiger J. Evidence that changes in platelet cyclic AMP levels regulate the fibrinogen receptor on human platelets. *J Biol Chem*. 1982;257:14606-14609.

114. Peerschke EI. Time-dependent association between platelet-bound fibrinogen and the Triton X-100 insoluble cytoskeleton. *Blood*. 1991;77:508-514.

115. Frojmovic M, Wong T, van de Ven T. Dynamic measurements of the platelet membrane glycoprotein IIb-IIIa receptor for fibrinogen by flow cytometry. I. Methodology, theory and results for two distinct activators. *Biophys J*. 1991;59:815-827.

116. Shattil SJ, Weisel JW, Kieber-Emmons T. Use of monoclonal antibodies to study the interaction between an integrin adhesion receptor, GP IIb-IIIa, and its physiological ligand, fibrinogen. *Immunomethods*. 1992;1:53-63.

117. Peerschke EI. Observations on the effects of cytochalasin B and cytochalasin D on ADP- and chymotrypsin-treated platelets. *Proc Soc Exp Biol Med*. 1984;175:109-115.

118. Shattil SJ, Haimovich B, Cunningham M, Lipfert L, Parsons JT, Ginsberg MH, Brugge JS. Tyrosine phosphorylation of pp125FAK in platelets requires coordinated signaling through integrin and agonist receptors. *J Biol Chem*. 1994;269:14738-14745.

119. Saitoh M, Salzman EW, Smith M, Ware JA. Activation of protein kinase C in platelets by epinephrine and A23187: correlation with fibrinogen binding. *Blood.* 1989;74:2001-2006.

120. Walker TR, Watson SP. Synergy between Ca2+ and protein kinase C is the major factor in determining the level of secretion from human platelets. *Biochem J.* 1993;289:277-282.

121. Shattil SJ, Cunningham M, Wiedmer T, Zhao J, Sims PJ, Brass LF. Regulation of glycoprotein IIb-IIIa receptor function studied with platelets permeabilized by the pore-forming complement proteins C5b-9. *J Biol Chem.* 1992;267:18424-18431.

122. Rink TJ. Cytosolic calcium in platelet activation. *Experientia.* 1988;44:97-100.

123. Ashby B, Daniel JL, Smith JB. Mechanisms of platelet activation and inhibition. *Hematol Oncol Clin North Am.* 1990;4:1-26.

124. Sage SO, Sargeant P, Heemskerk JW, Mahaut-Smith MP. Calcium influx mechanisms and signal organisation in human platelets. *Adv Exp Med Biol.* 1993;344:69-82.

125. Briddon SJ, Watson SP. Evidence for the involvement of p59fyn and p53/56lyn in collagen receptor signalling in human platelets. *Biochem J.* 1999;338:203-209.

126. Gibbins JM, Okuma M, Farndale R, Barnes M, Watson SP. Glycoprotein VI is the collagen receptor in platelets which underlies tyrosine phosphorylation of the Fc receptor gamma-chain. *FEBS Lett.* 1997;413:255-259.

127. Tsuji M, Ezumi Y, Arai M, Takayama H. A novel association of Fc receptor gamma-chain with glycoprotein VI and their co-expression as a collagen receptor in human platelets. *J Biol Chem.* 1997;272:23528-23531.

128. Kehrel B, Wierwille S, Clemetson KJ, Anders O, Steiner M, Knight CG, Farndale RW, Okuma M, Barnes MJ. Glycoprotein VI is a major collagen receptor for platelet activation: it recognizes the platelet-activating quaternary structure of collagen, whereas CD36, glycoprotein IIb/IIIa, and von Willebrand factor do not. *Blood.* 1998;91:491-499.

129. Alberio L, Dale GL. Review article: platelet-collagen interactions: membrane receptors and intracellular signalling pathways [In Process Citation]. *Eur J Clin Invest.* 1999;29:1066-1076.

130. Laudano AP, Doolittle RF. Synthetic peptide derivatives that bind to fibrinogen and prevent the polymerization of fibrin monomers. *Proc Natl Acad Sci U S A.* 1978;75:3085-3089.

131. Plow EF, Marguerie G. Inhibition of fibrinogen binding to human platelets by the tetrapeptide glycyl-L-prolyl-L-arginyl-L-proline. *Proc Natl Acad Sci U S A.* 1982;79:3711-3715.

132. Hayashi Y, Takenaka S, Kohmura C, Ikeda H. Preparation of discoid washed platelets by differential centrifugation. *Clin Chim Acta.* 1998;275:99-105.

133. Read NG, Radomski MW, Goodwin DA, Moncada S. An ultrastructural study of stored human platelets after washing using prostacyclin. *Br J Haematol.* 1985;60:305-314.

134. Bertagnolli ME, Beckerle MC. Evidence for the selective association of a subpopulation of GPIIb-IIIa with the actin cytoskeletons of thrombin-activated platelets. *J Cell Biol.* 1993;121:1329-1342.

135. Gudi S, Nolan JP, Frangos JA. Modulation of GTPase activity of G proteins by fluid shear stress and phospholipid composition. *Proc Natl Acad Sci U S A.* 1998;95:2515-2519.

136. Savage B, Shattil SJ, Ruggeri ZM. Modulation of platelet function through adhesion receptors. A dual role for glycoprotein IIb-IIIa (integrin alpha IIb beta 3) mediated by fibrinogen and glycoprotein Ib-von Willebrand factor. *J Biol Chem.* 1992;267:11300-11306.

137. Savage B, Ginsberg MH, Ruggeri ZM. Influence of fibrillar collagen structure on the mechanisms of platelet thrombus formation under flow. *Blood.* 1999;94:2704-2715.

138. Siljander P, Lassila R. Studies of adhesion-dependent platelet activation: distinct roles for different participating receptors can be dissociated by proteolysis of collagen. *Arterioscler Thromb Vasc Biol.* 1999;19:3033-3043.

139. Hartwig JH. Mechanisms of actin rearrangements mediating platelet activation. *J Cell Biol.* 1992;118:1421-1442.

140. Furman MI, Gardner TM, Goldschmidt-Clermont PJ. Mechanisms of cytoskeletal reorganization during platelet activation. *Thromb Haemost.* 1993;70:229-232.

141. Fox JE. The platelet cytoskeleton. *Thromb Haemost.* 1993;70:884-893.

142. Barkalow K, Hartwig JH. The role of actin filament barbed-end exposure in cytoskeletal dynamics and cell motility. *Biochem Soc Trans.* 1995;23:451-456.

143. Alberio L, Dale GL. Flow cytometric analysis of platelet activation by different collagen types present in the vessel wall. *Br J Haematol.* 1998;102:1212-1218.

144. Parmentier S, McGregor L, Catimel B, Leung LL, McGregor JL. Inhibition of platelet functions by a monoclonal antibody (LYP20) directed against a granule membrane glycoprotein (GMP-140/PADGEM). *Blood.* 1991;77:1734-1739.

145. Boukerche H, Ruchaud-Sparagano MH, Rouen C, Brochier J, Kaplan C, McGregor JL. A monoclonal antibody directed against a granule membrane glycoprotein (GMP-140/PADGEM, P-selectin, CD62P) inhibits ristocetin-induced platelet aggregation. *Br J Haematol.* 1996;92:442-451.

146. Federici AB, Bader R, Pagani S, Colibretti ML, De Marco L, Mannucci PM. Binding of von Willebrand factor to glycoproteins Ib and IIb/IIIa complex: affinity is related to multimeric size. *Br J Haematol.* 1989;73:93-99.

147. Furlan M. Von Willebrand factor: molecular size and functional activity. *Ann Hematol.* 1996;72:341-348.

148. Sixma JJ. Interaction of blood platelets with the vessel wall. In: Bloom AL, Forbes CD, Thomas DP, Tuddenham EGD, eds. *Haemostasis and Thrombosis.* 3rd ed. Edinburgh: Churchill Livingstone; 1994:259-285.

149. Mohri H, Fujimura Y, Shima M, Yoshioka A, Houghten RA, Ruggeri ZM, Zimmerman TS. Structure of the von Willebrand factor domain interacting with glycoprotein Ib. *J Biol Chem.* 1988;263:17901-17904.

150. Mohri H, Yoshioka A, Zimmerman TS, Ruggeri ZM. Isolation of the von Willebrand factor domain interacting with platelet glycoprotein Ib, heparin, and collagen and characterization of its three distinct functional sites. *J Biol Chem.* 1989;264:17361-17367.

151. Denis C, Baruch D, Kielty CM, Ajzenberg N, Christophe O, Meyer D. Localization of von Willebrand factor binding domains to endothelial extracellular matrix and to type VI collagen. *Arterioscler Thromb.* 1993;13:398-406.

152. Hoylaerts MF, Yamamoto H, Nuyts K, Vreys I, Deckmyn H, Vermylen J. von Willebrand factor binds to native collagen VI primarily via its A1 domain. *Biochem J.* 1997;324:185-191.

153. Mazzucato M, Spessotto P, Masotti A, De Appollonia L, Cozzi MR, Yoshioka A, Perris R, Colombatti A, De Marco L. Identification of domains responsible for von Willebrand factor type VI collagen interaction mediating platelet adhesion under high flow. *J Biol Chem.* 1999;274:3033-3041.

154. Kalafatis M, Takahashi Y, Girma JP, Meyer D. Localization of a collagen-interactive domain of human von Willebrand factor between amino acid residues Gly 911 and Glu 1,365. *Blood.* 1987;70:1577-1583.

155. Williams S, Gralnick H. Inhibition of von Willebrand factor binding to platelets by two recognition site peptides: the pentadecapeptide of the carboxy terminus of the fibrinogen gamma chain and the tetrapeptide arg-gly-asp-ser. *Thromb Res.* 1987;46:457-471.

156. Lawrence JB, Kramer WS, McKeown LP, Williams SB, Gralnick HR. Arginine-glycine-aspartic acid- and fibrinogen gamma-chain carboxyterminal peptides inhibit platelet adherence to arterial subendothelium at high wall shear rates. An effect dissociable from interference with adhesive protein binding. *J Clin Invest.* 1990;86:1715-1722.

157. Berndt MC, Ward CM, Booth WJ, Castaldi PA, Mazurov AV, Andrews RK. Identification of aspartic acid 514 through glutamic acid 542 as a glycoprotein Ib-IX complex receptor recognition sequence in von Willebrand factor. Mechanism of modulation of von Willebrand factor by ristocetin and botrocetin. *Biochemistry.* 1992;31:11144-11151.

158. Lopez JA, Dong JF. Structure and function of the glycoprotein Ib-IX-V complex. *Curr Opin Hematol.* 1997;4:323-329.

159. Clemetson KJ. Platelet GPIb-V-IX complex. *Thromb Haemost.* 1997;78:266-270.

160. Vicente V, Houghten RA, Ruggeri ZM. Identification of a site in the alpha chain of platelet glycoprotein Ib that participates in von Willebrand factor binding. *J Biol Chem.* 1990;265:274-280.

161. Katagiri Y, Hayashi Y, Yamamoto K, Tanoue K, Kosaki G, Yamazaki H. Localization of von Willebrand factor and thrombin-interactive domains on human platelet glycoprotein Ib. *Thromb Haemost.* 1990;63:122-126.

162. Tsuji T, Tsunehisa S, Watanabe Y, Yamamoto K, Tohyama H, Osawa T. The carbohydrate moiety of human platelet glycocalicin. *J Biol Chem.* 1983;258:6335-6339.

163. Coller BS. Biochemical and electrostatic considerations in primary platelet aggregation. *Ann N Y Acad Sci.* 1983;416:693-708.

164. Fox JE, Aggerbeck LP, Berndt MC. Structure of the glycoprotein Ib.IX complex from platelet membranes. *J Biol Chem.* 1988;263:4882-4890.

165. Lopez JA, Ludwig EH, McCarthy BJ. Polymorphism of human glycoprotein Ib alpha results from a variable number of tandem repeats of a 13-amino acid sequence in the mucin-like macroglycopeptide region. Structure/function implications. *J Biol Chem.* 1992;267:10055-10061.

166. Andrews RK, Fox JE. Identification of a region in the cytoplasmic domain of the platelet membrane glycoprotein Ib-IX complex that binds to purified actin-binding protein. *J Biol Chem.* 1992;267:18605-18611.

167. Fox JE, Boyles JK, Berndt MC, Steffen PK, Anderson LK. Identification of a membrane skeleton in platelets. *J Cell Biol.* 1988;106:1525-1538.

168. Fox JE, Lipfert L, Clark EA, Reynolds CC, Austin CD, Brugge JS. On the role of the platelet membrane skeleton in mediating signal transduction. Association of GP IIb-IIIa, pp60c-src, pp62c-yes, and the p21ras GTPase-activating protein with the membrane skeleton. *J Biol Chem.* 1993;268:25973-25984.

169. Cooray P, Yuan Y, Schoenwaelder SM, Mitchell CA, Salem HH, Jackson SP. Focal adhesion kinase (pp125FAK) cleavage and regulation by calpain. *Biochem J.* 1996;318:41-47.

170. Fox JE, Berndt MC. Cyclic AMP-dependent phosphorylation of glycoprotein Ib inhibits collagen-induced polymerization of actin in platelets. *J Biol Chem.* 1989;264:9520-9526.

171. Wardell MR, Reynolds CC, Berndt MC, Wallace RW, Fox JE. Platelet glycoprotein Ib beta is phosphorylated on serine 166 by cyclic AMP-dependent protein kinase. *J Biol Chem.* 1989;264:15656-15661.

172. Du X, Harris SJ, Tetaz TJ, Ginsberg MH, Berndt MC. Association of a phospholipase A2 (14-3-3 protein) with the platelet glycoprotein Ib-IX complex. *J Biol Chem.* 1994;269:18287-18290.

173. Sullam PM, Hyun WC, Szollosi J, Dong J, Foss WM, Lopez JA. Physical proximity and functional interplay of the glycoprotein Ib-IX-V complex and the Fc receptor FcgammaRIIA on the platelet plasma membrane. *J Biol Chem.* 1998;273:5331-5336.

174. Lawrence MB, Smith CW, Eskin SG, McIntire LV. Effect of venous shear stress on CD18-mediated neutrophil adhesion to cultured endothelium. *Blood.* 1990;75:227-237.

175. Lawrence MB, Springer TA. Leukocytes roll on a selectin at physiologic flow rates: distinction from and prerequisite for adhesion through integrins. *Cell.* 1991;65:859-873.

176. Alon R, Hammer DA, Springer TA. Lifetime of the P-selectin-carbohydrate bond and its response to tensile force in hydrodynamic flow [published erratum appears in Nature 1995 Sep 7;376(6544):86]. *Nature.* 1995;374:539-542.

177. Tees DF, Coenen O, Goldsmith HL. Interaction forces between red cells agglutinated by antibody. IV. Time and force dependence of break-up. *Biophys J.* 1993;65:1318-1334.

178. Tees DF, Goldsmith HL. Kinetics and locus of failure of receptor-ligand-mediated adhesion between latex spheres. I. Protein-carbohydrate bond. *Biophys J.* 1996;71:1102-1114.

179. Amblard F. Method to Assess the Strength of Cell-Cell Adhesion Using a Modified Flow Cytometer. In: Bongrand P, Claesson PM, Curtis ASG, eds. *Studying Cell Adhesion.* Heidelberg: Springer-Verlag; 1994:93-109.

180. Amblard F, Auffray C, Sekaly R, Fischer A. Molecular analysis of antigen-independent adhesion forces between T and B lymphocytes. *Proc Natl Acad Sci U S A.* 1994;91:3628-3632.

181. Shattil SJ, Brass LF, Bennett JS, Pandhi P. Biochemical and functional consequences of dissociation of the platelet membrane glycoprotein IIb-IIIa complex. *Blood.* 1985;66:92-98.

182. Smoluchowski MV. Vensuch einer mathematischen theorie der koagulation kinetic kolloider losungen. *Zeitschrift fur Physikalische Chemie.* 1917;92:129-168.

183. Girma JP, Fressinaud E, Christophe O, Rouault C, Obert B, Takahashi Y, Meyer D. Aurin tricarboxylic acid inhibits platelet adhesion to collagen by binding to the 509-695 disulphide loop of von Willebrand factor and competing with glycoprotein Ib. *Thromb Haemost.* 1992;68:707-713.

184. Fewell ME, Hellums JD. The secondary flow of Newtonian fluids in cone-and-plate viscometers. *Trans. Soc. Rheol.* 1977;21:535-565.

185. Cranmer SL, Ulsemer P, Cooke BM, Salem HH, de la Salle C, Lanza F, Jackson SP. Glycoprotein (GP) Ib-IX-transfected cells roll on a von Willebrand factor matrix under flow. Importance of the GPib/actin-binding protein (ABP-280) interaction in maintaining adhesion under high shear. *J Biol Chem.* 1999;274:6097-6106.

186. Schade AJ. Interactions of the Platelet GP Ib-IX-V Complex with Immobilized von Willebrand Factor under Flow Conditions. In:: Rice University; 1999.

187. Sheikh S, Nash GB. Treatment of neutrophils with cytochalasins converts rolling to stationary adhesion on P-selectin. *J Cell Physiol.* 1998;174:206-216.

188. Dembo M, Torney DC, Saxman K, Hammer D. The reaction-limited kinetics of membrane-to-surface adhesion and detachment. *Proc R Soc Lond B Biol Sci.* 1988;234:55-83.

189. Evans E, Leung A. Adhesivity and rigidity of erythrocyte membrane in relation to wheat germ agglutinin binding. *J Cell Biol.* 1984;98:1201-1208.

190. Goodman SL, Cooper SL, Albrecht RM. The effects of substrate-adsorbed albumin on platelet spreading. *J Biomater Sci Polym Ed.* 1991;2:147-159.

191. Mori A, Ito Y, Sisido M, Imanishi Y. Interaction of polystyrene/poly(gamma-benzyl L-glutamate) and poly(methyl methacrylate)/poly(gamma-benzyl L-glutamate) block copolymers with plasma proteins and platelets. *Biomaterials.* 1986;7:386-392.

192. Hofer M, Perktold K. Computer simulation of concentrated fluid-particle suspension flows in axisymmetric geometries. *Biorheology.* 1997;34:261-279.

193. Alon R, Chen S, Puri KD, Finger EB, Springer TA. The kinetics of L-selectin tethers and the mechanics of selectin-mediated rolling. *J Cell Biol.* 1997;138:1169-1180.

194. Florin EL, Moy VT, Gaub HE. Adhesion forces between individual ligand-receptor pairs. *Science.* 1994;264:415-417.

195. Fisher TE, Marszalek PE, Oberhauser AF, Carrion-Vazquez M, Fernandez JM. The micro-mechanics of single molecules studied with atomic force microscopy. *J Physiol (Lond).* 1999;520 Pt 1:5-14.